A MATHEMATICAL MODEL OF A BIPHASIC DNA AMPLIFICATION REACTION

by

Danielle Kristine Ciesielski

A dissertation submitted in partial fulfillment
of the requirements for the degree

of

Doctor of Philosophy

in

Mathematics

MONTANA STATE UNIVERSITY
Bozeman, Montana

April 2019

©COPYRIGHT

by

Danielle Kristine Ciesielski

2019

All Rights Reserved

DEDICATION

For my parents, who always help me go the extra mile.

Even when it took me to Montana.

ACKNOWLEDGEMENTS

I foremost want to acknowledge my committee, Dr. Tomáš Gedeon, Dr. Stephanie McCalla, Dr. Lisa Davis, Dr. Mark Pernarowski, and Dr. Jack Dockery, for providing mentoring and support throughout my time at Montana State. Your kindness, patience, and guidance is appreciated! Thank you also to Dr. Tianyu Zhang, Dr. Dominique Zosso, and Dr. Aaron Goodwin for developing my coding skills. And of course, thank you, Katie Sutich, for the endless geniality and support.

I'm so grateful to my parents for all their love, support, guidance, and effort to help me get where I am today. To my K-12 students, for modeling strength in the face of adversity; and my fellow teachers, especially Kim Bowman and Christine Gerling, for modeling unconditional compassion. To my dear friends Allison Morphis, Milica Koscica, and Catherine Potts for the endless cheerleading. And to Kai Jensen for keeping me grounded through this process.

This research was supported by the Office of the Assistant Secretary of Defense for Health Affairs, through the Peer Reviewed Medical Research Program, Discovery Award under Award No. W81XWH-17-1-0319. Dr. Gedeon was partially supported by NSF grant DMS-1361240, USDA 2015-51106-23970, DARPA grant FA8750-17-C-0054, and NIH grant 1R01GM126555-01. My final year of work was supported by the U.S. Army TRADOC Analyis Center through the SMART Scholarship program.

TABLE OF CONTENTS

1. INTRODUCTION 1

2. HYPOTHESES AND MODEL CONSTRUCTION 12

2.1 Model Description 16
2.1.1 Parameter ranges 21
2.1.2 Measuring DNA 23
2.2 Results 25
2.2.1 *Model 1:* No deactivation or recycling of amplifiers 29
2.2.2 *Model 2:* Deactivation but no recycling of amplifiers 30
2.2.3 *Model 3:* Polymerase is not limiting 31
2.3 Discussion 32
2.4 Methods 35
2.4.1 Reagents 35
2.4.2 UDAR setup 35
2.4.3 UDAR time series 36
2.5 Supplemental Computations 36
2.5.1 Calculation of $k_{+/-}$ 36
2.5.2 Calculating the upper bound of k_6 38

3. EQUILIBRIUM AND PERTURBATION ANALYSIS 40

3.1 Partial Model Equilibrium Analysis 45
3.1.1 General considerations 46
3.1.2 Model 1: *No deactivation or recycling of amplifiers* 47
3.1.3 Model 2: *Deactivation but no recycling of amplifiers* 54
3.1.4 Model 3: *Polymerase is not limiting* 58
3.1.5 Model 4: *Full Model* 65
3.2 Multiple Time Scale Analysis 73
3.2.1 Polymerase approximation 76
3.2.2 Analysis for $y < 10$ 79
3.2.2.1 Model I: $\mathcal{O}(1)$ *system* 80
3.2.2.2 Model II: $\mathcal{O}(10^{-4})$ *system,* $y < 10$ 81
3.2.3 Analysis for $y \geq 10$ 86

4. PROOFS 89

4.1 Proofs for Partial Model Equilibrium Analysis 89
4.1.1 Preliminary results 89
4.1.2 Proof of Theorem 1 for Model 1 96

TABLE OF CONTENTS – CONTINUED

4.1.3 Proof of Theorem 2 for Model 2 103
4.1.4 Proof of Theorem 3 for Model 3 106
4.1.5 Proof of Theorem 4 for Model 4 *(Full Model)* 115
4.2 Proofs for Multiple Time Scale Analysis 125
4.2.1 Proof of Theorem 5 for Model I 125
4.2.2 Proof of Theorem 6 for Model II 127
4.2.3 Center Manifold Dynamics for Model II 129

5. CONCLUSION 133

REFERENCES CITED 137

APPENDICES 143

APPENDIX A : Mathematica Code 144
A.1 Model 1 145
A.2 Model 2 147
A.3 Model 3 148
A.4 Model 4 *(Full Model)* 153
A.5 Model II 159
APPENDIX B : MATLAB Code 162

LIST OF TABLES

Table Page

2.1 Parameter ranges and simulation values 24

2.2 Parameters for initial binding event 37

3.1 Model 3 equilibria for simulation values 65

3.2 Model 4 equilibria for simulation values 71

A.1 Model 3 computations for simulation values 152

A.2 Model 4 computations for simulation values 158

LIST OF FIGURES

Figure Page

1.1 Schematic PCR diagram 4
1.2 Schematic EXPAR diagram 5
1.3 Schematic UDAR diagram 7
2.1 Example EXPAR, UDAR Type I and II amplification 13
2.2 UDAR model design 17
2.3 DNA size approximations 25
2.4 Simulation fit to experimental data 26
2.5 Model 1 simulation 29
2.6 Model 2 simulation 30
2.7 Model 3 simulation 31
3.1 UDAR time series for Type I and II templates 41
3.2 Model 1 with late initiation 51
3.3 Model 1 with extended run time 52
3.4 Model 1 with simulation values 53
3.5 Model 2 with simulation values 58
3.6 Model 2 with extended run time (detail) 59
3.7 Model 3 with simulation values 63
3.8 Model 3 with extended run time 64
3.9 Model 3 equilibria detail 66
3.10 Model 3 equilibria detail (inset) 67
3.11 Model 4 with late initiation 69
3.12 Model 4 with simulation values 70
3.13 Model 4 equilibria detail 72
3.14 Model 4 equilibria detail (inset) 73

LIST OF FIGURES – CONTINUED

Figure Page

3.15 Concentration time series 77

3.16 Concentration of $Z + V$ 78

3.17 Concentration of $Y(Y + J)$ 79

3.18 Recycling, dimerization rate approximations 87

ABSTRACT

Isothermal DNA amplification reactions have many applications ranging from analyte detection to DNA circuits. EXPonential Amplification Reaction (EXPAR) is a popular isothermal DNA amplification method that exponentially amplifies short DNA oligonucleotides. A recent modification of this technique using an energetically stable looped template with palindromic binding regions demonstrated unexpected biphasic amplification and much higher DNA yield than EXPAR. This Ultrasensitive DNA Amplification Reaction (UDAR) shows high-gain, switch-like DNA output from low concentrations of DNA input. Here we present the first mathematical model of UDAR based on four reaction mechanisms. We show that the model can reproduce the experimentally observed biphasic behavior. Furthermore, we show that three of these mechanisms are necessary to reproduce biphasic experimental results. The reaction mechanisms are (i) positively cooperative multistep binding caused by two palindromic trigger binding sites on the template; (ii) gradual template deactivation; (iii) recycling of deactivated templates into active templates; and (iv) polymerase sequestration. Understanding of these mechanisms also illuminates behavior of EXPAR and other nucleic acid amplification reactions. For a deeper understanding of the roles these mechanisms play in DNA amplification reactions, we apply dynamical systems analysis to the model. We first consider the long term behavior of partial models that lack key reaction mechanisms described above to see how their omission impacts the system's overall behavior. Then we use perturbation theory to examine the time scales on which these mechanisms operate and how their interaction leads to biphasic growth. We find that mechanisms (i) and (ii) together create a stable equilibrium reminiscent of EXPAR reactions, but the addition of mechanism (iii) changes the stability of this equilibrium and generates UDAR's characteristic high amplification. Finally, mechanism (iv) introduces a second stable equilibrium that indicates that polymerase sequestration is the mechanism that ends the second fast amplification phase. In addition, throughout this work we identify which rate constants shape different parts of the biphasic growth. These results can guide future work in rational design of molecular detection assays.

CHAPTER ONE

INTRODUCTION

Prior to the 1990s, the study of DNA, of its function, and of related information processing focused on genes: particular DNA sequences that contain all the necessary information for making functional RNA and mRNA coding for proteins. The remaining non-protein-coding portions of the genome, consisting mostly of repeated segments scattered throughout the genome, were considered "junk" [1]. In the early 1990s, researchers began to realize that these elements actually interact with the genomic environment in a way that invites genetic recombination and provides new signals for regulating gene expression. When the human genome was mapped, researchers found that less than 2% of the genome is protein-coding and a significant portion of the rest are these adaptive strands that take on different regulatory roles [2].

MicroRNAs (miRNAs) are a significant subset of the non-protein-coding RNAs. We now know these tiny DNA segments (approximately 22 nucleotides in length) degrade and repress translation of messenger RNA after transcription, thus regulating gene expression. With every discovery of a new miRNA and its regulatory target, the scope of miRNA-directed gene regulation is being revealed [3]. While miRNA transcription mechanisms aren't fully understood, it's been shown that major cellular functions such as development, differentiation, growth, metabolism, and apoptosis are regulated by miRNAs [4]. Because of their pervasive roles in the genome, altered expression of miRNA has been linked to heart diseases [5], neuro-developmental disorders [6], autoimmune diseases [7], and cancer [8]. miRNAs play a formative role in these and other conditions, so altered patterns of miRNA expression in cells

are an early indicator of oncoming disease. To accurately inform disease diagnosis, researchers need objective, quantifiable evidence of biological markers (biomarkers). An ideal biomarker is highly specific and sensitive, can be detected by minimally invasive procedures, and can indicate the current state of the disease [9].

Because miRNAs are uniquely associated with biological processes, they're extremely precise reporters of disease and, when measured accurately, can indicate diverse disease states [10], [11]. Furthermore, due to their relatively short length, they can be obtained from minimally invasive procedures. For decades, researchers examined diseases using formalin-fixed, paraffin-embedded tissue specimens where long RNA strands were always fragmented by ribonuclease activity. However, the expression profile of the extremely short miRNAs in these samples closely resembles the miRNA profile found in fresh tissue [12]. Based on this promising result, researchers found that miRNA are surprisingly stable in plasma and serum as well [13], then subsequently in saliva, urine, cerebrospinal fluid, and other eukaryotic fluids carrying exosomes [14]. These exciting results led to further research into circulating miRNA biomarkers for cancer [13], nervous system disorders [15], cardiovascular disorders and diabetes [16], conditions such as acetometaphin hepatotoxicity [17] and traumatic brain injuries [18], viral/bacterial/parasitic infectious diseases (hepatitis, tuberculosis, malaria) [19], and more. The stability of circulating miRNAs would allow not only less invasive diagnosis for patients but also samples that are easier to store and transport along with more cost-efficient diagnosis techniques.

Unfortunately, the final hurdle in using miRNA as biomarkers, specificity, is a huge challenge due to their short length, the high homology of false positives, and the low concentration of circulating miRNA. Since irrelevant miRNA may differ from a targeted biomarker by as little as one nucleotide [20], miRNA recognition struggles with the high homology of false positives. Conventional techniques to

detect RNA, such as microarrays and RNA sequencing, require micrograms of a target DNA whereas circulating miRNA appears on the order of nanograms. Finally, because sample preparation and RNA purification can impact yield, human error can have a profound impact on sample throughput. The combination of these technical challenges and the significant potential impact of miRNA biomarkers on human medicine has made molecular recognition scheme research a high interest field.

One effective molecular recognition scheme is the Polymerase Chain Reaction (PCR) which can accurately amplify specific miRNAs to detectable concentrations [21]. However, the process was designed to amplify longer, double stranded DNA and isn't ideal for miRNA detection. In this process, a small DNA segment (called a primer) with a high affinity for the 3' end of a targeted DNA strand is mixed with the sample in question and put in a thermocycler. The thermocycler first raises the temperature to denature (melt apart and separate) the DNA strands, then lowers the temperature so the strands can anneal (bind together). Because of the relatively higher concentration of primer, the separated strands will more likely bind to a primer than each other. Then the primers are elongated by a DNA polymerase enzyme to replicate the original double stranded DNA segment and therefore create two strands from each original as show in Figure 1.1. The theromcycling process is repeated until the DNA strand concentration reaches a detectable level.

PCR amplifies longer segments of double stranded DNA, so using PCR for miRNA detection requires additional DNA constructions to make it a suitable target. Along with this additional technical step, PCR is constrained by time and expensive instrumentation. The process itself is limited by the fact that only two-fold amplification can be achieved each cycle. Furthermore, traditional flouorophore used for DNA detection binds with high affinity and low specificity, generating potential false positives. While these false positives can be avoided with careful primer design

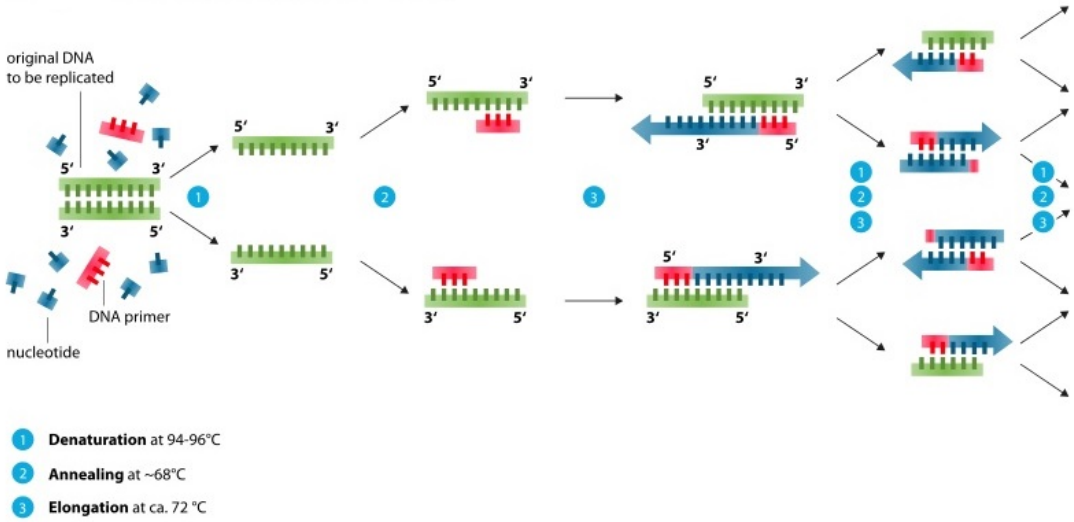

Figure 1.1: The PCR cycle *(by Enzoklop, licensed under CC BY-SA 3.0)*

and melt curve analysis, this is more difficult for miRNA because they're so small and can have close homology of sequence [4]. Clearly advances in speed, specificity, sensitivity, and simplicity would be most welcome.

Isothermal amplification is currently being developed as an effective alternative for molecular recognition. Because it doesn't use thermocyclers, isothermal amplification reduces time and cost considerations [22]. These techniques use single strand templates that are longer than their target DNA strands, so they're well suited for detecting miRNA. In specific cases, isothermal amplification techniques have optimized specificity to single nucleotide resolution and the femtomolar and attomolar concentration levels [23]. One popular isothermal technique is the EXPonential Amplification Reaction (EXPAR) [24], Figure 1.2. In this reaction, a linear template with two binding sites complementary to the target DNA sequence (red τ in Figure 1.2) is combined with the sample to be analyzed. Between the binding sites, the template has a restriction and nicking site (gray and green boxes in Figure 1.2). The target DNA (blue σ in Figure 1.2) binds to the complementary binding site on the 3'

end of the template (χ in Figure 1.2) and is extended by DNA polymerase through the rest of the template to form a double stranded DNA. Then the endonuclease binds to the restriction site and cleaves at the nicking site, freeing the synthesized sequence. Because this sequence was synthesized over a region complementary to the triggering DNA, it's a replica of the trigger which can then trigger the process to begin on another template, creating a chain reaction of amplification. The original template can continue to be extended by DNA polymerase and cleaved by endonuclease, creating the Linear Amplification cycle (r in Figure 1.2).

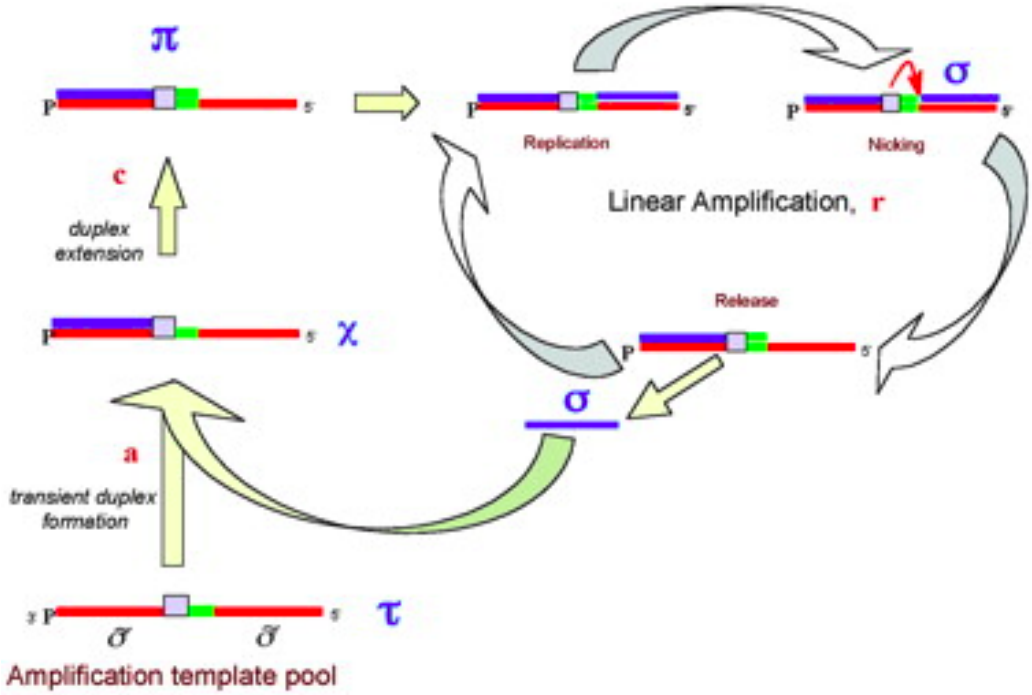

Figure 1.2: The EXPAR cycle *(Van Ness et al., 2003 [24])*

Because EXPAR doesn't need to denature and anneal to replicate target DNA, the reaction speed depends mostly on molecule interaction rates. It's been observed that EXPAR can exhibit either linear or exponential growth depending on template design and can amplify initial concentrations up to six orders of magnitude. While

EXPAR is easier to implement and shows improved speed over PCR, it struggles with specificity [25]. The templates are designed to have a high affinity for the correct miRNA at low concentrations, making them attractive binding sites for near homologous sequences as well. This is problematic when searching for target miRNA in a pool of non-target miRNA. Unlike PCR, where the target replicates itself, EXPAR templates create a perfect replica of the target even when triggered by an incorrect sequence. Since this initiates a chain reaction, the binding of an incorrect sequence therefore leads to production of correct sequences and a strong a false positive. Cut off times between specific and nonspecific amplification change frequently from trial to trial, particularly with low concentrations of target miRNA. This makes it difficult to distinguish between detection of target miRNA and a false positive.

Still, the medical promise of miRNA biomarkers and the advantages of isothermal amplification make it tempting to improve on the existing EXPAR design. As such, researchers are working to keep the essential ideas of EXPAR while curbing the potential for false positives. One such attempt is the Ultrasensitive DNA Amplification Reaction (UDAR) [26], see Figure 1.3. The key feature of UDAR templates is that the pair of binding sites for the target DNA are palindromic, creating an affinity for the binding sites to bind to each other and form a stable hairpin structure shown in Figure 1.3. While in this closed configuration, the restriction site and second binding region are enclosed within the loop. Because the template forms a stable loop, it has a lower affinity for near homologous sequences. To make sure the correct target DNA can access the binding site, the 3' end of the template has a toehold structure (t' in Figure 1.3) that encourages strand displacement [27]. However, the binding energy between a short trigger DNA (miRNA in Figure 1.3) and the looped template is lower than the energy of the closed structure. Because of this, amplification is unlikely to begin unless a second trigger binds to the second

palindromic site directly after a first trigger has opened the template (middle green boxes in Figure 1.3). The structure of a template with two bound triggers is then energetically favorable to extend in the same manner as EXPAR templates and begin a chain reaction amplification process (bottom white boxes in Figure 1.3).

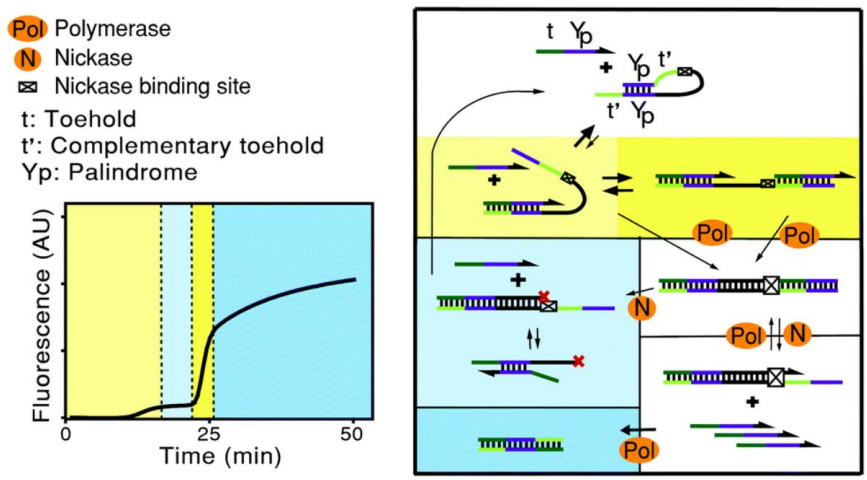

Figure 1.3: The UDAR cycle *(Özay et al., 2018 [26])*

UDAR has two unique features that are the focus of this dissertation.

1. Amplification is up to 100 times larger than standard EXPAR.

2. UDAR trials generally exhibit a pause in DNA amplification when it reaches amplification levels expected for EXPAR.

It was first suggested that the termination of fast amplification in EXPAR trials was caused by a loss of integrity of nicking endonuclease [24] and later suggested that extension errors could create double bound templates that are unable to produce replicates [28]. Özay et al. argue the second theory must be true [26]. If the reagents were limited at EXPAR's final levels of amplification, UDAR could never attain such dramatically higher levels. Furthermore, Özay et al. argue that UDAR templates have the capacity to rescue deactivated complexes by a positively cooperative process.

They posit that with a sufficient concentration of replicated trigger, the trigger's affinity for the toehold enhancements can cause displacement of deactivated tops strand (light blue boxes in Figure 1.3) and returning them back into active amplifying complexes. Because these templates exhibit distinct amplification phases, Özay et al. examine the kinetic features based on DNA association thermodynamics. They experimentally observe that, for certain designs of UDAR templates, the second amplification period can be sharpened to an almost ultrasensitive jump. This indicates the templates can be rationally designed for switch-like behavior. If true, this can lead to the creation of an UDAR-based miRNA detection assay that reacts decisively to true signal while filtering out noise.

In this work, we examine the novel system of chemical reactions motivating the UDAR template's response to trigger by use of a reaction kinetic based ODE model. We explore the following key mechanisms proposed by Özay et al. [26]

1. Multistep initiation, where a DNA trigger opens a template and another trigger binds immediately afterwards. This double binding allows the reaction to begin.

2. Template deactivation, where synthesis errors in the polymerase extension event create complexes that can no longer amplify the trigger DNA.

3. Template recycling, where the many palindromic binding sites in an amplifying complex encourages a high concentration of replicated trigger DNA molecules to dislodge inactive strands.

4. Polymerase sequestration, when increasing concentrations of palindromic DNA trigger causes these molecules to dimerize and extend so frequently that the extension process competes with the amplification reaction extensions and dramatically decreases the final rate of amplification.

We analyze this system by comparing the rates of the reactions and examining solutions of the model lacking key mechanisms both numerically and analytically.

In Chapter 2, we outline our hypotheses about the physical conditions that control the reaction and guide our model construction. We explore physically plausible ranges for the many parameters of this model based on similar experiments in literature. Because multistep initiation, template deactivation, and template recycling have not been experimentally studied yet, we fit the remaining parameters to show how our model can reproduce the unusual biphasic amplification that characterizes UDAR.

We then consider a series of partial models,

1. *Model 1*: No deactivation or recycling of amplifiers
2. *Model 2*: Deactivation but no recycling of amplifiers
3. *Model 3*: Polymerase is not limiting
4. *Model 4*: Full Model.

We use numerical simulation to see if these partial models can reproduce the predicted behavior of the system without key components. This provides insight into the precise roles of different reaction mechanisms.

In Chapter 3, we consider the long term behavior of the partial models from Chapter 2 and interpret our results using plausible reaction rate ranges. Because of UDAR's secondary growth phase, EXPAR reaction cannot terminate because of limited reagents. In fact, our analysis of long term behavior of *Model 1* indicates that, without deactivation, the reaction would produce even higher gain than UDAR. We also show in *Model 2* that, with deactivation but not recycling, the reaction would only amplify to the levels observed in EXPAR experiments. We then consider the

full model, both with the decreased availability of polymerase due to an increasing number of reactions that use it, *Model 4*, and also with the polymerase concentration remaining constant throughout the experiment, *Model 3*. We find the full model exhibits two partial equilibria, one corresponding to the plateau phase and one corresponding to the final level of growth. Using linearization of a reduced system, we determine the lower partial equilibrium is unstable and the higher equilibrium is stable. This reveals the possibility that the plateau phase may be a consequence of trajectories passing close to an unstable saddle equilibrium before diverging along the unstable manifold toward the higher, stable equilibrium.

We then use perturbation theory to look at the phases of delayed initiation and primary amplification in a second series of models. This series will be enumerated by Roman numerals. We see that after a few templates are opened and extended, the reaction remains in the initial state of slow amplification where templates are in excess of trigger due to tiny concentration of trigger DNA *(Model I)*. When enough trigger DNA has been replicated, there's an equilibrium not far from the equilibrium of the leading order terms where all components are at almost imperceptible concentrations. However, this equilibrium is degenerate and has second order instabilities that, given enough time, cause the concentration of replicated trigger DNA to increase until it's no longer limiting *(Model II)*. The time spent near this degenerate equilibrium corresponds to UDAR's extended initiation phase compared to EXPAR. After escaping the neighborhood of this equilibrium, we observe an ultrasensitive switch as the trigger DNA concentration exceeds the availability of the templates. This second equilibrium is stable and corresponds to the plateau phase. This multiple time scale analysis shows that, once recycling begins, dimerization and recycling operate on highly variable orders of magnitude and the most appropriate analysis is the asymptotic limit analysis of full model from the previous section.

Modeling isothermal amplification reactions and understanding the central mechanisms can help improve the specificity and sensitivity of UDAR and other isothermal amplification reactions. By identifying the mechanisms and rates that drive the slow and fast growth phases, templates can be rationally designed to consistently reproduce high gain in the presence of the signal. If nonspecific amplification cannot be eliminated entirely, it may be possible to construct templates in such a way that true signal response occurs in consistent time frames that can be easily distinguished from nonspecific amplification.

While not all questions have been answered, our dynamical systems approach to a kinetic model has continually raised questions that challenged common beliefs regarding isothermal DNA amplification. Wielded appropriately, dynamical systems theory can continue to hone our understanding of the molecular processes at play and thereby our ability to construct successful, highly specific, sensitive assays for specific miRNA sequences. Furthermore, as this work is based on fundamental principles of biokinetics and rigorous mathematics, the insights developed here can extrapolate to more general molecular recognition assays and encourage their rational design.

CHAPTER TWO

HYPOTHESES AND MODEL CONSTRUCTION

DNA amplification technologies are a cornerstone of molecular diagnostics. While Polymerase Chain Reaction (PCR) provides a gold standard for accuracy and sensitivity of nucleic acid detection, it requires complex laboratory equipment and trained personnel. Isothermal DNA amplification reactions that require less energy, time, and equipment than PCR [22] have become an increasingly popular alternative for molecular detection. These reactions can even be run without electricity [29], which is particularly attractive for point of care and limited resource molecular diagnostics. Identification of specific DNA or RNA sequences in these situations could inform medical professionals and potentially curb health crises. EXPonential Amplification Reaction (EXPAR) is a popular isothermal DNA amplification method that exponentially replicates short oligonucleotide triggers [24]. The central elements of EXPAR design are (1) a DNA trigger oligonucleotide that is either the target molecule or is produced by a target molecule, (2) a single stranded DNA template, and (3) polymerase and nickase enzymes. The trigger binds to a complementary region on the single stranded DNA template and then is extended by the polymerase enzyme through a restriction site and a second identical complementary region. Extending over the second complementary region creates a copy of the original trigger which then is released from the template by a nicking endonuclease that recognizes the restriction site. Repeated extension and nicking of these complexes forms a core amplification loop and leads to rapid increase of trigger concentration. As the short oligonucleotide triggers can be created by proteins [30, 31], microRNA [32], DNA [33, 34], and RNA [35], amplification reactions of this type are a popular tool

for molecular recognition schemes. These types of reactions also are used in DNA circuits [36] that show promise in synthetic biology.

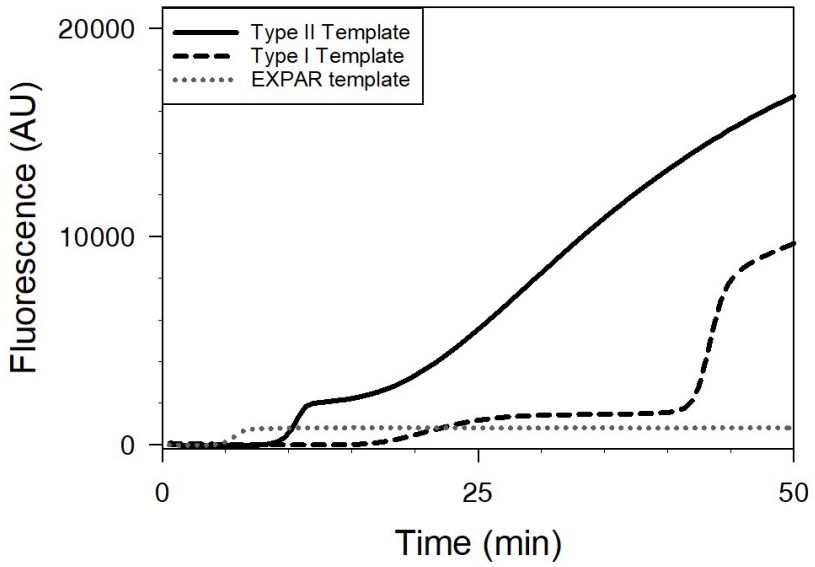

Figure 2.1: **Biphasic DNA amplification output**: Representative outputs of the biphasic DNA amplification reaction UDAR from different template designs; Type II experimental data is modeled in this study. The EXPAR template was reproduced from [37]. The fluorescent signal is produced by the DNA dye SYBR Green II intercalating into the reaction products.

Recently, we constructed an isothermal DNA amplifying template where the complementary binding regions contain palindromic sequences. This construction produces intriguing biphasic amplification behavior [26] (Figure 2.1). The pair of palindromic sequences cause the templates to fold into an energetically favorable hairpin structure which remains closed in the absence of trigger. To ensure the template opens in the presence of the appropriate trigger, the binding regions are enhanced with toeholds [27]. The triggers bind to the toeholds to initiate strand displacement, open the hairpin, and begin the amplification process. The initial behavior of these templates show a quick amplification burst followed by a slow rising plateau similar to EXPAR. However, the plateau is interrupted by a

secondary amplification phase where total DNA produced reaches 10-100 times the levels of standard EXPAR. Since this second phase greatly increases output signal, it's important to understand the factors that cause amplification to resume in this biphasic reaction. The goal of this work is to first mathematically model key reaction mechanisms suggested in [26] that may explain each phase of this reaction and then to simulate the mechanisms with reasonable approximations for each kinetic component. We compare this model to experimental data produced from a UDAR template and show that, without the key reaction mechanisms, the model deviates from the data. Our ultimate goal is to predict and control the timing, duration, and trigger concentration at the plateaus based on known DNA association and dissociation kinetics. To achieve this, we constructed a differential equation model based on four proposed reaction mechanisms.

(i.) *Multistep binding*: A trigger bound at the 3' end of the template can open the template and create an amplifier complex. However, if a second DNA trigger doesn't bind quickly to the formerly concealed palindromic binding region, it's more energetically favorable for the template to reform the stable hairpin and knock off the first binding trigger than to create an amplifier complex. For example, the melting temperature of the looped template structure used in this study is 11.3° C higher than that of a single trigger associated with the template. Thus the template favors the closed configuration and the forward reaction is extremely unlikely when only a single DNA trigger is bound. Because of this, we simplify the reaction for modeling purposes by assuming a second trigger must bind to the template simultaneously to prevent the template from returning to the closed form. A second trigger molecule can only bind after a first trigger has opened the loop, so we consider this a positively cooperative multistep binding event. The trigger will more likely open the loop at the 3'

toehold as the external toehold has association kinetics 10-100 times higher than the internal toehold located inside the loop [38].

(ii.) *Template deactivation*: During the amplification process, an infrequent polymerase error leaves a complementary top strand bound to the template in a complex that cannot be nicked. This reaction mechanism was posited by Rondelez et al. [28], but the incidence and prevalence of this process has yet to be investigated. We assume this mechanism causes deactivation of amplifier complexes which, in turn, dramatically reduces trigger production and often causes the appearance of a plateau.

(iii.) *Template recycling*: We hypothesize that the secondary phase of the trigger amplification is due to an accumulation of trigger replicates that can associate with one of four palindromic binding sites on the deactivated amplifier. The triggers can aid in dislodging the complementary top strand that deactivated the amplifier and thereby rescue the original template. The rescued template can then reform its preferred looped structure and become a functional amplifier again. Because the top strand is complementary, it also has two palindromic sites and, therefore, an affinity for a closed loop form. Due to the energetic favorability of binding with the excess replicated trigger or creating a closed loop form, it's less likely for the separated UDAR template strands to reassociate than for the complementary strands of a standard EXPAR template to do so.

(iv.) *Polymerase sequestration*: Finally, a palindromic trigger can bind to itself and be extended by polymerase to produce an inactive dimer. This reaction was shown to occur when complementary palindromic regions are included in EXPAR templates [26, 39] and was hypothesized to slow the reaction due to limiting the concentration of free trigger molecules. This model incorporates

this effect and the subsequent competition for DNA polymerase that will limit the amplification reaction rate and cause a slow down of amplification. The polymerase concentration used in UDAR and EXPAR experiments is typically approximately 5 nanomolar and will become limiting as the reaction proceeds to produce 10-100 micromolar of product.

Using reasonable parameter estimates based on values reported in literature, we found that this model explains the characteristics of the biphasic reaction described in [26]. Our model reproduces two distinct DNA amplification periods and three periods of stalled growth as observed in UDAR trials. We show that partial models lacking the last three mechanisms described above fail to reproduce biphasic behavior. Our results support the hypothesis that template deactivation hinders EXPAR amplification, which was originally ascribed to deactivation of the nickase [24].

Mathematical models of DNA amplification reactions are uncommon, presenting a significant challenge for researchers working on a broad range of applications. This work is relevant for general kinetic modeling of DNA amplification reactions used in DNA circuits [36], as well as quantitative molecular recognition [40].

2.1 Model Description

The main chemical reactions we assume to occur during UDAR trials are presented in Figure 2.2. The variables in our model represent molar concentrations of different types of oligonucleotides measured in micromolar (μM). We refer to a molecule type by the same name as its concentration, i.e. the concentration of trigger oligonucleotide is denoted by $[Y]$ and we will refer to an oligonucleotide of this type as trigger Y. We now describe the assumptions on which our model is based.

- Let Y be a DNA *trigger*, which is the short DNA oligonucleotide that triggers

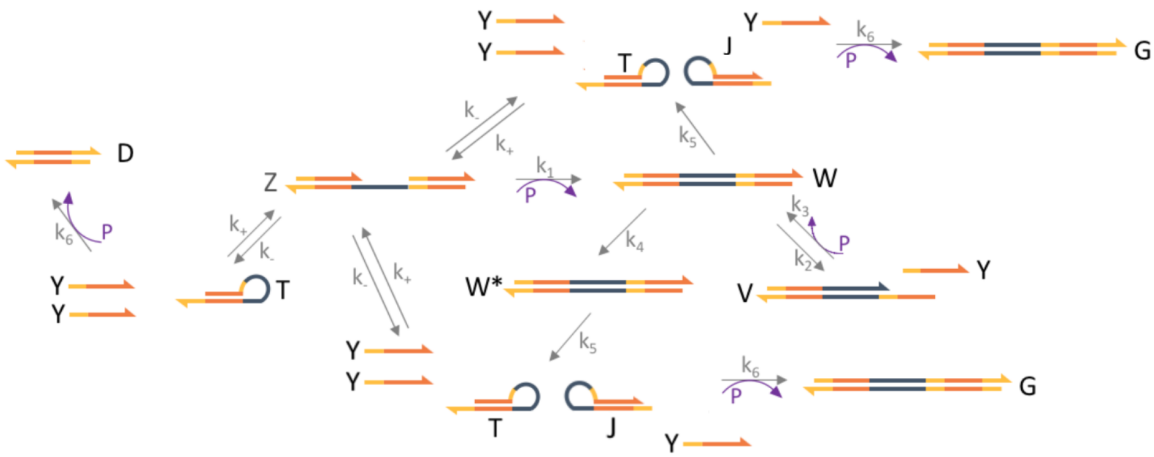

Legend		
DNA trigger (Y)	Double bound template (Z)	Deactivated amplifier (W^*)
Amplifier template (T)	Complete amplifier (W)	Available polymerase (P)
Top strand (J)	Nicked amplifier (V)	Inactive dimers (D) and byproduct (G)

Figure 2.2: **The Full Model diagram** Yellow segments indicate toehold sequences, orange segments indicate palindromic sequences, and navy segments indicate restriction sites. Arrows indicate the direction of elongation. Segments bind when (1.) the colors match (sequences are complementary) and (2.) their direction of elongation is opposite. Toehold sequences have the strongest affinity for binding, followed by palindrome sequences.

its own amplification. Let T be an UDAR *template* consisting of two toehold enhanced palindromic binding sites separated by a restriction site. Because UDAR templates have a stronger affinity for the closed loop configuration than the open configuration with a single Y bound, we simplify the model by assuming single Y bound to T can't extend and that two Ys must cooperatively bind to T to initiate amplification. Let Z be this template with two bound triggers. The simplified multistep binding reaction creates Z complexes at a rate of k_+ and the rate of the inverse reaction is k_-. Computations to estimate the values k_+ and k_- that characterize this multistep process are in §2.5.

- Let W be a *complete amplifier*, the double-stranded complex formed when a

polymerase extends a Z complex. As polymerase extends a Y bound to the 3' end of T, it displaces the Y bound to the 5' end. The rate of extension is proportional to polymerase availability with rate constant k_1.

- Let V be a *nicked amplifier*, a partially double stranded complex formed when nickase releases the replicated Y from W. The rate of nicking is k_2 and V are extended into W proportional to the availability of polymerase at a rate k_3. We assume the process of extending V deactivates complete amplifiers at a rate k_4 and denote these *deactivated amplifiers* by W^*.

- Because Y can weakly dimerize in sufficient concentrations, the abundance of Y replicated in UDAR trials will eventually sequester itself into *inactive dimers*, D [26, 39]. Y molecules associate at their palindromic regions and available polymerase extends through the toeholds, creating strongly associated dimers. The rate of formation of D is proportional to the amount of available polymerase and Y with rate constant k_6. The initial dimerization event has association constant κ_A. For the experimental data used here, the palindromic regions are 6 nucleotides long and Y weakly dimerizes at the reaction temperature.

- W and W^* consist of two strands; the original template T and a complementary *top strand*, J. J has a Y embedded in both ends with a restriction site between, see Figure 2.2. We assume the Y molecules embedded in J or their complementary binding sites in T may be exposed by fraying ends which can lead to separation of complete and deactivated amplifiers, W and W^*, into single strands T and J. This *template recycling* occurs at a rate k_5. Because there are four sites where Y can initiate strand separation, we model the recycling reaction as positively cooperative with a Hill function using Y as the ligand, Hill coefficient 4, and half-saturation constant κ_R. We note that D may also

aid in recycling by separating into individual strands that can bind to both the T and J strands of an amplifier at the same binding sites as Y. However, the strongly associated D is energetically stable at the reaction temperature and therefore sequestered in the double-stranded form. Accordingly, we only consider Y-mediated recycling in this model. Both T and J can either form a stable looped structure or immediately bind with two more Y molecules. For T, this restarts a core amplification loop. For J, this creates an *inactive byproduct* G, which we describe next.

- Because there are two Y molecules embedded in J, excess Y can weakly bind to J at either of these locations with the same affinity with which J forms a closed loop. Y bound to J in this manner can be extended by polymerase at a rate k_6 to form G. Because a Y bound on the 3' end will extend through the restriction site and release any Y that may have previously bound on the 5' end, we assume the process of forming G only removes one Y molecule from the pool of free Y molecules. When a Y bound to the 5' end is removed, it may have been extended by polymerase to form a strand identical to a single strand of the inactive dimer D. This strand then has an affinity for both free Y and strands identical to itself, either of which will then form D. Since Y bound on the 5' end of J is not extendable to a double stranded G, we assume for simplicity that Y only binds to J at the 3' end.

- Because the polymerase becomes occupied during several reactions, the concentration of free polymerase, P, is estimated by

$$P := \frac{P_0}{1 + \frac{[Z]+[V]}{\kappa_{P_1}} + \frac{\kappa_A([J][Y]+[Y]^2)}{\kappa_{P_2}}}, \tag{2.1}$$

where P_0 is the initial concentration of polymerase, κ_{P_1} is the dissociation constant for oligonucleotides longer than 10 nt, κ_{P_2} is the dissociation constant for oligonucleotides shorter than 10 nt, and κ_A is the association constant for the dimerization event described above.

The resulting set of equations to measure concentrations of each DNA form is

$$
\begin{aligned}
[\dot{Y}] &= -2k_+[T][Y]^2 + 2k_-[Z] + k_1[Z][P] + k_2[W] - k_6[P][Y]\big(2[Y] + [J]\big) \\
[\dot{T}] &= -k_+[T][Y]^2 + k_-[Z] + k_5\left(\frac{[Y]^n}{\kappa_R^n + [Y]^n}\right)\big([W] + [W^*]\big) \\
[\dot{Z}] &= k_+[T][Y]^2 - k_-[Z] - k_1[Z][P] \\
[\dot{W}] &= k_1[Z][P] - k_2[W] + k_3[V][P] - k_4[W] - k_5\left(\frac{[Y]^n}{\kappa_R^n + [Y]^n}\right)[W] \\
[\dot{V}] &= k_2[W] - k_3[V][P] \\
[\dot{W}^*] &= k_4[W] - k_5\left(\frac{[Y]^n}{\kappa_R^n + [Y]^n}\right)[W^*] \\
[\dot{J}] &= k_5\left(\frac{[Y]^n}{\kappa_R^n + [Y]^n}\right)\big([W] + [W^*]\big) - k_6[J][Y][P] \\
[\dot{G}] &= k_6[J][Y][P] \\
[\dot{D}] &= k_6[Y]^2[P]
\end{aligned}
\tag{2.2}
$$

where we use Newton's dot notation to indicate a derivative with respect to time. Furthermore, we compute free polymerase $[P]$ using (2.1) and impose the constraint

$$
[T] := T(0) - [Z] - [V] - [W] - [W^*] \tag{2.3}
$$

which comes from a conservation law of the system. The initial conditions are

$$(Y(0), T(0), P(0), Z(0), W(0), V(0), V^*(0), J(0), G(0), D(0)) = (Y_0, T_0, P_0, 0, 0, 0, 0, 0, 0, 0).$$

2.1.1 Parameter ranges

Our model contains 12 parameters: k_+, k_-, k_1, k_2, k_3, k_4, k_5, k_6, κ_R, κ_{P_1}, κ_{P_2}, κ_A. Most of these parameters have known ranges as listed in Table 2.1, which we elaborated on presently.

- $k_{+/-}$ *(binding two Y to one T)* The rate of binding for a ten nucleotide complex at a range of temperatures hass been reported in [41]. Using these correlations, we calculated the rate of a single trigger association to a template as 3.8×10^7 and trigger dissociation as 7.9 s^{-1} for a ten nucleotide trigger. The rate of binding of two triggers to a looped template is not specifically available in literature. To estimate the on and off rates of this association, we used MATLAB to fit estimates of the first and second trigger association (bimolecular rate constants) to dual trigger association (trimolecular rate constants). Details of these calculations are provided in §2.5. Because $k_{+/-}$ primarily affects the initiation of the first phase of trigger expansion, these parameters shift the time of the initial rise. The final parameters were chosen to fit the reaction initiation observed in experimental data for the template studied in this work while keeping reasonable values for the DNA association kinetics.

- k_1 *(extension of Z to W)* The previously reported parameter for a polymerization event of a transient complex for traditional EXPAR is 2 s^{-1} [24]. We adjusted this parameter to reflect the addition of available polymerase in the

equation using the initial value of polymerase, $P_0 = 0.005\ \mu M$, making k_1 approximately $2/P_0 = 400\ s^{-1}\mu M^{-1}$.

- k_2 *(nicking of W)* The original EXPAR model calculated nicking and extension of an amplifying complex (W) as 0.4 s^{-1} [24]. We chose a similar rate to represent the nicking step.

- k_3 *(extension of V to W)* For the template studied in this work, a nicked amplifier V has 12 unbound nucleotides and a double bound template Z has 22. Thus extending V requires synthesizing about half as many nucleotides as Z, so this rate was chosen to be twice as fast a extension of Z to W.

- k_4 *(template deactivation)* Analysis of UDAR trials with the template considered in this study showed that an initial concentration of 0.1 μM of template produced 5 μM of trigger before pausing at the first plateau. We therefore assume templates become deactivated after approximately 50 extension events, corresponding to a deactivation rate approximately 50 times lower than the extension rate, $k_3 P_0$. Our chosen parameter is in this range.

- k_5 *and* κ_R *(recycling)* We signify by κ_R the concentration of Y at which recycling operates at half its maximum rate. We chose this to be between the concentration at the first plateau (approximately 5 μM) and final growth (approximately 50 μM). The rate k_5 is a free parameter describing the speed of recycling. It was chosen to fit the data as template recycling is a completely unexplored phenomenon.

- k_6 *(inactive dimer formation)* This parameter has an upper bound calculated by employing a quasi-steady state assumption: association of the triggers to

form a dimer is assumed to equilibrate quickly compared to the association of dimers with the polymerase. Details of this calculation can be found in §2.5.

- $\kappa_{P_{1,2}}$ *(polymerase dissociation constants)* The affinity of DNA polymerase to DNA substrate is highly variable and can change with parameters such as DNA sequence. For example, measurements of polymerase dissociation constants can range from $5\ nM - 200\ nM$. The trials used for this study use Bst, a family A polymerase. Complete extension of complexes Z and V, which require more than 10 base pairs to be filled in, are modeled with a dissociation constant $\kappa_{P_1} = 15\ nM$. This is similar to the $K_d = 5\ nM$ of Pol I [42], a different family A polymerase. Another family A polymerase showed decreased initiation kinetics when primers were less than 10 base pairs [43]. These primers likely have a higher dissociation constant than longer priming regions. Thus we chose a value on the order of the highest dissociation constant found in literature, $225\ nM$ for κ_{P_2} [44]. This is appropriate for binding the short primer strands ($6\ nt$) creating during dimerization of Y.

- κ_A *(association constant of palindrome-palindrome binding)* The association constant for palindrome sites binding together, such as free Y binding to itself or an unbound top strand, was calculated using the DINAmelt web server [45].

2.1.2 Measuring DNA

The measured reaction output is created by the fluorescent intercalating dye SYBR Green II, which produces a signal assumed to be approximately proportional to the length of DNA. To compare model simulations to experimental results, simulated concentrations were converted to the number of nucleotides incorporated into the DNA reaction products. The product of the reaction was shown to be primarily

Parameter	Range	Simulation Value	Citation
k_+	$\mathcal{O}(10^2 - 10^3)\ \mu M^{-2}s^{-1}$	$2,000\ \mu M^{-2}s^{-1}$	[41], SI
k_-	$\mathcal{O}(1 - 10)\ s^{-1}$	$45\ s^{-1}$	[41], SI
k_1	$400\ \mu M^{-1}s^{-1}$	$400\ \mu M^{-1}s^{-1}$	[24]
k_2	$0.4\ s^{-1}$	$0.625\ s^{-1}$	[24]
k_3	$\mathcal{O}(k_1)\ \mu M^{-1}s^{-1}$	$800\ \mu M^{-1}s^{-1}$	–
k_4	$\mathcal{O}(\frac{k_1 P_0}{50}) = \mathcal{O}(0.04)\ s^{-1}$	$0.013\ s^{-1}$	[24], [26]
k_5	–	$0.1\ s^{-1}$	–
κ_R	–	$14\ \mu M$	–
k_6	Less than $k_1\kappa_A = 3\ \mu M^{-2}s^{-1}$	$0.01\ \mu M^{-2}s^{-1}$	[45], SI
κ_A	$7.5 \times 10^{-3}\ \mu M^{-1}$	$0.0075\ \mu M^{-1}$	[45]
$\kappa_{P_1}, \kappa_{P_2}$	$0.001 - 0.2$	0.015, 0.225	[44], [42], [43]

Table 2.1: **Parameter ranges and simulation values** Note this work is introducing the idea of recycling templates, so κ_R and k_5 have no comparable values in present literature.

free trigger (Y) with a growing number of inactive dimers (D). The approximate concentration of reaction products was determined using calibrated SYBR Green II fluorescence of 12 nucleotide triggers. Experimental data and model output are both reported as the equivalent μM of incorporated nucleotides. All oligonucleotides in our model are comprised of three fundamental sequences: the toehold, the palindrome binding site, and the restriction site, see Figure 2.3. Each sequence length is expressed in nucleotides and can differ between experiments. We denote the length of toehold by $\mathcal{T}$, the length of the palindrome site by $\mathcal{P}$, and the length of the restriction site by $\mathcal{R}$. The length of each oligonucleotide can be expressed in terms of the three basic lengths, Figure 2.3. We note that G can take on two forms, G_1 or G_2, based on which trigger binds first. However, consistent with the assumptions described in §2.1, we estimate total DNA in G form by the length of G_2. The total DNA (Σ) in terms of

incorporated nucleotides, is

$$\begin{aligned}\Sigma =&(\mathcal{T}+\mathcal{P})[Y]+(2\mathcal{T}+2\mathcal{P}+\mathcal{R})([T]+[J])+\big(4\mathcal{T}+4\mathcal{P}+\mathcal{R})[Z]\\&+(3\mathcal{T}+3\mathcal{P}+2\mathcal{R})[V]+(4\mathcal{T}+4\mathcal{P}+2\mathcal{R})\big([W]+[W^*]\big)+(4\mathcal{T}+2\mathcal{P})[D]\\&+(6\mathcal{T}+4\mathcal{P}+2\mathcal{R})[G]\end{aligned}$$

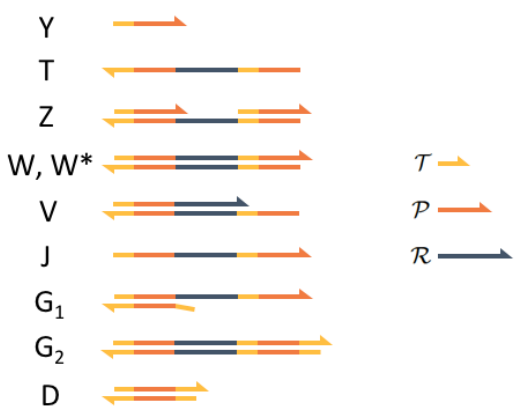

Length of Y:	$\mathcal{T}+\mathcal{P}$
Length of T, J:	$2\mathcal{T}+2\mathcal{P}+\mathcal{R}$
Length of Z :	$4\mathcal{T}+4\mathcal{P}+\mathcal{R}$
Length of W, W^*:	$4\mathcal{T}+4\mathcal{P}+2\mathcal{R}$
Length of V:	$3\mathcal{T}+3\mathcal{P}+2\mathcal{R}$
Length of G_1:	$4\mathcal{T}+3\mathcal{P}+\mathcal{R}$
Length of G_2:	$6\mathcal{T}+4\mathcal{P}+2\mathcal{R}$
Length of D:	$4\mathcal{T}+2\mathcal{P}$

Figure 2.3: Length and structure of various oligonucleotides in terms of three basic sequences, $\mathcal{T}$, $\mathcal{P}$, and $\mathcal{R}$

2.2 Results

Our model, constructed from proposed reaction mechanisms (i.)-(iv.) as described in the chapter introduction and using parameters within biologically plausible ranges (Table 2.1), is able to closely match experimental amplification time series from UDAR trials first reported in [26], see Figure 2.4. The reaction has five distinct phases,

I. *Initiation*, a period where total DNA stays near initial levels;

II. *Primary amplification*, a brief period where total DNA rapidly increases;

III. *Plateau*, a period where the DNA amplification rate significantly decreases;

IV. *Secondary amplification*, a second period where total DNA rapidly increases;

V. *Slow final growth*, a final period where the total DNA growth rate decelerates.

The proposed reaction mechanisms successfully reproduce these features. We justify the connections between the reaction mechanisms and the above phases as follows.

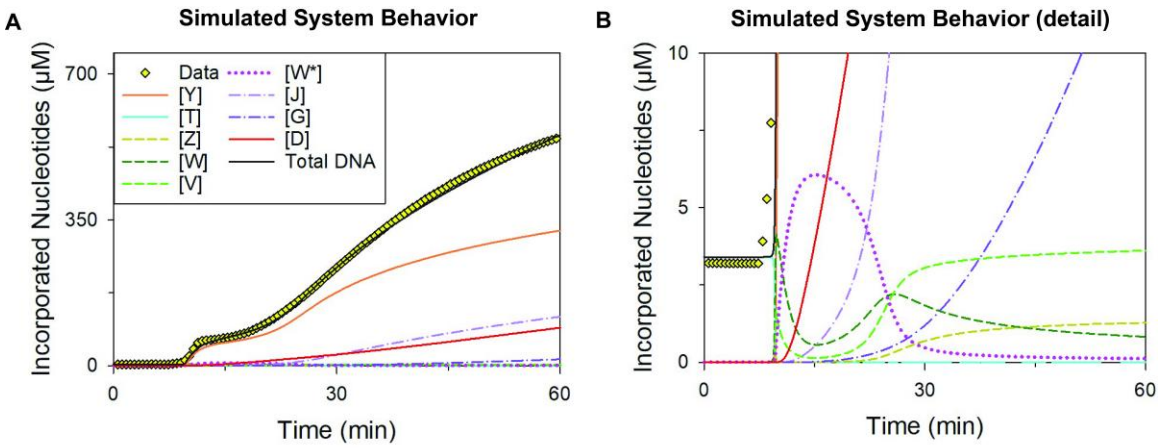

Figure 2.4: **Simulation fit to data:** (a) Fit of experimental data to total DNA predicted by the full model with parameters within range of best estimates for the experimental conditions. Concentrations of each reaction product are also shown; (b) Detail *(note the vertical axis scale)* of non-monotonic concentration values that drives the biphasic behavior

I. The initial concentration of T is much larger than the initial concentration of Y. Mechanism (i) requires multistep binding to initiate amplification, so the reaction is limited by an insufficient concentration of Y to bind two molecules to a T at once. Assuming multistep binding does occur infrequently during initiation, a small concentration of W will be produced. These complete amplifiers begin core amplification loops: W is nicked to form V, releasing a replicated Y, then being extended back into W to close the loop. However until a sufficient concentration of Y is replicated, this phase appears static.

II. The transition from initiation to primary amplification exhibits behavior similar to ultrasensitive switches as reported by [46], see Figure 2.4(b). When Y approaches a concentration where it's is no longer limiting, T has sufficient trigger available to immediately form stable Z complexes. These then rapidly transform into W complexes and abundantly replicate Y. Thus we see the jump in amplification that characterizes the primary amplification phase.

III. As posited in mechanism (ii), W amplifiers are regularly deactivated by polymerase errors during extension. As the W concentration rises, this deactivation becomes more pronounced. The accumulation of W^* and decline in W, observed in Figure 2.4(b), reduces the availability of operational core amplification loops, slows the production of Y, and initiates the first plateau. During the plateau, most W amplifiers are deactivated so this phase is characterized by extremely subtle amplification. Mechanism (iii), however, postulates that Y can split inactive W^* complexes into separate hairpin shaped J and T strands. Because the W and W^* structures are energetically favorable compared to Y association with the already bound palindromic regions of W, recycling is delayed until Y is concentrated enough to displace J. As there's continued slow growth in Y during the plateau phase, Y will eventually attain the critical concentration required to start recycling W and W^*.

IV. When this second critical concentration of Y is attained, we again observe switch-like behavior as recycling becomes energetically favored. The critical concentration of Y that triggers recycling is much higher than the critical concentration of Y needed for template opening, so recycled templates immediately form W complexes. Furthermore, this concentration of Y is sufficient to recycle W^*. This means the amplification process at this stage follows a *secondary*

amplification loop: two Ys immediately bind to the newly free T and extend to form W. W will then complete approximately 50 core amplification loops before being deactivated and recycled (or directly recycled without deactivation), releasing the template to repeat the process. This secondary loop drives the secondary amplification phase.

V. The final amplification deceleration is caused by mechanism (iv) as polymerase becomes saturated by an increased demand for extension late in the reaction. The concentration of Y and J increase to the point that weak dimerization becomes a dominant reaction. When Y binds to another Y or a J, the polymerase either synthesizes the complimentary toeholds (creating D) or the length of J (creating G). As the concentration of Y is much higher than the concentration of J, D is produced more rapidly than G. These reactions compete with the core and secondary amplification loops for polymerase, sequestering the availability of polymerase and slowing all reactions during the second half of the experiment. The lack of available polymerase leads to accumulation of V in the core amplification loop, accumulation of Z in the secondary amplification loop, and a corresponding decrease in concentration of W. Since W produces Y, this decreases production of Y.

To show the proposed mechanisms are essential to reconstruct all five phases of the reaction, we present simulations of a series of partial models that satisfy some, but not all, of these hypotheses:

1. *Model 1: No deactivation or recycling of amplifiers*, omitting mechanisms (ii)-(iii)

2. *Model 2: Deactivation but no recycling of amplifiers*, omitting mechanism (iii)

3. *Model 3: Polymerase is not limiting*, omitting mechanism (iv)

In each partial model, we use the parameters from Table 2.1 except that parameters corresponding to omitted mechanisms are set to zero. We simulate the resulting model from the experimental initial conditions and discuss our findings in the following sections.

2.2.1 *Model 1:* No deactivation or recycling of amplifiers

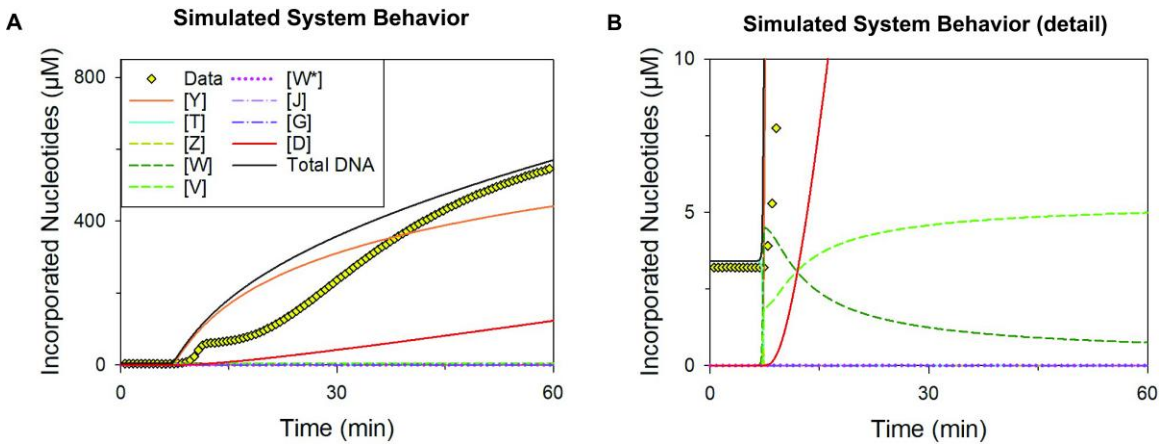

Figure 2.5: **Partial Model 1 ($k_4 = k_5 = 0$):** (a) Total DNA and individual reaction products, shown with experimental data; (b) Detail of primary amplification

In this model we use only mechanisms (i) and (iv). We represent this by setting

$$k_4 = k_5 = 0.$$

All other parameters are from Table 2.1. In this simplified model,

$$[W^*] \equiv 0, \qquad [J] \equiv 0, \qquad [G] \equiv 0.$$

The numerical simulation, shown in Figure 2.5, does not reproduce the five phases that characterize the UDAR trials. It reproduces (I.) initiation, (II.) primary amplification, and (V.) slow final growth, but does not exhibit the initial plateau or secondary

amplification phases. Deactivation reduces the number of active core amplification loops, so the omission of deactivation reduces the time required to achieve the critical concentration of Y needed to trigger the primary growth. This model does not reproduce the plateau because the only limitation on the growth of the DNA is sequestration of polymerase by the formation of inactive dimers D.

2.2.2 *Model 2:* Deactivation but no recycling of amplifiers

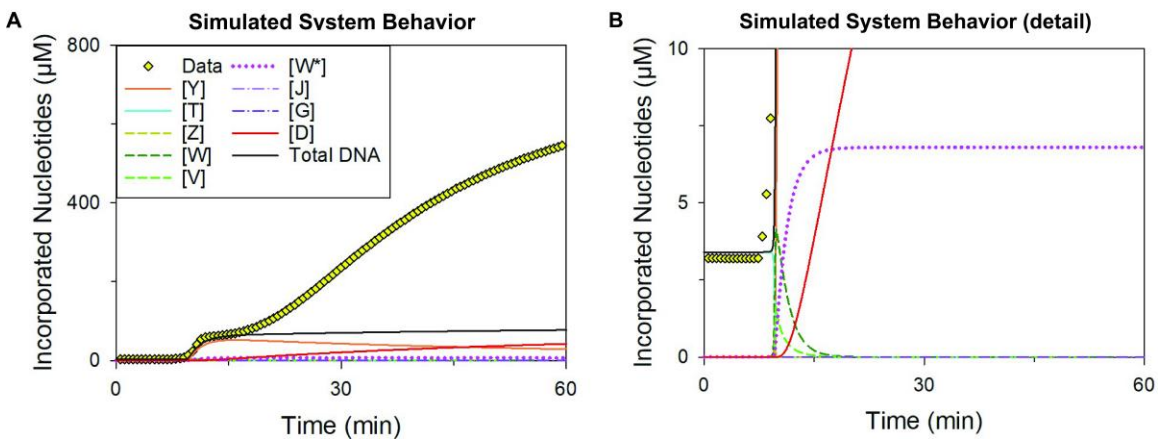

Figure 2.6: **Partial Model 2 ($k_5 = 0$):** (a) Total DNA and individual reaction products, shown with experimental data; (b) Detail of primary amplification

In the second partial model we use mechanisms (i), (ii), and (iv). We represent the lack of mechanism (iii) by setting

$$k_5 = 0.$$

All other parameters are from Table 2.1. This leads to a simplified model where

$$[J] \equiv 0, \qquad [G] \equiv 0.$$

The numerical simulation shown in Figure 2.6 reproduces the amplitude of DNA

production during the (II.) primary amplification phase and the (III.) plateau phase observed experimentally. This indicates the plateau is indeed caused by template deactivation. Note that the total DNA closely approximates concentrations reported in EXPAR experiments. However, the model does not reproduce (IV.) the secondary amplification phase. Since the only mechanism still missing is (iii.), the recycling, we conclude that secondary amplification is caused by template recycling.

Without recycling, the deactivation of templates lowers the concentration of core amplification loops until trigger replication nearly ceases. Total DNA growth after the core amplification loops are deactivated is mostly due to dimerization of Y. When polymerase synthesizes over the toehold regions to create strongly associated inactive dimers D, the size of the strand is increased (Figure 2.3), so total DNA continues to rise at a significantly diminished rate (note the decrease in Y and corresponding increase in D in Figure 2.6(b)).

2.2.3 *Model 3:* Polymerase is not limiting

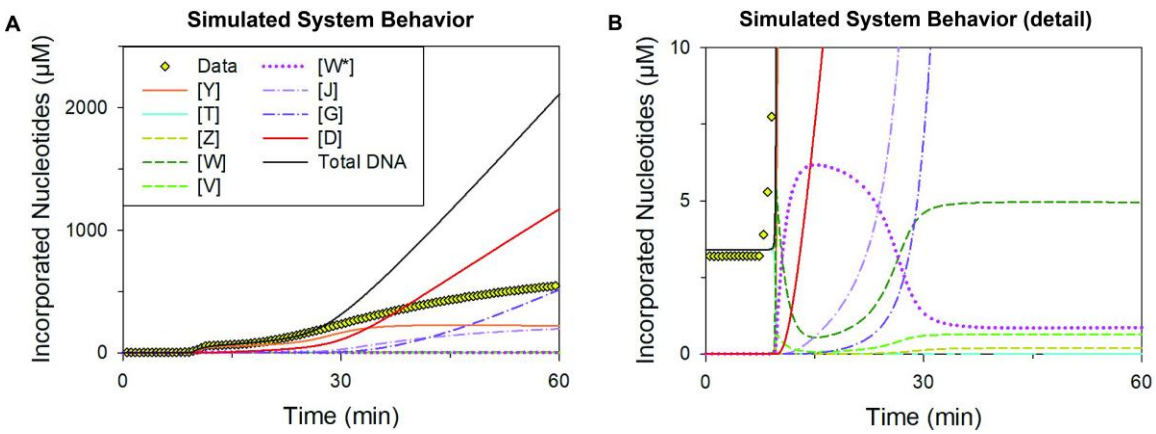

Figure 2.7: **Model III ($[P] \equiv P_0$):** (a) Total DNA and individual reaction products, shown with experimental data; (b) Detail of the primary amplification process

In the final partial model, we use mechanisms (i)-(iii), but not (iv), replacing the polymerase availability equation (2.1) by the assumption that polymerase stays

at its initial level, P_0, throughout the reaction. All parameters are from Table 2.1.

The numerical simulation, shown in Figure 2.7, reproduces the (I.) initiation, (II.) primary amplification, (III.) plateau, and (IV.) secondary amplification phases. However, the total DNA growth does not slow down at the rate observed in the experimental data. This suggests the reduced production of free trigger that drives the final deceleration is caused by competition for available polymerase.

In this simulation, inactive dimers form rapidly due to constant trigger production and extend the secondary amplification phase. Because polymerase will synthesize over the toeholds of the triggers, one inactive dimer is larger than two triggers, see Figure 2.3. As polymerase is not limiting, the core amplification loops continue to produce trigger which rapidly form inactive dimers. This results in the linear-like growth that continues past the experimental time frame and leads to a significant increase in predicted total DNA production compared to experimental data. We expect that EXPAR templates would show the same linear growth without template deactivation. Thus the fact that EXPAR experiments stop amplifying at the levels they do again indicates the template deactivation is responsible for termination of EXPAR amplification.

2.3 Discussion

In this paper, we propose the first mathematical model that reproduces the biphasic behavior of UDAR templates [26]. We propose that the necessary ingredients for successful reproduction of all five characteristic phases of these biphasic experiments include gradual amplifier deactivation, recycling of deactivated amplifiers back into single stranded templates, and polymerase sequestration. Our model incorporates these three assumptions with parameters informed by experimental literature and successfully reproduces all essential features observed in UDAR trials.

Furthermore, a sequence of partial models where some of these mechanisms are omitted fail to reproduce key aspects of the UDAR process.

The proposed mechanisms of template deactivation, template recycling, and polymerase sequestration are not included in previous models of isothermal DNA amplification reactions [24, 36, 39]. These mechanisms have implications for other isothermal DNA amplification processes, including the popular reaction EXPAR. Because EXPAR trials produce final amplification levels comparable to the first plateau of an UDAR template, our model suggests the core amplification loops of EXPAR templates stop replicating permanently due to template deactivation. Based on the presented model, template recycling spurs the secondary amplification phase of UDAR templates. We expect that recycling of non-palindromic templates (such as those used in EXPAR) is energetically unfavorable and hence very rare. The palindromic binding sites make recycling more likely in two ways. First, trigger molecules can separate deactivated UDAR complexes at two different locations on either strand, while non-palindromic complementary sites only allow trigger to attach to the template and not the complementary top strand. Second, the complementary top strand with palindromic sequences will form a hairpin loop. Because both the UDAR template and complementary top strand prefer to close when separated, the strands are less likely to reassociate. Linear templates like those used in EXPAR, however, have a strong affinity for their complementary top strand and are more likely to return to the deactivated state than be recycled.

It's worth noting that the biphasic behavior observed in UDAR trials is not a requisite feature for the increased amplification levels. As noted in [26], a few templates fail to produce a plateau but do nevertheless attain much larger final concentrations than EXPAR templates. We expect the trigger concentration required for recycling these templates is lower and therefore attained before template

deactivation noticeably slows the amplification. We further expect that templates lacking strong enough trigger associations to recycle amplifiers or that cannot produce the critical concentration of trigger will not enter the second amplification phase during the experimental time frame.

While this is the only comprehensive model to date incorporating polymerase sequestration as well as the only mathematical model describing a biphasic DNA amplification reaction, there are several limitations to be addressed in future work. First, a more detailed study of several different template types could identify the relationship between DNA association thermodynamics with each reaction mechanism. Second, future studies will focus on identifying unknown specific parameters, such as an experimentally determined trimolecular rate constant (for dual trigger binding to a template) and dimerization, as both were estimated by simplified order of magnitude approximations. Finally, future work will include investigation of kinetic parameters k_5 and κ_R that describe the novel mechanism of template recycling and understanding the effect of reactions that were not included in the model. Our model describes a basic reaction set that occurs during UDAR and informs mathematical understanding of isothermal DNA amplification reactions such as EXPAR. The scope of this work is to identify the critical reaction mechanisms required to reproduce biphasic amplification output. A mechanistic understanding of this reaction can help researchers predict and control the kinetics and trigger output of UDAR based on known DNA association and dissociation kinetics. This kind of understanding will in turn produce more accurate models of isothermal amplification reactions. This model can be adapted to aid in design of molecular diagnostics, DNA circuits, and synthetic biology applications.

2.4 Methods

2.4.1 Reagents

SYBR Green II RNA Gel Stain were purchased from Thermo Fisher Scientific (Waltham, MA). Nuclease-free water, Oligo length standard 10/60 and desalted amplification templates (suspended in IDTE Buffer at a concentration of 100 μM and modified with an amino group on the 3 end to prevent template extension) were purchased from Integrated DNA Technologies, Inc. (Coralville, IA). Nt.BstNBI nicking enzyme, Bst 2.0 WarmStart DNA Polymerase, 10x ThermoPol I Buffer, dNTPs, BSA, and 100 mM $MgSO_4$ were purchased from New England Biolabs (Beverly, MA). The template (LS3, 5' - CGCGCGGTTTGGTAATGACTCTCGCGCGGTTTGG - 3') and trigger (5' - CCAAACCGCGCG - 3') were described in [26]. The traditional EXPAR template design is from [37], with template (5' - CTCACGCTACGGAC-GACTCTCTCACGCTAC - 3') and trigger (5' - GTAGCGTGAG - 3').

2.4.2 UDAR setup

Reactions were prepared at 4° C. The amplification reaction mixture contained 1x ThermoPol I Buffer [20 mM Tris-HCl (pH 8.8), 10 mM $(NH_4)_2SO_4$, 10 mM KCl, 2 $mMMgSO_4$, 0.1% Triton X-100], 25 mM Tris-HCl (pH 8), 6 mM $MgSO_4$, 50 mM KCl, 0.5 mM each dNTP, 0.1 mg/mL BSA, 0.2 $U/\mu L$ Nt.BstNBI, and 0.0267 $U/\mu L$ Bst 2.0 WarmStart DNA Polymerase ($75,000$ U/mg, 67 kDa). Amplification templates were diluted in nuclease-free water and added at a final concentration of 100 nM. SYBR Green II (10,000x stock in DMSO) was added to the reaction mixture to a final concentration of 4x. The experimental data was triggered by 10 pM of trigger. Fluorescent measurements were taken every 20 seconds with a 12 second imaging step in a BioRad CFX Connect Thermocycler (Hercules,

CA) at 55° C. Completed reactions were stored at $-20°$ C for further analysis.

2.4.3 UDAR time series

To determine the conversion factor between the real-time fluorescence and the total DNA produced, 9 tubes of 20 μL UDAR reactions were produced according to above protocol without the addition of trigger, which can be non-specifically produced during EXPAR and UDAR reactions [26]. One tube for each time point (0, 8.5, 10.2, 12.3, 19.4, 31.1, 60 min) was taken out of the thermocycler and placed on ice to terminate the reaction. The concentrations of the reaction products were determined using calibrated SYBR gold fluorescence of the 12 nucleotide trigger, and used to calculate the μM/Fluorescent Unit. From these time points we found that the conversion between fluorescense from the real-time thermal cycler and μM of products was 0.0026 ± 0.0004 μM/ Fluorescence Unit after background correction. The number of nucleotides incorporated into the reaction products was calculated by multiplying the μM of measured reaction products by 12, as SYBR dye fluorescence is approximately correlated with length of the products and reaction products are largely composed of trigger Y. This conversion factor was used to calculate the concentration of reaction products in the trigger-initiated reaction described above.

2.5 Supplemental Computations

2.5.1 Calculation of $k_{+/-}$

The equations for bimolecular association for Z_1 (one trigger associated with a template) and Z (two triggers associated with a template) are:

$$[\dot{Z}_1] = k_{a_1}[T][Y] - k_{d_1}[Z_1] - k_{a_2}[Z_1][Y] + k_{d_2}[Z]$$

$$[\dot{Z}] = k_{a_2} Z_1[Y] - k_{d_2}[Z]$$

The equation for a trimolecular association, which is the assembly of two triggers Y with one template T, is given by:

$$[\dot{Z}] = k_+[T][Y]^2 - k_-[Z]$$

The parameters for k_{a_2} and k_{d_2} were approximated using experimental data from literature [41], which provides a temperature-dependent formula for calculating kinetics of association and dissociation of complimentary DNA strands that were 10 and 20 nucleotides. Using a temperature of 55° C and a DNA length of 10 gives a $k_a = 37.8$ μM and $k_d = 7.9$ $1/s$. As our trigger is slightly longer than 10 nucleotides (12 nucleotides), we have assumed a slightly larger k_{a_2} and a smaller k_{d_2} than those of the 10 nucleotide sequence, but ones that are still below and above that of the 20 nucleotides sequence. The parameters for k_{a_1} and k_{d_1} were assumed to be smaller and larger, respectively, due to the presence of the strong template loop. In the case of the experimental data shown here, the template loop has a melting temperature that is 11.3° C higher than the trigger Y association with the template T. The concentration of complex Z over time was calculated using MATLAB ODE solver `ode15s` and the parameters/initial conditions shown in Table 2.2. The final parameters approximating

Parameter	Value
k_{a_1}	$25\ \mu M^{-1}s^{-1}$
k_{a_2}	$50\ \mu M^{-1}s^{-1}$
k_{d_1}	$22.8\ s^{-1}$
k_{d_2}	$1\ s^{-1}$
k_+	$2000\ \mu M^{-2}s^{-1}$
k_-	$45\ s^{-1}$
Initial Values	$[Y, T, Z] = [10^{-5}, 0.1, 0]\ \mu M$

Table 2.2: Bimolecular and trimolecular kinetic parameters describing template (T) trigger (Y) binding

trimolecular association, k_+ and k_-, were chosen to match the initiation of the first phase of DNA ouput seen in the UDAR experimental data. To verify that $k_{+/-}$ were in a reasonable range for a trimolecular binding constant, we used the values for k_{a_1}, k_{a_2}, k_{d_2} approximated from literature and calculated the concentration of Z given by the two-step bimolecular association and one-step trimolecular association. We then used the MATLAB optimization function `fminsearch` to find the value of k_{d_1} that produced the same concentration of Z as the one-step trimolecular association. We assume that the dissociation constant changes much more than the association constant; for example, between 10 and 20 nucleotides the association constant changes by a factor of two, but the dissociation constant changes by over four orders of magnitude. The fitted value of k_{d_1} is approximately 20 times greater than k_{d_2}, which is reasonably larger than the first association constant.

2.5.2 Calculating the upper bound of k_6

The parameter k_6 is a combination of trigger dimerization and subsequent polymerase binding. As the dimerization of triggers has a high on/off rate, we assume it equilibrates quickly and that polymerization is the rate limiting step. The association constant of dimerization was calculated using the DINAmelt web server as described in the main text [45]. Using the pseudo-steady state approximation

$$\kappa_A = \frac{[YY]}{[Y][Y]} = 0.0075\ \mu M^{-1},$$

it follows that

$$[YY] = [Y][Y]\kappa_A.$$

A decrease in initial polymerization rates when using primers that have less than 10 base pairs is observed in other family A polymerases [43], as well as in polymerases

from thermophilic archea [47]. We previously observed that looped templates with triggers less than 10 nucleotides showed much lower amplification efficiency regardless of the strength of the trigger [26]. The palindrome of the trigger that produced this experimental data is 6 nucleotides long. Therefore, the rate of polymerization of double stranded trigger $[YY]$ to form the stable double-stranded inactive dimer D must be lower than the rate of polymerization of the trigger-bound template Z to the double stranded template W. It follows that $k_1 << k_1'$, where k_1' is the rate of polymerization of the dimerized triggers to D. By definition,

$$k_6[Y][Y][P] = k_1'[YY][P].$$

Plugging in the expression for [YY] found above, we find that

$$k_6 = k_1'\kappa_A << k_1\kappa_A.$$

CHAPTER THREE

EQUILIBRIUM AND PERTURBATION ANALYSIS

As noted in Chapter 2, this research is one of the first attempts to model DNA amplification reactions. The field of dynamical systems has many tools to interpret the long term behavior of systems, but defining features of biochemical reactions can be transient. Equilibria, periodic orbits, connecting orbits, and their stability therefore may be only marginally relevant for describing how UDAR templates behave in the presence of low target miRNA concentrations. However, the experimental data (Figure 3.1) clearly shows an intriguing dynamic process that occurs consistently with various template designs. To access information regarding these finite time dynamics rigorously, we first analyze the long term behavior of the system by determining its equilibria. In this process, we compare the full results with behavior of systems lacking the key mechanisms described in Chapter 2. Then we investigate the delayed initiation and primary amplification growth phases using perturbation theory where we treat the multistep binding event as an unperturbed system and the subsequent slower reactions leading to the plateau phase as perturbing the system. In this section, we assume reaction mechanisms with higher order rate constants approach their equilibrium before reaction mechanisms with lower order rate constants impact the system. This piecemeal use of equilibrium and stability analysis with perturbation theory provides a basis from which we explain the unique biphasic behavior of the experimental UDAR trials.

This analysis gives novel insight into not only key mechanisms for Type II templates in the UDAR reaction but hints at important reaction mechanisms for other UDAR templates (Figure 3.1) [26] as well as more general DNA amplification

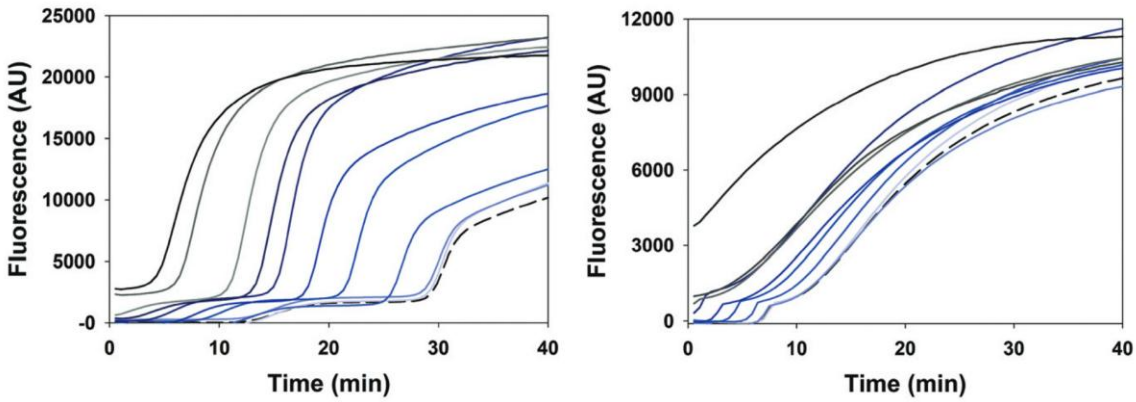

Figure 3.1: **UDAR experimental data as reported in [26]:** Left figure are fluorescence time series for several templates displaying Type I behavior, Right figure are fluorescence time series for several templates displaying Type II behavior

reactions. Furthermore, the dynamical systems based approach used here may motivate future analysis of biochemical reactions exhibiting nonlinear behavior. To make this work broadly applicable, much analysis is completed with general rate constants. When necessary, appropriate, or simply illuminating, we'll assume either that our parameters lie in the ranges described in Table 2.1 or that they take on the actual values used in Chapter 2 (found in the same table). Where appropriate, we present the formulas needed to replicate numerical simulations and computations with different parameter sets. In this way, our analysis provides a framework for understanding the key mechanisms of UDAR amplification beyond just the current knowledge of acceptable parameter ranges.

We analyze the general UDAR model,

$$
\begin{aligned}
[\dot{Y}] &= -2k_+[T][Y]^2 + 2k_-[Z] + k_1[Z][P] + k_2[W] - k_6[P][Y]\left(2[Y] + [J]\right) \\
[\dot{T}] &= -k_+[T][Y]^2 + k_-[Z] + k_5\left([W] + [W^*]\right)\left(\frac{[Y]^4}{\kappa_R^4 + [Y]^4}\right) \\
[\dot{Z}] &= k_+[T][Y]^2 - k_-[Z] - k_1[Z][P] \\
[\dot{W}] &= k_1[Z][P] - k_2[W] + k_3[V][P] - k_4[W] - k_5[W]\left(\frac{[Y]^4}{\kappa_R^4 + [Y]^4}\right) \\
[\dot{V}] &= k_2[W] - k_3[V][P] \\
[\dot{W^*}] &= k_4[W] - k_5[W^*]\left(\frac{[Y]^4}{\kappa_R^4 + [Y]^4}\right) \\
[\dot{J}] &= k_5\left([W] + [W^*]\right)\left(\frac{[Y]^4}{\kappa_R^4 + [Y]^4}\right) - k_6[P][J][Y] \\
[\dot{G}] &= k_6[P][J][Y] \\
[\dot{D}] &= k_6[P][Y]^2
\end{aligned}
\tag{3.1}
$$

with initial conditions

$$
(Y(0), T(0), Z(0), W(0), V(0), W^*(0), J(0), G(0), D(0)) = (Y_0, T_0, 0, 0, 0, 0, 0, 0, 0) \tag{3.2}
$$

and where the available polymerase concentration is measured

$$
[P] = \frac{P_0}{1 + \frac{[Z]+[V]}{\kappa_{P_1}} + \frac{\kappa_A([Y][J]+[Y]^2)}{\kappa_{P_2}}}. \tag{3.3}
$$

Recall that the system admits a conservation law,

$$
[T] + [Z] + [W] + [V] + [W^*] = T_0. \tag{3.4}
$$

This system, as presented in Chapter 2, uses capitalized Latin letters to indicate

time dependent concentration functions, indexed values k_i to indicate fixed rates, indexed values κ_i to indicate fixed dissociation/association constants, and Newton's dot notation indicates a derivative with respect to time. Concentration functions are nonnegative while rates and dissociation/association constants are strictly positive. For simplicity, we omit the concentration brackets in future references. We use the capital letters to represent both concentration and a molecule of the same type.

We first consider the equilibrium analysis of the partial models from Chapter 2,

(1.) no deactivation or recycling of amplifiers (§2.2.1),

(2.) deactivation but no recycling of amplifiers (§2.2.2),

(3.) and the model with constant polymerase concentration (§2.2.3),

to determine how the different mechanisms affect the behavior of the system. Finally, we analyze the full model, *Model 4*. We refer to these models throughout the document using the western arabic numerals (1, 2, 3,...) as associated above. The parameter ranges in Table 2.1 generally lead to reaction systems that would continue amplifying DNA indefinitely if not for the experimental constraints. However, numerical simulation shows that only the full model produces results consistent with the biphasic behavior observed during the one hour experimental run time. We further verify that, using the values from Table 2.1, the outcomes from the partial models either don't reproduce UDAR's characteristic high amplification gain or don't decelerate amplification as rapidly as observed in UDAR trials.

While the equilibrium analysis is focused on determining if our proposed mechanisms are essential for UDAR's biphasic amplification, in the second part of the analysis we direct our focus to the temporal behavior of the system. Because the parameters of this model can range from $\mathcal{O}(10^{-5})$ to $\mathcal{O}(10^{3})$, we apply

perturbation theory to identify the reactions that drive UDAR's five temporally distinct amplification phases,

(I.) Initiation *(slow)*

(II.) Primary amplification *(fast)*

(III.) Plateau *(slow)*

(IV.) Secondary amplification *(fast)*

(V.) Slow final growth *(slow)*.

These were described in detail in §2.2. Figure 3.1 shows these phases can differ in length and duration based on template design, but seem to be an innate feature of UDAR templates.

We find that some reaction mechanisms operate on a time scale as slow as $\mathcal{O}\left(10^{-10}\right)$ during the initiation phase. We interpret the long initiation phase as a stable equilibrium of the faster reactions that becomes unstable when the slower reactions start impacting the system. This change in stability causes the primary amplification phase which equilibrates and creates the plateau phase. However, this equilibrium also becomes destabilized by the slowest reactions: recycling, dimerization of surplus trigger, and the subsequent sequestration of available polymerase, which initiate when free trigger reaches specific critical concentrations.

There exist conditions under which UDAR templates attain the characteristic high gain but the plateau phase is not observed [26]. We'll show that the plateau phase is an equilibrium value that becomes unstable when the concentration of trigger passes a certain critical value. If this critical value is passed quickly during primary amplification, the subsequent amplification will be caused by simultaneous activity of core and secondary amplification loops, rather than the more typical sequential

activity. Thus while not all UDAR templates exhibit biphasic behavior, most do and our analysis indicates that the plateau is indeed an innate feature of UDAR templates.

3.1 Partial Model Equilibrium Analysis

In this section, we analyze the long term behavior of a series of partial models to substantiate the results presented via simulation in Chapter 2. For each model, we use stability theory to examine the asymptotic properties of solutions and trajectories. We consider equilibrium points for each system and the linearization of the systems near those equilibrium points [48], [49].

Model 1 (§2.2.1) excludes the reactions that model deactivation and recycling. Numerical simulations show this model predicts appropriate total growth for the expected total DNA growth in the one hour experimental run time, but lacks the mechanisms for the intricate dynamic behavior of the plateau and two distinct amplification periods. Next we include the deactivation of amplifiers *(Model 2)* (§2.2.2) and observe that deactivation causes the amplification reaction to stop. Since the limiting equilibrium is highly degenerate, simulations show that the amplification reaction decelerates to imperceptible levels in the experimental run time. Before considering the full system, we analyze a version where polymerase doesn't become burdened by the many reactions requiring it *(Model 3)* (§2.2.3). This model examines whether polymerase sequestration is indeed the mechanism causing the deceleration of final growth. The long term behavior of this system parallels the behavior of the full model, but numerical simulations show the characteristic slow final growth phase doesn't occur in the experimental run time.

Finally we show that, with both trigger mediated recycling of deactivated amplifiers and sequestration of polymerase, the full model reproduces the characteristic high amplification gain. Furthermore, we numerically observe the biphasic growth

and slow final growth phase after the secondary amplification phase, meaning the full model reproduces all UDAR's observed characteristics. We explore the biphasic growth mechanisms further in §3.2.

3.1.1 General considerations

In any partial model of the system (3.1), functions $T(t)$, $Z(t)$, $V(t)$, $W(t)$, $W^*(t)$ are bounded because they obey the conservation law (3.4). The functions $Y(t)$, $J(t)$, $D(t)$, $G(t)$ are not a priori bounded. We prove that the functions $Y(t)$ and $J(t)$ are bounded in all of our models in Theorems 4.3, 4.7, and 4.8, but the functions measuring the concentration of inert byproduct, $G(t)$ and $D(t)$, may still diverge to infinity. However $G(t)$ and $D(t)$ are decoupled from the system and don't affect the dynamics of the other functions. Therefore in the following analysis, we always assume the functions $T(t)$, $Z(t)$, $V(t)$, $W(t)$, $W^*(t)$, $Y(t)$, and, when appropriate, $J(t)$ converge to an equilibrium value. In each partial model, we'll discuss if $D(t)$ and $G(t)$ converge or diverge. Typically we find a family of partial equilibria parameterized by a nonzero value of Y_∞. This will imply that $D(t)$ and, when it's part of the model, $G(t)$ will diverge to infinity.

When the limit at infinity of a function $\Omega(t)$ of any model is known or assumed to exist, we use the notation

$$\Omega_\infty := \lim_{t\to\infty} \Omega(t).$$

Instead of using (3.3) to determine the amount of polymerase available, we use a simplified form

$$P(t) := \frac{P_0}{1 + \frac{Z(t)+V(t)+\kappa_2([Y(t)]^2+J(t)Y(t))}{\kappa_1}} \tag{3.5}$$

where

$$\kappa_1 = \kappa_{P_1}, \qquad \kappa_2 = \frac{\kappa_{P_1}\kappa_A}{\kappa_{P_2}}.$$

The MATLAB code used to simulate models and generate figures is found in Appendix B. All the proofs of the theorems are relegated to §4.1.

3.1.2 Model 1: *No deactivation or recycling of amplifiers*

Our first model assumes that complete amplifiers W and W^* are never deactivated. If recycling were to occur, it would simply send a template back to a core amplification loop described in §2.1, so for simplicity we also assume there's no recycling. We represent this in the system by setting

$$k_4 = k_5 = 0 \ \frac{1}{s}$$

which creates the system

$$\begin{aligned}
\dot{Y} &= -2k_+TY^2 + 2k_-Z + k_1ZP + k_2W - 2k_6Y^2P \\
\dot{T} &= -k_+TY^2 + k_-Z \\
\dot{Z} &= k_+TY^2 - k_-Z - k_1ZP \\
\dot{W} &= k_1ZP - k_2W + k_3VP \\
\dot{V} &= k_2W - k_3VP \\
\dot{D} &= k_6Y^2P
\end{aligned} \tag{3.6}$$

with initial conditions

$$(Y(0), T(0), Z(0), W(0), V(0), D(0)) = (Y_0, T_0, 0, 0, 0, 0), \tag{3.7}$$

reduced conservation law

$$T + Z + W + V = T_0, \tag{3.8}$$

and where

$$P = \frac{P_0}{1 + \frac{Z+V+\kappa_2 Y^2}{\kappa_1}}. \tag{3.9}$$

The omitted reactions of the full model and the initial conditions (3.2) imply immediately that

$$W^*(t) \equiv 0, \qquad J(t) \equiv 0, \qquad G(t) \equiv 0$$

We have the following result.

Theorem 1. *Consider system (3.6) with initial conditions (3.7). Assume that*

$$\dot{T}_\infty,\ \dot{Z}_\infty,\ \dot{W}_\infty,\ \dot{V}_\infty,\ \dot{Y}_\infty \text{ exist and are finite.}$$

Then either

(A.)

$$\lim_{t\to\infty}(Y, T, Z, W, V, D) = (0, T_0, 0, 0, 0, D_\infty)$$

where

$$D_\infty := \lim_{t\to\infty} k_6 \int_0^t \frac{\kappa_1 P_0 [Y(\tau)]^2}{\kappa_1 + Z(\tau) + V(\tau) + \kappa_2 [Y(\tau)]^2} d\tau$$

(B.) or

$$\lim_{t\to\infty}(Y, T, Z, W, V) = (Y_\infty, 0, 0, W_\infty, V_\infty^+)$$

where V_∞^+ is the positive root of

$$k_2(2k_6 + \kappa_2 k_3)V_\infty^2 + \left(2\kappa_1 k_6(k_2 + k_3 P_0) - k_2 T_0(2k_6 + \kappa_2 k_3)\right) V_\infty - 2\kappa_1 k_2 k_6 T_0 = 0$$

and its value determines the remaining limits,

$$
\begin{aligned}
Y_\infty &= \sqrt{\frac{k_3 V_\infty^+}{2k_6}}, \\
P_\infty &= \frac{2\kappa_1 k_6 P_0}{2\kappa_1 k_6 + (2k_6 + \kappa_2 k_3) V_\infty^+}, \\
W_\infty &= \frac{2\kappa_1 k_3 k_6 P_0 V_\infty^+}{k_2 \left(2\kappa_1 k_6 + (2k_6 + \kappa_2 k_3) V_\infty^+\right)}.
\end{aligned}
$$

Finally, D diverges to infinity.

Note that expression for D_∞ in (A.) allows it to be infinite as well.

The solutions presented in Theorem 1 may not be equilibria in case $(A.)$ and never are in $(B.)$ because $\lim_{t\to\infty} D$ may diverge to infinity in $(A.)$ and definitely must in $(B.)$. We call these solutions **partial equilibria**, where some of the components converge to a finite value, while others (here, D) may diverge. To examine actual equilibria, we note that the last equation in (3.6) satisfies $\dot{D} \geq 0$ for all t and the function D does not enter into the other equations. In addition, the conservation law (3.8) allows us to remove the $\dot{T}$ from the system. Then we can consider a reduced set of equations,

$$
\begin{aligned}
\dot{Y} &= -2k_+ \left(T_0 - Z - W - V\right) Y^2 + 2k_- Z + k_1 Z P + k_2 W - 2k_6 Y^2 P \\
\dot{Z} &= k_+ \left(T_0 - Z - W - V\right) Y^2 - k_- Z - k_1 Z P \\
\dot{W} &= k_1 Z P - k_2 W + k_3 V P \\
\dot{V} &= k_2 W - k_3 V P.
\end{aligned}
\tag{3.10}
$$

The equilibria of this system are in one-to-one correspondence with the partial equilibria of the system (3.6). We analyze their stability next.

Corollary 1.1. *Consider the reduced system (3.10). For any partial equilibrium of Theorem 1(A.), the corresponding equilibrium of (3.10)*

$$(Y_\infty, Z_\infty, W_\infty, V_\infty) = (0, 0, 0, 0)$$

has Jacobian Matrix

$$\mathcal{J}(0, 0, W_\infty, 0) = \begin{bmatrix} 0 & 2k_- + k_1 P_0 & k_2 & 0 \\ 0 & -k_- - k_1 P_0 & 0 & 0 \\ 0 & k_1 P_0 & -k_2 & k_3 P_0 \\ 0 & 0 & k_2 & -k_3 P_0 \end{bmatrix}.$$

This Jacobian has eigenvalues

$$\chi_1 = 0, \quad \chi_2 = -k_- - k_1 P_0, \quad \chi_3 = -k_2 - k_3 P_0$$

where χ_1 has multiplicity 2 with eigenvector

$$\vec{v} = (1,\ 0,\ 0,\ 0)$$

and generalized eigenvector

$$\vec{g} = \left(0,\ 0,\ \frac{1}{k_2},\ \frac{1}{k_3 P_0}\right).$$

Since a generic solution in the zero eigenspace grows linearly with time t, any equilibrium where $Y_\infty = 0$ is unstable. Because solutions of the reduced system represent solutions of the system (3.6) when paired with the equation $\dot{D} = k_6 Y^2 P$, any partial equilibrium of system (3.6) where $Y_\infty = 0$ is unstable.

The proof of Theorem 1 is in §4.1.2. The computations for Corollary 1.1 are in Appendix A.1. By the corollary, we conclude that any solution described in Theorem 1(A.) represents an unstable partial equilibrium. To illustrate this numerically, we present a simulation result (Figure 3.2) using most of the values from Table 2.1 except that key factors for initiation are altered to unreasonable levels. In Figure 3.2, the multistep binding rate k_+ has been lowered 100 fold, the inverse binding rate k_- has been doubled, and the rate at which double bound templates extend to amplifiers k_1 is one sixteenth of its value in the values (Table 2.1). In agreement with the analysis in Corollary 1.1 that the equilibrium of Theorem 1(A.), the simulation eventually initiates (after approximately 8 hours).

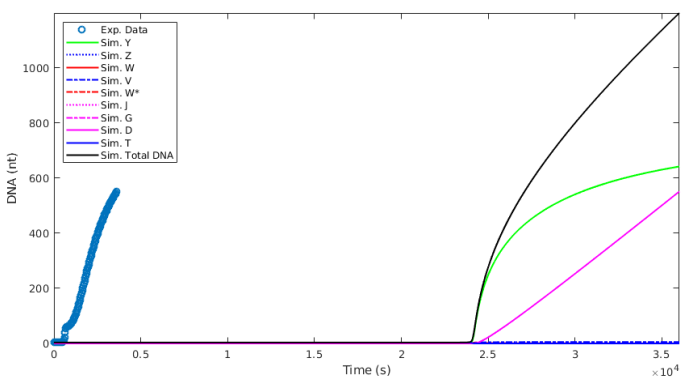

Parameter	Value
T_0	$0.1\ \mu M$
Y_0	$10^{-5}\ \mu M$
P_0	$0.005\ \mu M$
κ_R	$14\ \mu M$
κ_{P_1}	0.015
κ_{P_2}	0.225
κ_A	$0.0075\ \frac{1}{\mu M}$
k_+	$20\ \frac{1}{s\ \mu M^2}$
k_-	$100\ \frac{1}{s}$
k_1	$25\ \frac{1}{s\ \mu M}$
k_2	$0.625\ \frac{1}{s\ \mu M}$
k_3	$800\ \frac{1}{s\ \mu M}$
k_4	$0\ \frac{1}{s}$
k_5	$0\ \frac{1}{s}$
k_6	$0.01\ \frac{1}{s\ \mu M^2}$

Figure 3.2: Model 1 with modified parameters showing eventual initiation

We now analyze the partial equilibrium of Theorem 1(B.).

Corollary 1.2. *Consider the reduced system (3.10) for the values from Table 2.1. The Jacobian matrix for the reduced system evaluated at the partial equilibrium of*

Theorem 1(B.) has eigenvalues

$$\chi_1 \approx -7.63705 \times 10^6, \quad \chi_2 \approx -0.654707,$$
$$\chi_3 \approx -0.0148535, \quad \chi_4 \approx -9.17863 \times 10^{-5}.$$

Thus this equilibrium is asymptotically stable for the values from Table 2.1.

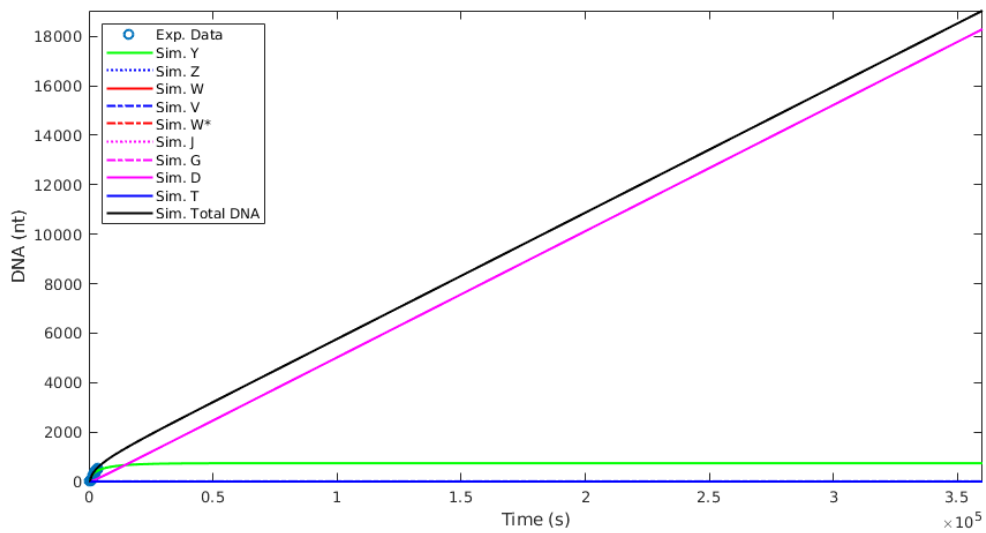

Figure 3.3: Model 1 with simulation parameters and extended run time

The computations for Corollary 1.2 are in Appendix A.1. This result implies there's continued amplification past the end of the experimental run time, which is consistent with experimental observations. The simulation results with values from Table 2.1 is shown in Figure 3.4. We can compute the concentration function limit values for this parameter set (Appendix A.1),

$$V_\infty^+ \approx 0.0954625\ \mu M, \quad Y_\infty \approx 61.794\ \mu M,$$
$$P_\infty \approx 3.7134 \times 10^{-5}\ \mu M, \quad W_\infty \approx 0.00453748\ \mu M.$$

Therefore the model predicts that the concentration of Y will converge to approximately 60 μM which is insufficient to sequester enough polymerase to slow the reaction. We see this is true in Figure 3.3 where the formation of the inactive dimers D continues for at least 100 hours, indicating that polymerase availability on the order of 10^{-5} μM is sufficient for extending dimers. Furthermore, Figure 3.4 shows that with values from Table 2.1 in appropriate physical ranges, Model I cannot reproduce the plateau phase that should be generated for this parameter set. While this simulation may mimic the experimental trials where the plateau is missing, the model gives no indication it's capable of reproducing the much more common solutions that exhibit plateaus. The equilibrium analysis is not entirely conclusive, but numerical simulation supports the conclusion that *solutions of system (3.6) do not match the experimental data.*

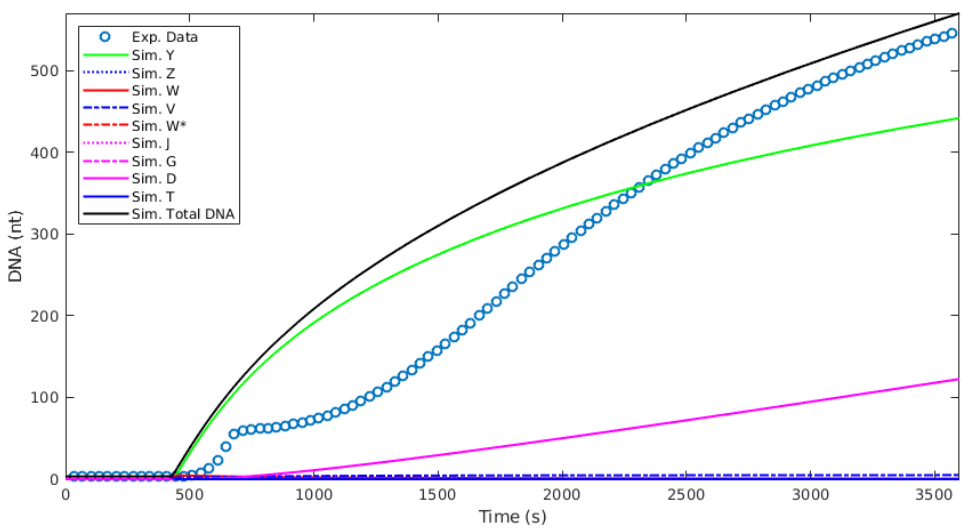

Figure 3.4: Model 1 with values from Table 2.1 and experimental run time

3.1.3 Model 2: *Deactivation but no recycling of amplifiers*

Our second model assumes complete amplifiers W gradually deactivate. We also assume that once a trigger has bound to a template, it will never disassociate to let the template be recycled. We represent this in the system by setting

$$k_5 = 0 \ \frac{1}{s}$$

which creates the system

$$\begin{aligned}
\dot{Y} &= -2k_+TY^2 + 2k_-Z + k_1ZP + k_2W - 2k_6Y^2P \\
\dot{T} &= -k_+TY^2 + k_-Z \\
\dot{Z} &= k_+TY^2 - k_-Z - k_1ZP \\
\dot{W} &= k_1ZP - k_2W + k_3VP - k_4W \\
\dot{V} &= k_2W - k_3VP \\
\dot{W}^* &= k_4W \\
\dot{D} &= k_6Y^2P
\end{aligned} \tag{3.11}$$

with initial conditions

$$(Y(0), T(0), Z(0), W(0), V(0), W^*(0), D(0)) = (Y_0, T_0, 0, 0, 0, 0, 0), \tag{3.12}$$

conservation law (3.4), and where P is computed by (3.9). The omitted equations and initial conditions (3.2) imply immediately that

$$J(t) \equiv 0, \qquad G(t) \equiv 0$$

We have the following result.

Theorem 2. *Consider system (3.11) with initial conditions (3.12). Assume that*

$$\dot{T}_\infty,\ \dot{Z}_\infty,\ \dot{W}_\infty,\ \dot{V}_\infty,\ \dot{W}^*_\infty,\ \dot{Y}_\infty \text{ exist and are finite.}$$

Then

(A.) Y is bounded

(B.) and

$$\lim_{t\to\infty}(Y,T,Z,W,V,W^*,D) = (0,T_\infty,0,0,0,W^*_\infty,D_\infty)$$

where

$$\begin{aligned}
T_\infty &:= \lim_{t\to\infty} \frac{\int_0^t e^{\int_0^\tau k_+[Y(s)]^2 ds} k_- Z(\tau)d\tau + T_0}{e^{\int_0^t k_+[Y(\tau)]^2 d\tau}} \\
W^*_\infty &:= \lim_{t\to\infty} \int_0^t \frac{k_4 \int_0^\tau e^{(k_2+k_4)s}[k_1 Z(s) + k_3 V(s)]P(s)ds}{e^{(k_2+k_4)\tau}} d\tau \\
D_\infty &:= \lim_{t\to\infty} k_6 \int_0^t \frac{\kappa_1 P_0 [Y(\tau)]^2}{\kappa_1 + Z(\tau) + V(\tau) + \kappa_2[Y(\tau)]^2} d\tau
\end{aligned}$$

and $T_\infty + W^*_\infty = T_0$. Note that D_∞ may be infinite.

The limiting values in Theorem 2 may not be equilibria as D_∞ may not be finite. We therefore analyze a reduced system where we omit the last equation because D does not enter the right hand side of the other equations. In addition, we use

conservation law (3.4) remove the $\dot{T}$ equation and obtain the reduced system

$$
\begin{aligned}
\dot{Y} &= -2k_+(T_0 - Z - V - W - W^*)Y^2 + 2k_-Z + k_1ZP + k_2W - 2k_6Y^2P \\
\dot{Z} &= k_+\left(T_0 - Z - V - W - W^*\right)Y^2 - k_-Z - k_1ZP \\
\dot{W} &= k_1ZP - k_2W + k_3VP - k_4W \\
\dot{V} &= k_2W - k_3VP \\
\dot{W}^* &= k_4W
\end{aligned}
\tag{3.13}
$$

Corollary 2.1. *Consider the reduced system (3.13). For any partial equilibrium of Theorem 2, the corresponding equilibrium of (3.13),*

$$(Y_\infty, Z_\infty, W_\infty, V_\infty, W^*_\infty) = (0, 0, 0, 0, W^*_\infty),$$

has Jacobian Matrix

$$
\mathcal{J}(0,0,0,0,W^*_\infty) = \begin{bmatrix}
0 & 2k_- + k_1P_0 & k_2 & 0 & 0 \\
0 & -k_- - k_1P_0 & 0 & 0 & 0 \\
0 & k_1P_0 & -k_2 - k_4 & k_3P_0 & 0 \\
0 & 0 & k_2 & -k_3P_0 & 0 \\
0 & 0 & k_4 & 0 & 0
\end{bmatrix}.
$$

This Jacobian has eigenvalues

$$
\begin{aligned}
\chi_1 = 0, \quad \chi_2 &= -k_- - k_1P_0, \\
\chi_{3,4} &= -\frac{1}{2}\left(k_2 + k_4 + k_3P_0 \pm \sqrt{(k_2 + k + 4 + k_3P_0)^2 - 4k_3k_4P_0}\right)
\end{aligned}
$$

where χ_1 has multiplicity 2 with linearly independent eigenvectors

$$\vec{v}_1 = (1,\ 0,\ 0,\ 0,\ 0), \quad \vec{v}_2 = (0,\ 0,\ 0,\ 0,\ 1).$$

The proof of Theorem 2 is in §4.1.3. The computations for Corollary 2.1 are in Appendix A.2. By Corollary 2.1, the equilibrium is degenerate. Since Theorem 2*(A.)* ensures Y is bounded and all other functions are bounded due to the conservation law (3.4), all solutions of the reduced system are bounded. Since system (3.11) only allows the partial equilibrium from Theorem 2*(B.)*, which is the equilibrium of (3.13), the solutions must converge to this equilibrium. Clearly, another possibility would be for solutions to converge to a bounded nontrivial attractor, like a periodic orbit or chaotic attractor. While we cannot exclude this possibility, we have not seen any hint of nontrivial dynamics in any numerical simulations, which are generally similar to Figure 3.5. We conclude that the degenerate equilibrium attracts all solutions but, due to its degeneracy, convergence is extremely slow. In Figure 3.6, we see that D can still slowly grow well after the experimental run time of one hour. This is due to the extremely slow convergence of Y. Furthermore, because we don't know how slowly Y converges, it remains possible for D to diverge.

Using the values from Table 2.1 and the experimental run time, Figure 3.5 shows that primary amplification occurs but the reaction terminates with the total DNA reaching only the level of the the first plateau. As a consequence, our numerical simulation shows that *solutions of system (3.11) do not match the experimental data*. As discussed in §2.2.2, this behavior is similar to the DNA amplification levels observed in EXPAR trials.

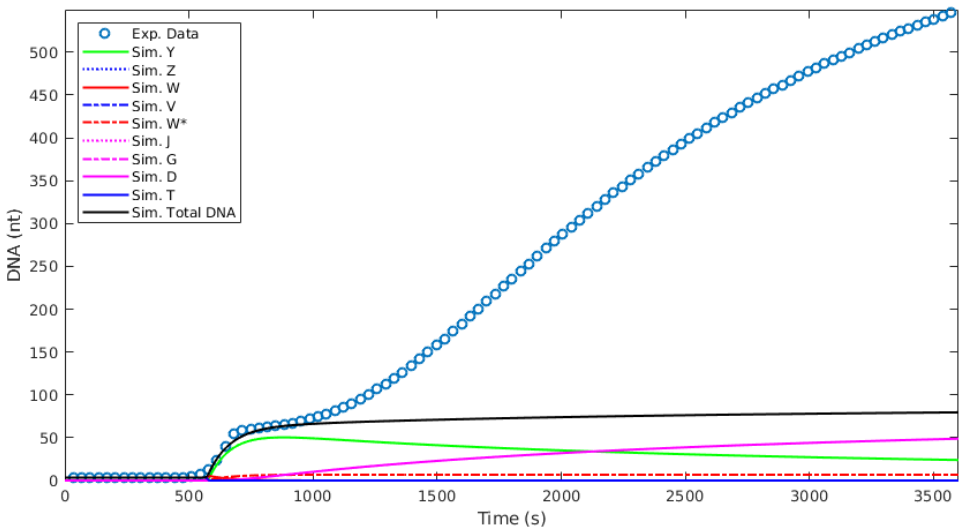

Figure 3.5: Model 2 with values from Table 2.1 and experimental run time

3.1.4 Model 3: *Polymerase is not limiting*

We now consider a system similar to the full system except that the equation that tracks available polymerase, (3.5), is replaced by the constant value P_0. The

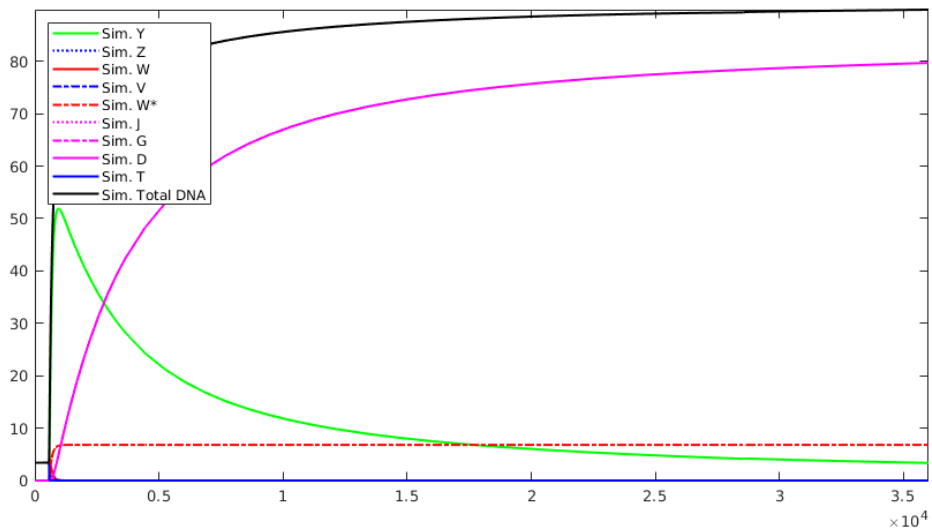

Figure 3.6: Model 2 (detail) with values from Table 2.1 and extended run time

modified system is

$$
\begin{aligned}
\dot{Y} &= -2k_+TY^2 + 2k_-Z + k_1P_0Z + k_2W - k_6P_0Y(2Y + J) \\
\dot{T} &= -k_+TY^2 + k_-Z + k_5f(Y)(W + W^*) \\
\dot{Z} &= k_+TY^2 - k_-Z - k_1P_0Z \\
\dot{W} &= k_1P_0Z - k_2W + k_3P_0V - k_4W - k_5f(Y)W \\
\dot{V} &= k_2W - k_3P_0V \\
\dot{W}^* &= k_4W - k_5f(Y)W^* \\
\dot{J} &= k_5f(Y)(W + W^*) - k_6P_0JY \\
\dot{G} &= k_6P_0JY \\
\dot{D} &= k_6P_0Y^2
\end{aligned}
\tag{3.14}
$$

with initial conditions (3.2), conservation law (3.4) and where

$$f(Y) := \frac{Y^4}{\kappa_R^4 + Y^4}.$$

We have the following result.

Theorem 3. *Consider system (3.14) with initial conditions (3.2). Assume that*

$$\dot{T}_\infty,\ \dot{Z}_\infty,\ \dot{W}_\infty,\ \dot{V}_\infty,\ \dot{W}^*_\infty,\ \dot{Y}_\infty,\ \dot{J}_\infty \text{ exist and are finite.}$$

Then either

(A.)

$$\lim_{t\to\infty}(Y, T, Z, W, V, W^*, J, G, D) = (0, T_\infty, 0, 0, 0, W^*_\infty, J_\infty, G_\infty, D_\infty)$$

where

$$\begin{aligned}
T_\infty &= \lim_{t\to\infty} \frac{\int_0^t e^{\int_0^s k_+[Y(\tau)]^2 d\tau}(k_- Z(s) + k_5 h(Y(s))[W(s) + W^*(s)])ds + T_0}{e^{\int_0^t k_+[Y(\tau)]^2 d\tau}} \\
W^*_\infty &= \lim_{t\to\infty} \frac{\int_0^t e^{\int_0^s k_5 h(Y(\tau))d\tau} k_4 W(s) ds}{e^{\int_0^t k_5 h(Y(\tau))d\tau}} \\
J_\infty &= \lim_{t\to\infty} \frac{\int_0^t e^{\int_0^s k_6 P_0 Y(\tau)d\tau} k_5 h(Y(s))[W(s) + W^*(s)]ds}{e^{\int_0^t k_6 P_0 Y(\tau)d\tau}} \\
G_\infty &= \lim_{t\to\infty} k_6 P_0 \int_0^t J(t)Y(t)dt \\
D_\infty &= \lim_{t\to\infty} k_6 P_0 \int_0^t [Y(W + W^*)]^2 dt
\end{aligned}$$

and $T_\infty + W^*_\infty = T_0$,

(B.) or there's a fourth order polynomial $\mathcal{P}(Y^2)$ *such that* Y_∞ *can correspond to positive, real roots of* $\mathcal{P}(Y^2) = 0$. *Furthermore, when real values for* Y_∞ *exist, there are rational functions* $\mathcal{T}(Y)$, $\mathcal{Z}(Y)$, $\mathcal{W}(Y)$, $\mathcal{V}(Y)$, $\mathcal{W}^*(Y)$, *and* $\mathcal{J}(Y)$ *such*

that

$$T_\infty = \mathcal{T}(Y_\infty),\ Z_\infty = \mathcal{Z}(Y_\infty),\ W_\infty = \mathcal{W}(Y_\infty),$$

$$V_\infty = \mathcal{V}(Y_\infty),\ W^*_\infty = \mathcal{W}^*(Y_\infty),\ J_\infty = \mathcal{J}(Y_\infty),$$

and D, G will diverge to infinity.

Note that expressions for D_∞, G_∞ in (A.) allow them to be infinite.

To probe the stability of the solutions in Theorem 3, we analyze a reduced system where we omit the last two equations and use conservation law (3.4) to remove the $\dot{T}$ equation. We thereby obtain the reduced system

$$\begin{aligned}
\dot{Y} &= -2k_+\left(T_0 - Z - W - V - W^*\right)Y^2 + 2k_-Z + k_1P_0Z + k_2W - k_6P_0Y(2Y + J)\\
\dot{Z} &= k_+\left(T_0 - Z - W - V - W^*\right)Y^2 - k_-Z - k_1P_0Z\\
\dot{W} &= k_1P_0Z - k_2W + k_3P_0V - k_4W - k_5Wf(Y)\\
\dot{V} &= k_2W - k_3P_0V\\
\dot{W}^* &= k_4W - k_5W^*f(Y)\\
\dot{J} &= k_5(W + W^*)f(Y) - k_6P_0JY.
\end{aligned} \tag{3.15}$$

Corollary 3.1. *Consider the reduced system (3.15). For any partial equilibrium of Theorem 3(A.), the corresponding equilibrium of (3.15),*

$$(Y_\infty, Z_\infty, W_\infty, V_\infty, W^*_\infty, J_\infty) = (0, 0, 0, 0, W^*_\infty, J_\infty),$$

has Jacobian matrix

$$\mathcal{J}(0,0,0,0,W_\infty^*,J_\infty) = \begin{bmatrix} -k_6 J_\infty P_0 & 2k_- + k_1 P_0 & k_2 & 0 & 0 & 0 \\ 0 & -k_- - k_1 P_0 & 0 & 0 & 0 & 0 \\ 0 & k_1 P_0 & -k_2 - k_4 & k_3 P_0 & 0 & 0 \\ 0 & 0 & k_2 & -k_3 P_0 & 0 & 0 \\ 0 & 0 & k_4 & 0 & 0 & 0 \\ -k_6 J_\infty P_0 & 0 & 0 & 0 & 0 & 0 \end{bmatrix}$$

This Jacobian has eigenvalues

$$\chi_1 = 0, \quad \chi_2 = -k_- - k_1 P_0, \quad \chi_3 = -k_6 J_\infty P_0,$$
$$\chi_{4,5} = -\frac{1}{2}\left(k_2 + k_4 + k_3 P_0 \pm \sqrt{(k_2+k_3+k_4)^2 - 4k_3 k_4 P_0}\right)$$

where χ_1 has multiplicity 2 with linearly independent eigenvectors

$$\vec{v}_1 = (0,\ 0,\ 0,\ 0,\ 0,\ 1,), \quad \vec{v}_2 = (0,\ 0,\ 0,\ 0,\ 1,\ 0).$$

The proof of Theorem 3 is in §4.1.4. The computations for Corollary 3.1 are in Appendix A.3. The characteristics of zero eigenvalue in Corollary 3.1 are consistent with the possibility that an equilibrium with Y_∞ as described in Theorem 3(A.) is nonlinearly stable. However, simulations using the values in Table 2.1, displayed in Figure 3.7, are consistent with Theorem 3(B.). Because the growth rate of D and G depend on Y, if Y_∞ approached zero, we would see deceleration in the growth rates of G and D. Figure 3.8 shows this is not the case.

We now analyze the equilibria of the reduced system (3.15) that correspond to partial equilibria of system (3.14) determined in Theorem 3*(B.)*.

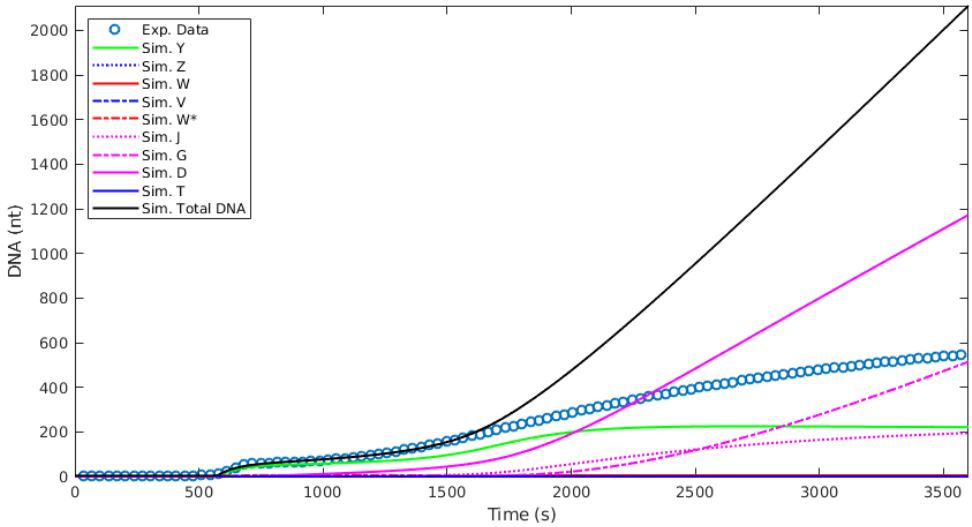

Figure 3.7: Model 3 with values from Table 2.1 and experimental run time

Corollary 3.2. *Consider the reduced system (3.15) for the values from Table 2.1. The solutions of Theorem 3(B.) yield two nonzero values,*

$$Y_{\infty_1} \approx 2.85082\ \mu M \ \textit{and}\ Y_{\infty_2} \approx 21.4478\ \mu M.$$

These values give rise to two equilibria of the reduced system (3.15), $\mathcal{E}_1$ *and* $\mathcal{E}_2$ *respectively, see Table 3.1. The Jacobian Matrix for the reduced system (3.15) at* $\mathcal{E}_1$ *has eigenvalues*

$$\chi_1 \approx -36,299.3, \quad \chi_2 \approx -4.6268, \quad \chi_3 \approx -1.99463,$$
$$\chi_4 \approx -0.0124928, \quad \chi_5 \approx 4.72093 \times 10^{-4}, \quad \chi_6 \approx -1.38747 \times 10^{-4}.$$

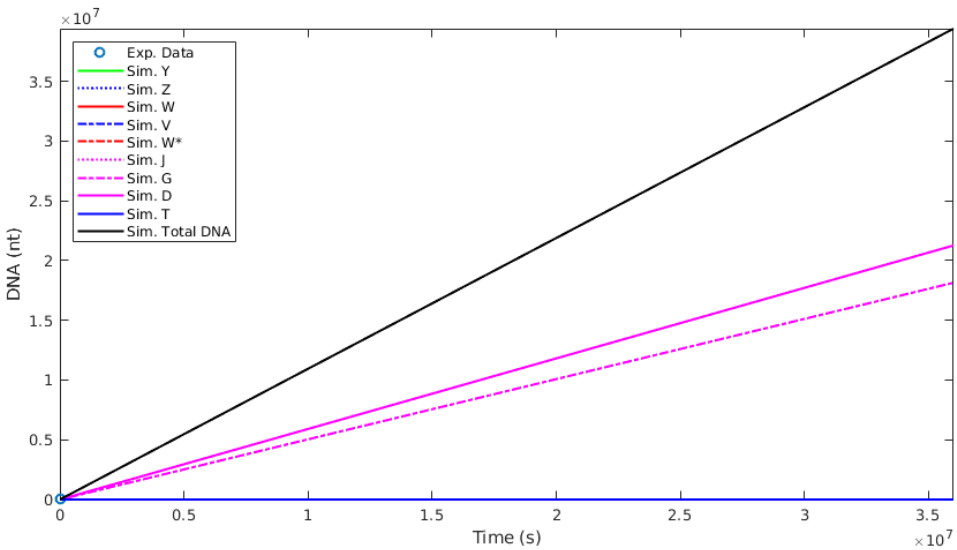

Figure 3.8: Detail of Model 3 with values from Table 2.1 and extended run time

and the Jacobian of the reduced system (3.15) at $\mathcal{E}_2$ has eigenvalues

$$\chi_1 \approx -920,062, \quad \chi_2 \approx -4.64748, \quad \chi_3 \approx -2.06395,$$
$$\chi_4 \approx -0.0960804, \quad \chi_5 \approx -4.74393 \times 10^{-3}, \quad \chi_6 \approx -1.03166 \times 10^{-3}.$$

Therefore $\mathcal{E}_1$ is a saddle point with one-dimensional unstable manifold and $\mathcal{E}_2$ is asymptotically stable.

The computations for Corollaries 3.1 and 3.2 are in Appendix A.3. We now numerically investigate how the behavior of Model 3 reflects the existence of partial equilibria $\mathcal{E}_1$ and $\mathcal{E}_2$. We first note that Figure 3.8 shows that the functions G, D, and consequently, the overall production of DNA, grow indefinitely through any reasonable run time. Therefore, based on our numerical simulations, *solutions of system (3.14) do not match experimental data.* However, we are interested in behavior of the other functions, in particular Y.

	$Y_{\infty_1} \approx 2.85082$	$Y_{\infty_2} \approx 21.4478$
T_∞	$2.47627 \times 10^{-8}\ \mu M$	$1.83554 \times 10^{-7}\ \mu M$
Z_∞	$8.56384 \times 10^{-6}\ \mu M$	$3.59304 \times 10^{-3}\ \mu M$
W_∞	$1.30035 \times 10^{-3}\ \mu M$	$7.36014 \times 10^{-2}\ \mu M$
V_∞	$2.03179 \times 10^{-4}\ \mu M$	$1.15002 \times 10^{-2}\ \mu M$
W^*_∞	$9.84879 \times 10^{-2}\ \mu M$	$1.13052 \times 10^{-2}\ \mu M$
J_∞	$0.12016\ \mu M$	$6.70099\ \mu M$

Table 3.1: Limit approximations for concentration functions of Model 3 at each viable solution for Y_∞ for values from Table 2.1

Figure 3.9 shows convergence to the stable equilibrium $\mathcal{E}_2$ with value $Y_\infty \approx 21.4478\ \mu M$ (green trace). The solution also shows the primary amplification rate decreases slightly when Y is close to the value at the saddle point $\mathcal{E}_1$, $Y_\infty \approx 2.85082\ \mu M$. Note that this time interval, from 500 s to $1,000$ s corresponds to when almost all template is in deactivated amplifier form W^* (dashed red trace), see Figure 3.10. Therefore a plausible interpretation suggests that the characteristic UDAR plateau is due to the solution trajectory passing near a saddle point of the reduced system (3.15) that has relatively strong negative eigenvalues and a small $\mathcal{O}\left(10^{-5}\right)$ unstable eigenvalue.

3.1.5 Model 4: *Full Model*

We now consider the full system (3.1) with initial conditions (3.2) and obtain the following result.

Theorem 4. *Consider system (3.1) with initial conditions (3.2). Assume that*

$$\dot{T}_\infty,\ \dot{Z}_\infty,\ \dot{W}_\infty,\ \dot{V}_\infty,\ \dot{W}^*_\infty,\ \dot{Y}_\infty,\ \dot{J}_\infty \text{ exist and are finite.}$$

Then either

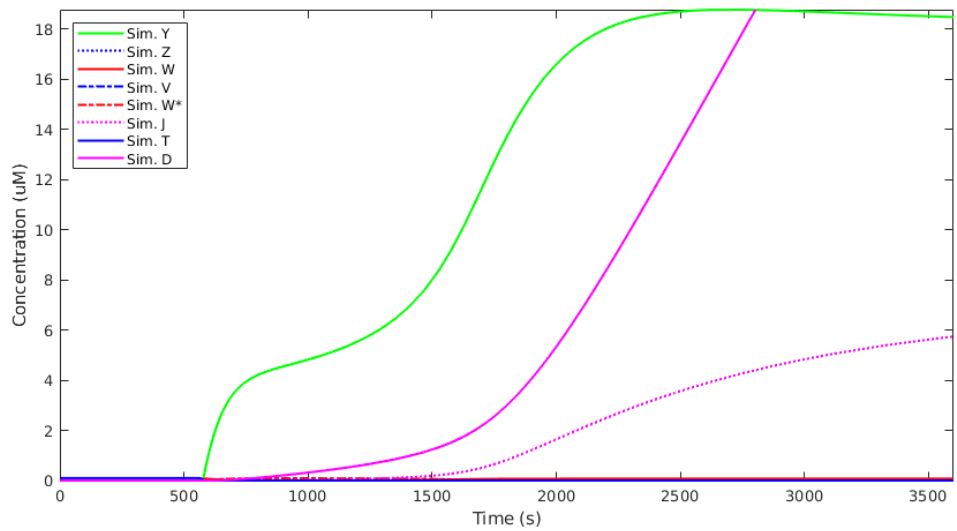

Figure 3.9: Detail of Model 3 concentration simulations with values from Table 2.1 and experimental run time

(A.)

$$\lim_{t\to\infty}(Y,T,Z,W,V,W^*,J,G,D) = (0,T_\infty,0,0,0,W^*_\infty,0,G_\infty,D_\infty)$$

where

$$T_\infty = \lim_{t\to\infty}\frac{\int_0^t e^{\int_0^s k_+[Y(\tau)]^2 d\tau}(k_- Z(s) + k_5 h(Y(s))[W(s)+W^*(s)])ds + T_0}{e^{\int_0^t k_+[Y(\tau)]^2 d\tau}}$$

$$W^*_\infty = \lim_{t\to\infty}\frac{\int_0^t e^{\int_0^s k_5 h(Y(\tau))d\tau} k_4 W(s)ds}{e^{\int_0^t k_5 h(Y(\tau))d\tau}}$$

$$G_\infty = \lim_{t\to\infty} k_6 \int_0^t \frac{\kappa_1 P_0 J(\tau)Y(\tau)}{\kappa_1 + Z(\tau) + V(\tau) + \kappa_2\left(J(\tau)Y(\tau) + [Y(\tau)]^2\right)}d\tau$$

$$D_\infty = \lim_{t\to\infty} k_6 \int_0^t \frac{\kappa_1 P_0 [Y(\tau)]^2}{\kappa_1 + Z(\tau) + V(\tau) + \kappa_2\left(J(\tau)Y(\tau) + [Y(\tau)]^2\right)}d\tau$$

and $T_\infty + W^*_\infty = T_0$,

(B.) or there's a seventh order polynomial $\mathcal{P}\left(Y^2\right)$ *such that* Y_∞ *can correspond to positive, real roots of* $\mathcal{P}\left(Y^2\right) = 0$. *Furthermore, when real values for* Y_∞ *exist,*

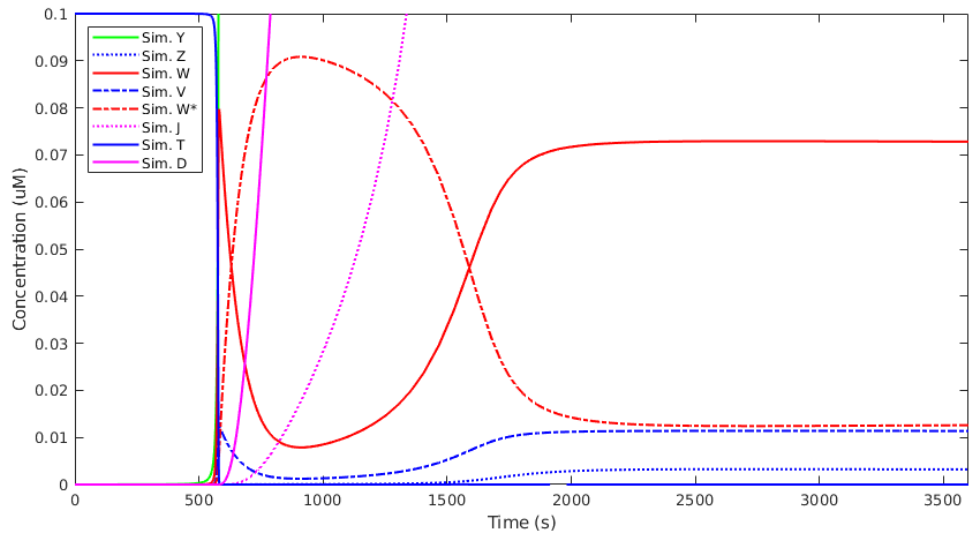

Figure 3.10: Detail of Model 3 functions constrained by conservation law (3.4) (inset of Figure 3.9)

there are rational functions $\mathcal{T}(Y)$, $\mathcal{Z}(Y)$, $\mathcal{W}(Y)$, $\mathcal{V}(Y)$, $\mathcal{W}^*(Y)$, *and* $\mathcal{J}(Y)$ *such that*

$$T_\infty = \mathcal{T}(Y_\infty),\ Z_\infty = \mathcal{Z}(Y_\infty),\ W_\infty = \mathcal{W}(Y_\infty),$$

$$V_\infty = \mathcal{V}(Y_\infty),\ W^*_\infty = \mathcal{W}^*(Y_\infty),\ J_\infty = \mathcal{J}(Y_\infty)$$

and D, G *will diverge to infinity.*

Note that expressions for D_∞, G_∞ *in (A.) allow them to be infinite.*

To analyze stability of the solutions in Theorem 4 we again introduce a reduced system where we omit the last two equations and use the conservation law (3.4) to

remove the $\dot{T}$ equation. This reduced system is

$$
\begin{aligned}
\dot{Y} &= -2k_+\left(T_0 - Z - W - V - W^*\right)Y^2 + 2k_-Z + k_1ZP + k_2W - k_6YP(2Y + J) \\
\dot{Z} &= k_+\left(T_0 - Z - W - V - W^*\right)Y^2 - k_-Z - k_1ZP \\
\dot{W} &= k_1ZP - k_2W + k_3VP - k_4W - k_5Wf(Y) \\
\dot{V} &= k_2W - k_3VP \\
\dot{W}^* &= k_4W - k_5W^*f(Y) \\
\dot{J} &= k_5(W + W^*)f(Y) - k_6PJY
\end{aligned}
\tag{3.16}
$$

Corollary 4.1. *Consider the reduced system (3.16). For any partial equilibrium of Theorem 4(A.), the corresponding equilibrium of (3.16),*

$$(Y_\infty, Z_\infty, W_\infty, V_\infty, W^*_\infty, J_\infty) = (0, 0, 0, 0, W^*_\infty, 0),$$

has Jacobian matrix

$$\mathcal{J}(0,0,0,0,W^*_\infty,0) = \begin{bmatrix} 0 & 2k_- + k_1P_\infty & k_2 & 0 & 0 & 0 \\ 0 & -k_- - k_1P_\infty & 0 & 0 & 0 & 0 \\ 0 & k_1P_\infty & -k_2 - k_4 & k_3P_\infty & 0 & 0 \\ 0 & 0 & k_2 & -k_3P_\infty & 0 & 0 \\ 0 & 0 & k_4 & 0 & 0 & 0 \\ 0 & 0 & 0 & 0 & 0 & 0 \end{bmatrix}.$$

This Jacobian has eigenvalues

$$
\begin{aligned}
\chi_1 = 0, \quad \chi_2 &= -k_- - k_1P_\infty, \\
\chi_{3,4} &= -\frac{1}{2}\left(k_2 + k_4 + k_3P_\infty \pm \sqrt{(k_2 + k_3 + k_4)^2 - 4k_3k_4P_\infty}\right)
\end{aligned}
$$

where χ_1 has multiplicity 3 with linearly independent eigenvectors

$$\vec{v}_1 = (0,\ 0,\ 0,\ 0,\ 0,\ 1), \quad \vec{v}_2 = (0,\ 0,\ 0,\ 0,\ 1,\ 0), \quad \vec{v}_3 = (1,\ 0,\ 0,\ 0,\ 0,\ 0)$$

The proof of Theorem 4 is in §4.1.5. The computations for Corollary 4.1 are in Appendix A.4. The results of Theorem 4 strongly parallel the results of Theorem 3. A key difference, however, is that in Theorem 4, the vector $\vec{e}_Y$ in the direction of the Y axis is in the zero eigenspace just as in Theorems 1 and 2. Therefore, we suspect the Theorem 4(A.) equilibrium will again be nonlinearly unstable in the full model. This is supported numerically using the same parameter modifications as in Figure 3.2 ($k_+ = 20$, $k_- = 100\frac{1}{s}$, $k_1 = 25\ \frac{1}{s\ \mu M}$) while keeping the remaining parameters at the values from Table 2.1, see Figure 3.11. The fact that the reaction eventually initiates from small initial data is consistent with this equilibrium being unstable.

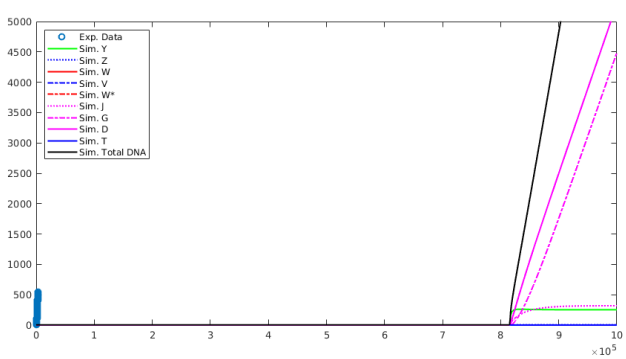

Parameter	Value
T_0	$0.1\ \mu M$
Y_0	$10^{-5}\ \mu M$
P_0	$0.005\ \mu M$
κ_R	$14\ \mu M$
κ_{P_1}	0.015
κ_{P_2}	0.225
κ_A	$0.0075\ \frac{1}{\mu M}$
k_+	$20\ \frac{1}{s\ \mu M^2}$
k_-	$100\ \frac{1}{s}$
k_1	$25\ \frac{1}{s\ \mu M}$
k_2	$0.625\ \frac{1}{s\ \mu M}$
k_3	$800\ \frac{1}{s\ \mu M}$
k_4	$0.013\ \frac{1}{s}$
k_5	$0.1\ \frac{1}{s}$
k_6	$0.01\ \frac{1}{s\ \mu M^2}$

Figure 3.11: Full Model with modified parameters showing eventual initiation

Numerical simulations using values from Table 2.1 show that solutions behave as described in Theorem 4(B.). This includes the unbounded DNA amplification as

shown in Figure 3.12. Because the experimental run time for UDAR trials lasts only an hour, these solutions model the reaction accurately over that time span. Based on Figure 3.12, we conclude that *there are appropriate solutions for system (3.1) that match experimental data.*

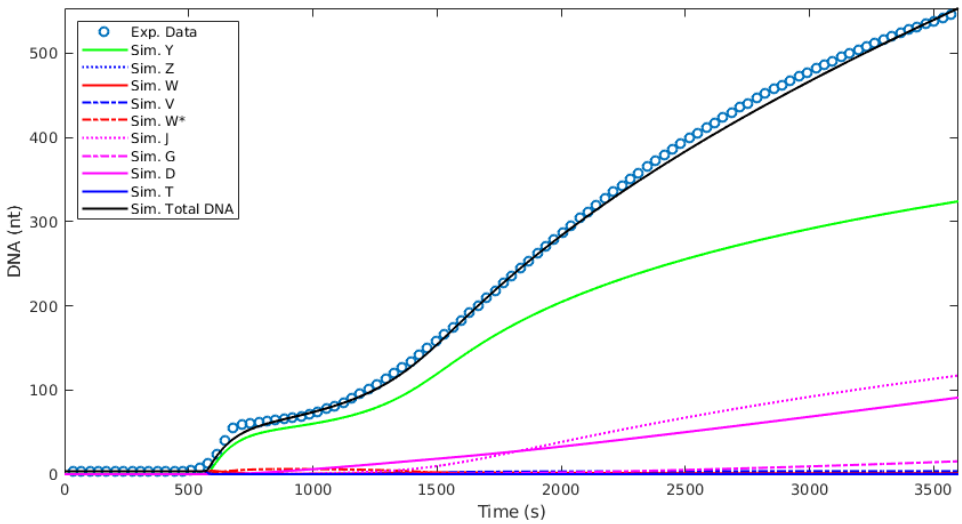

Figure 3.12: Simulation of Full Model with values from Table 2.1 and experimental run time

Finally, we address the equilibria of the reduced system (3.16) that correspond to partial equilibria of the system (3.1) determined in Theorem 4.

Corollary 4.2. *Consider the reduced system (3.16) for the values from Table 2.1. The solutions of Theorem 3(B.) are determined by two nonzero values,*

$$Y_{\infty_1} \approx 2.60126\ \mu M \ \textit{and}\ Y_{\infty_2} \approx 42.3847\ \mu M.$$

These values give rise to two equilibria of the reduced system (3.16), $\mathcal{E}_3$ *and* $\mathcal{E}_4$ *respectively, see Table 3.2. The Jacobian matrix for the reduced system (3.16) at*

$\mathcal{E}_3$ has eigenvalues

$$\chi_1 \approx -13,578.1, \quad \chi_2 \approx -3.83306, \quad \chi_3 \approx -1.59773,$$
$$\chi_4 \approx -0.011828, \quad \chi_5 \approx 3.87824 \times 10^{-4}, \quad \chi_6 \approx -1.01557 \times 10^{-4}$$

and the Jacobian Matrix of the reduced system (3.16) at $\mathcal{E}_4$ has eigenvalues

$$\chi_1 \approx -3.59297 \times 10^{6}, \quad \chi_2 \approx -0.773298, \quad \chi_3 \approx -0.099122,$$
$$\chi_4 \approx -0.0229107, \quad \chi_5 \approx -1.00093 \times 10^{-4}, \quad \chi_6 \approx -1.80379 \times 10^{-5}.$$

Therefore $\mathcal{E}_3$ is a saddle point with one-dimensional unstable manifold and $\mathcal{E}_4$ is asymptotically stable.

	$Y_{\infty_1} \approx 2.60126$	$Y_{\infty_2} \approx 42.3847$
T_∞	$2.55271 \times 10^{-8}\ \mu M$	$3.13583 \times 10^{-7}\ \mu M$
Z_∞	$7.41284 \times 10^{-6}\ \mu M$	$2.50263 \times 10^{-2}\ \mu M$
W_∞	$9.05737 \times 10^{-4}\ \mu M$	$4.45015 \times 10^{-3}\ \mu M$
V_∞	$1.76576 \times 10^{-4}\ \mu M$	$6.99379 \times 10^{-2}\ \mu M$
W^*_∞	$9.89102 \times 10^{-2}\ \mu M$	$5.85406 \times 10^{-4}\ \mu M$
J_∞	$0.113989\ \mu M$	$23.6182\ \mu M$
P_∞	$4.00737 \times 10^{-3}\ \mu M$	$4.9711 \times 10^{-5}\ \mu M$

Table 3.2: Limit approximations for concentration functions of Full Model at each viable solution for Y_∞ for values from Table 2.1

The computations for Corollary 4.2 are in Appendix A.4. We illustrate this analysis by numerical simulation, which parallels the analysis of Model 3. We again observe that the functions D and G diverge to infinity. Figure 3.13 shows the stable partial equilibrium $\mathcal{E}_4$, now at $Y_{\infty_2} \approx 42.3847\ \mu M$, and a slow down after Y reaches the neighborhood of a saddle equilibrium $\mathcal{E}_3$, $Y_{\infty_1} \approx 2.60126\ \mu M$. The functions constrained by conservation law (3.4), Figure 3.14, exhibit similar behavior as in

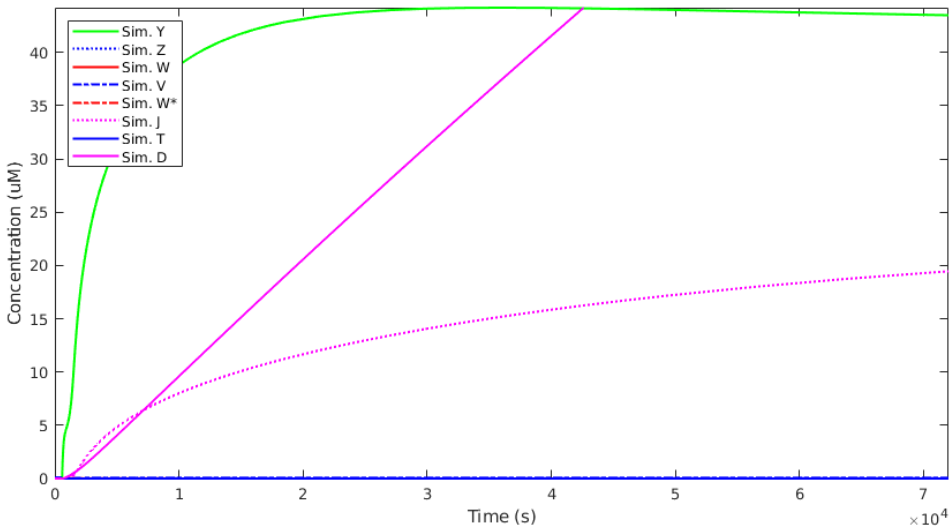

Figure 3.13: Detail of Full Model concentration simulations with values from Table 2.1 and extended run time

Model 3: during the plateau phase, most of the template T is trapped in the form of deactivated template W^*. Recycling of this template coincides with the start of the second amplification period. Thus we can again believe that the plateau phase is caused by a solution trajectory passing near a saddle point of the reduced system (3.16) that has strong negative eigenvalues and a small unstable eigenvalue.

The main conclusions of the equilibrium analysis are:

1. There's a degenerate partial equilibrium when $Y_\infty = 0$ that has an associated high dimensional zero eigenspace. This equilibrium is responsible for a slow start of the amplification for UDAR templates.

2. For the values in Table 2.1, we see two equilibria: one saddle with a low value for Y_{∞_1} and one asymptotically stable equilibrium with high value of Y_{∞_2}.

3. The saddle has a single unstable eigenvalue with small magnitude of $\mathcal{O}\left(10^{-5}\right)$. This may be responsible for a temporary attraction to this saddle before convergence

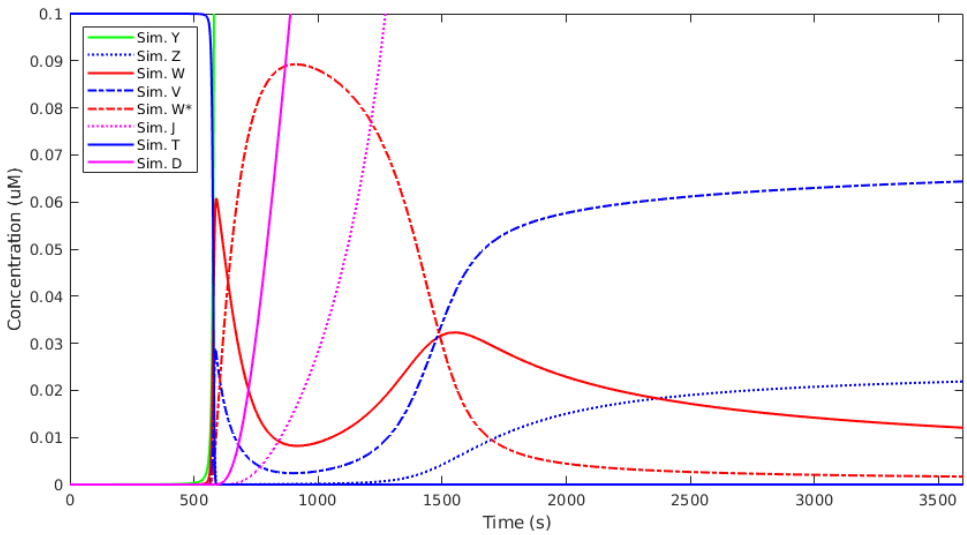

Figure 3.14: Detail of Full Model functions constrained by the conservation law *(bottom)*, values from Table 2.1 and experimental run time

to the stable equilibrium.

4. The temporary attraction to the saddle point may cause the plateau observed in experimental data.

3.2 Multiple Time Scale Analysis

Having shown that the full model is capable of reproducing the experimental results, we now want to understand the mechanisms causing the biphasic behavior. In this section, our emphasis is on understanding the behavior of UDAR templates at experimental parameter ranges (listed in 2.1), rather than on general analysis. The unusual alternating between fast and slow growth indicates the system operates on multiple time scales, so we approach the system as a regular perturbation problem and attempt to isolate the five key phases of the UDAR reaction,

(I.) Initiation *(slow)*

(II.) Primary Amplification *(fast)*

(III.) Plateau *(slow)*

(IV.) Secondary amplification *(fast)*

(V.) Slow final amplification *(slow)*

Because the $\dot{G}$ and $\dot{D}$ equations from the full system (3.1) only track inactive reaction byproducts and are decoupled from the rest of the system, we omit them in this section. Furthermore, we indicate unscaled time by $\mathfrak{t}$ and use Newton's dot derivative notation to indicate derivatives with respect to unscaled time. Based on conservation law (3.4), we employ the scaling,

$$Y = yT_0, \qquad T = tT_0, \qquad Z = zT_0, \qquad W = wT_0,$$

$$V = vT_0, \qquad W^* = uT_0, \qquad J = jT_0,$$

and the arbitrary time scale $\tau = \hat{\tau}\mathfrak{t}$ where Lagrange's prime notation denotes a derivative with respect to scaled time, τ. We also define

$$\varepsilon := \frac{Y_0}{T_0} = 10^{-4}$$

to capture the difference between the initial concentrations Y_0 and T_0. Substituting these terms into (3.1), we get

$$
\begin{aligned}
\hat{\tau} y' &= -2k_+ T_0^2 t y^2 + 2k_- z + k_1 P z + k_2 w - k_6 P T_0 y(2y + j) \\
\hat{\tau} t' &= -k_+ T_0^2 t y^2 + k_- z + k_5 (w + u) f(y) \\
\hat{\tau} z' &= k_+ T_0^2 t y^2 - k_- z - k_1 P z \\
\hat{\tau} w' &= k_1 P z - k_2 w + k_3 P v - k_4 w - k_5 w f(y) \\
\hat{\tau} v' &= k_2 w - k_3 P v \\
\hat{\tau} u' &= k_4 w - k_5 u f(y) \\
\hat{\tau} j' &= k_5 (w + u) f(y) - k_6 P T_0 y j
\end{aligned}
$$

where

$$
f(y) := \frac{y^4}{\left(\frac{\kappa_R}{T_0}\right)^4 + y^4}.
$$

Letting $\hat{\tau} := k_+ T_0^2$, the system becomes

$$
\begin{aligned}
y' &= -2ty^2 + 2\alpha z + \beta z + \gamma w - \zeta y(2y + j) \\
t' &= -ty^2 + \alpha z + (w + u) f(y) \\
z' &= ty^2 - \alpha z - \beta z \\
w' &= \beta z - \gamma w + \delta v - \lambda w - w f(y) \\
v' &= \gamma w - \delta v \\
u' &= \lambda w - u f(y) \\
j' &= (w + u) f(y) - \zeta y j
\end{aligned}
\tag{3.17}
$$

where

$$f(y) = \frac{\eta y^4}{\theta^4 + y^4}.$$

and

$$\alpha := \frac{k_-}{k_+ T_0^2}, \quad \beta(P) := \frac{k_1 P}{k_+ T_0^2}, \quad \gamma := \frac{k_2}{k_+ T_0^2}, \quad \delta(P) := \frac{k_3 P}{k_+ T_0^2},$$
$$\lambda := \frac{k_4}{k_+ T_0^2}, \quad \eta := \frac{k_5}{k_+ T_0^2}, \quad \zeta(P) := \frac{k_6 P}{k_+ T_0}, \quad \theta := \frac{\kappa_R}{T_0}.$$

Note that the scaled coefficients $\beta,\ \delta,\ \zeta$ are actually functions of available polymerase and must be considered accordingly.

3.2.1 Polymerase approximation

The key difference between this analysis and the long term behavior analysis of §3.1 is that systems analyzed here differ by the magnitude of the coefficients representing the biokinetic rate constants. Some coefficients depend on the availability of polymerase, which we'll assume is relatively constant over certain phases of amplification. As we'll show, available polymerase is approximately P_0 in the initiation and primary amplification phases of the reaction, but drops by one order of magnitude during secondary amplification. Recall from our analysis in §3.1.2 that even when P dropped by one order of magnitude, there was still sufficient polymerase to allow indefinite dimerization, see Figure 3.3.

First, based on the ranges outlined in Table 2.1,

$$\kappa_{P_1} \sim \mathcal{O}\left(10^{-2}\right), \quad \kappa_{P_2} \sim \mathcal{O}\left(10^{-1}\right), \quad \kappa_A \sim \mathcal{O}\left(10^{-3}\right).$$

During the first period of slow growth, lasting from two to ten minutes for various template designs (Figure 3.1), $Y \ll T_0$ and $J \approx 0$. Furthermore, simulations verify

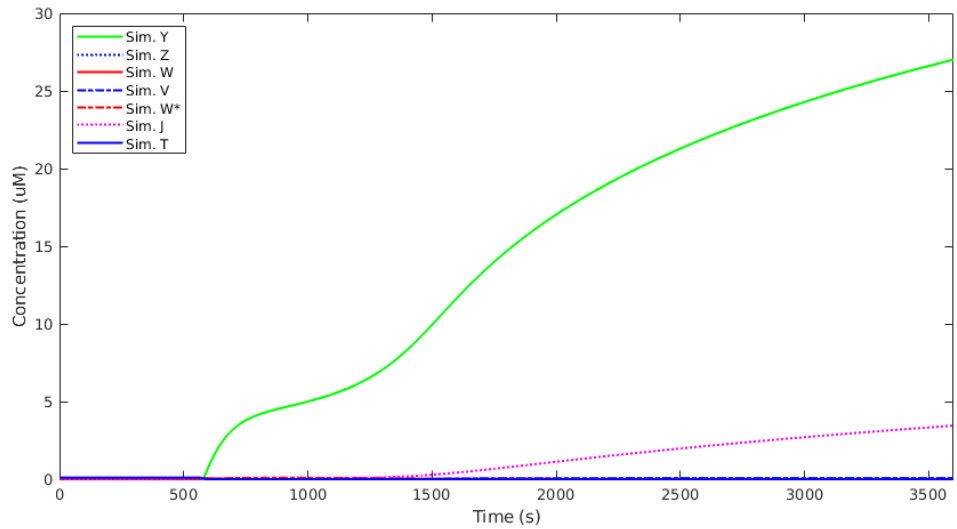

Figure 3.15: Concentration time series using unscaled values from Table 2.1 showing the key UDAR features in the concentration of Y

that $Z + V < Y_0$ until significant amplification can begin. With these facts, we use equation (3.3) to provide an initial lower bound for the concentration of available polymerase,

$$P \geq \frac{P_0}{1 + \frac{Y_0}{\kappa_{P_1}} + \frac{\kappa_A T_0^2}{\kappa_{P_2}}}.$$

Because

$$\frac{Y_0}{\kappa_{P_1}} \sim \mathcal{O}\left(10^{-3}\right) \text{ and } \frac{\kappa_A T_0^2}{\kappa_{P_2}} \sim \mathcal{O}\left(10^{-4}\right),$$

the approximation $P \approx P_0$ is accurate during the initiation phase and we can treat β, δ, and ζ as constant through the initiation phase.

To better estimate when β, δ, and ζ should be adjusted, we consider the size of the denominator terms in the expression for free polymerase P,

$$\frac{Z + V}{\kappa_{P_1}} \quad \text{and} \quad \frac{\kappa_A Y(Y + J)}{\kappa_{P_2}}.$$

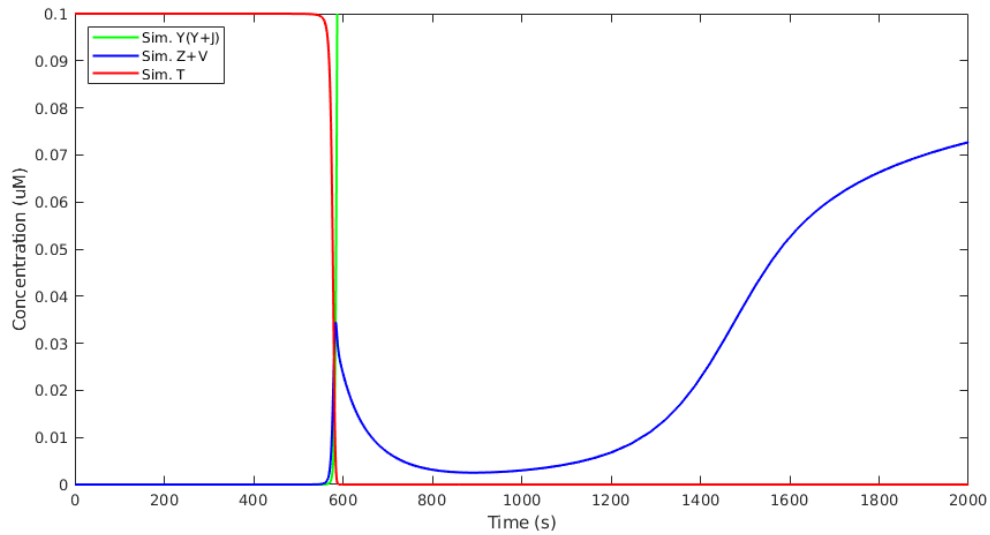

Figure 3.16: Concentration time series of $Z + V$ using unscaled values from Table 2.1. Primary amplification occurs around 500 s and secondary amplification occurs between 1,000 s and 1,500 s.

We first present a general analysis, then specify our results for the plausible ranges in Table 2.1. The concentration of $Z + V$ can decrease the concentration of available polymerase by an order of magnitude when $\frac{Z+V}{\kappa_{P_1}} \approx 10$, creating a condition

$$Z + V \approx 10\kappa_{P_1}.$$

On the other hand the presence of Y and J lowers the amount of available polymerase by one order of magnitude when $\frac{\kappa_A Y(Y+J)}{\kappa_{P_2}} \approx 10$, creating a second condition,

$$Y(Y + J) \approx 10\frac{\kappa_{P_2}}{\kappa_A}. \tag{3.18}$$

For the plausible ranges in Table 2.1, we have

$$10\kappa_{P_1} = 0.15, \quad 10\frac{\kappa_{P_2}}{\kappa_A} = 300.$$

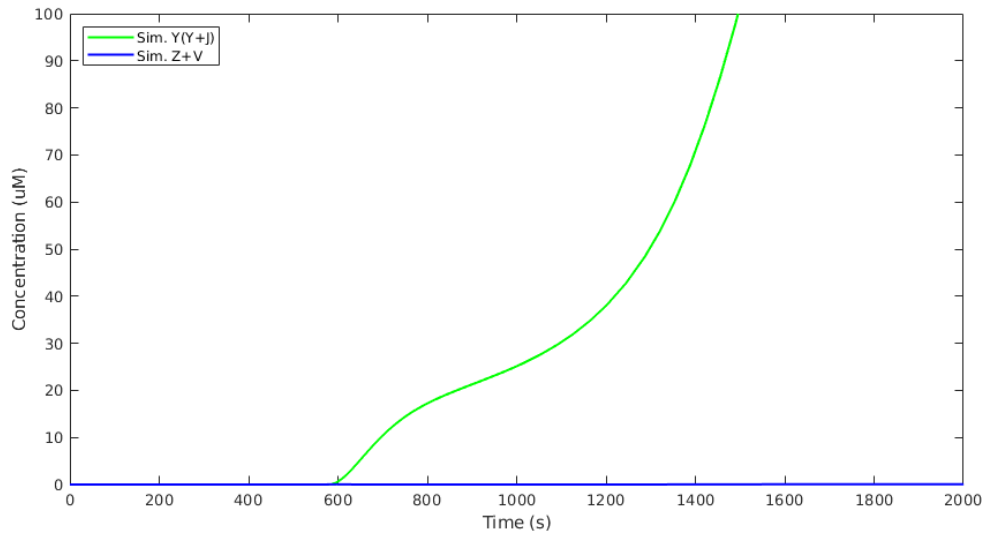

Figure 3.17: Concentration time series of $Y(Y+J)$ during the amplification phases using unscaled values from Table 2.1

Figure 3.16 shows that during the primary amplification phase, the sum $Z+V$ only raises to $Z+V \approx 0.035$. Figure 3.17 shows that $Y(Y+J) \approx 20$ during the primary amplification phase. Since both

$$Z+V << 0.15 \text{ and } Y(Y+J) << 300,$$

P_0 is not significantly depleted during the first amplification phase or during the plateau phase. Thus we will analyze systems where $Y < 1$ or, in the scaled values, $y < 10$, and assume $P \approx P_0$. When $y > 10$ and free polymerase drops by at least an order of magnitude and we will reevaluate the rates of the reactions.

3.2.2 Analysis for $y < 10$

In this stage, we assume

(a.) $P \approx P_0$,

(b.) $j \approx 0$,

(c.) $\zeta y(2y + j) \approx 0$,

(d.) and $f(y) \approx 0$.

We investigate system (3.17) by studying two partial systems. First, we consider just $\mathcal{O}(1)$ reactions. Then we look at reactions $\mathcal{O}\left(10^{-4}\right)$ and faster under the assumption that $y < 10$. Under these assumptions, the scaled parameters are approximately

$$\begin{gathered}\theta \sim \mathcal{O}\left(10^{2}\right), \quad \alpha \sim \mathcal{O}(1), \quad \beta, \delta \sim \mathcal{O}\left(10^{-1}\right), \quad \gamma \sim \mathcal{O}\left(10^{-2}\right), \\ \eta \sim \mathcal{O}\left(10^{-3}\right), \quad \lambda \sim \mathcal{O}\left(10^{-4}\right), \quad \zeta \sim \mathcal{O}\left(10^{-7}\right)\end{gathered} \tag{3.19}$$

based on the plausible ranges in Table 2.1. Assumption $(d.)$ holds because $f(y)$ is at most $\mathcal{O}(10^{-8})$ when $y \leq 10$.

3.2.2.1 Model I: $\mathcal{O}(1)$ *system* The dominant reaction is the process of binding two triggers to a template,

$$\begin{aligned} y' &= -2ty^2 + 2\alpha z \\ t' &= -ty^2 + \alpha z \\ z' &= ty^2 - \alpha z \\ w' &= 0 \\ v' &= 0 \\ u' &= 0 \\ j' &= 0 \end{aligned} \tag{3.20}$$

This system admits two conservation laws

$$2z + y = \varepsilon \tag{3.21}$$

$$z + t = 1 \tag{3.22}$$

and has initial conditions

$$(y_0, t_0, z_0, w_0, v_0, u_0, j_0) = (\varepsilon, 1, 0, 0, 0, 0, 0). \tag{3.23}$$

We have the following result.

Theorem 5. *Consider system (3.20) with initial conditions (3.23). Assume*

$$P \approx P_0, \quad j \approx 0, \quad \zeta y(2y + j) \approx 0, \quad f(y) \approx 0.$$

Then the system has one stable equilibrium,

$$(y_*, t_*, z_*, w_*, v_*, u_*, j_*) = (\varepsilon - 2z_*, 1 - z_*, z_*, 0, 0, 0, 0) \tag{3.24}$$

where $t_* \sim \mathcal{O}(1)$ *and* $y_*, z_* \sim \mathcal{O}\left(10^{-4}\right)$ *or smaller.*

The proof of Theorem 5 is in §4.2.1.

3.2.2.2 Model II: $\mathcal{O}\left(10^{-4}\right)$ *system,* $y < 10$ We now consider all reactions $\mathcal{O}\left(10^{-4}\right)$ and faster when $y < 10$. Because the $\mathcal{O}(1)$ system is converging toward the equilibrium from Theorem 5 for $t \in [0, \tau_1]$, before the $\mathcal{O}\left(10^{-1}\right) - \mathcal{O}\left(10^{-4}\right)$ reactions impact the system, we consider (3.24) from Theorem 5 as an approximate initial condition for Model II. This means $y(\tau_1) \approx \varepsilon - 2z_*$ and our assumptions for $y < 10$

still apply. The system is

$$
\begin{aligned}
y' &= -2ty^2 + (2\alpha + \beta)z + \gamma w \\
t' &= -ty^2 + \alpha z \\
z' &= ty^2 - (\alpha + \beta)z \\
w' &= \beta z + \delta v - (\gamma + \lambda)w \\
v' &= -\delta v + \gamma w \\
u' &= \lambda w \\
j' &= 0
\end{aligned}
\tag{3.25}
$$

with initial conditions near (3.24) at a time τ_1,

$$(y_{\tau_1}, t_{\tau_1}, z_{\tau_1}, w_{\tau_1}, v_{\tau_1}, u_{\tau_1}, j_{\tau_1}) = (\varepsilon - 2z_*, 1 - z_*, z_*, 0, 0, 0, 0)$$

and has conservation law

$$t + z + w + v + u = 1. \tag{3.26}$$

We have the following result.

Theorem 6. *Consider the system (3.25) with initial conditions near (3.24). Assume that*

$$\lim_{\tau\to\infty} y' = \lim_{\tau\to\infty} z' = \lim_{\tau\to\infty} w' = \lim_{\tau\to\infty} v' = \lim_{\tau\to\infty} u' = 0$$

and that the assumptions

$$y < 1, \quad P \approx P_0, \quad j \approx 0, \quad \zeta y(2y + j) \approx 0, \quad f(y) \approx 0$$

hold. Then there are two one-dimensional manifolds of equilibria,

$$E_1(u_*) = (y_*, t_*, z_*, w_*, v_*, u_*, j_*) = (0, 1 - u_*, 0, 0, 0, u_*, 0), \qquad u_* \in [0, 1] \tag{3.27}$$

$$E_2(y_*) = (y_*, t_*, z_*, w_*, v_*, u_*, j_*) = (y_*, 0, 0, 0, 0, 1, 0), \qquad y_* \in [0, \infty) \tag{3.28}$$

where the limit on u_* follows from conservation law (3.26).

The proof of Theorem 6 is in §4.2.2. To analyze the stability of the equilibria in Theorem 6, we introduce a reduced system where we omit the last equation and use conservation law (3.26) to remove the t' equation. This reduced system is

$$\begin{aligned}
y' &= -2(1 - z - w - v - u)y^2 + (2\alpha + \beta)z + \gamma w \\
z' &= (1 - z - w - v - u)y^2 - (\alpha + \beta)z \\
w' &= \beta z + \delta v - (\gamma + \lambda)w \\
v' &= -\delta v + \gamma w \\
u' &= \lambda w
\end{aligned} \tag{3.29}$$

The manifold of equilibria $E_1(u_*)$ corresponds to a manifold of equilibria in the reduced system (3.29),

$$\xi_1(u_*) = (y_*, z_*, w_*, v_*, u_*) = (0, 0, 0, 0, u_*),$$

and the manifold of equilibria $E_2(y_*)$ corresponds to a second manifold of equilibria in the reduced system (3.29),

$$\xi_2(y_*) = (y_*, z_*, w_*, v_*, u_*) = (y_*, 0, 0, 0, 1).$$

Corollary 6.1. *Consider the reduced system (3.29). The Jacobian matrix at any value in $x \in \xi_1$ is*

$$\mathcal{J}(x) = \begin{bmatrix} 0 & 2\alpha+\beta & \gamma & 0 & 0 \\ 0 & -\alpha-\beta & 0 & 0 & 0 \\ 0 & \beta & -\gamma-\lambda & \delta & 0 \\ 0 & 0 & \gamma & -\delta & 0 \\ 0 & 0 & \lambda & 0 & 0 \end{bmatrix}$$

and has eigenvalues

$$\chi_1 = 0, \quad \chi_2 = -\alpha-\beta, \quad \chi_{3,4} = -\frac{1}{2}\left(\gamma+\delta+\lambda \pm \sqrt{(\gamma+\delta+\lambda)^2 - 4\delta\lambda}\right).$$

The zero eigenspace spans $\{\vec{e}_y, \vec{e}_u\}$ along the y and u axes respectively. To investigate solutions that don't leave (or enter) a neighborhood of an equilibrium at an exponential rate determined by eigenvalues with positive (or negative) real parts, we study an approximation of the dynamics on a non-unique, two-dimensional center manifold W^c using center manifold reduction [49]. For any value in $x \in \xi_1$, the second order approximation of $W^c(x)$ is

$$z = \left(\frac{1}{\alpha+\beta}\right) y^2, \qquad w = \left(\frac{\beta}{\lambda(\alpha+\beta)}\right) y^2, \qquad v = \left(\frac{\beta\gamma}{\delta\lambda(\alpha+\beta)}\right) y^2$$

and the induced flow is

$$\begin{aligned} y' &= y^2\left[2(u_* - u) + \left(\frac{2(\delta\lambda+\beta\delta+\beta\gamma)}{\delta\lambda(\alpha+\beta)}\right) y^2 + \frac{\beta(\gamma-\lambda)}{\lambda(\alpha+\beta)}\right] \\ u' &= \left(\frac{\beta}{\alpha+\beta}\right) y^2. \end{aligned} \tag{3.30}$$

Computations for Corollary 6.1 are in §4.2.3. The flow (3.30) has a one-

dimensional manifold of equilibria, $\{(y, u) \mid y = 0\}$, corresponding to equilibria sets E_1 of the original system (3.25) and ξ_1 of the reduced system (3.29). Outside of this set, we know from our scaled approximations (3.19) that $\gamma > \lambda$ and so

$$y' > 0 \quad \text{and} \quad u' > 0.$$

and the reduced system is nonlinearly unstable near ξ_1. Extrapolating this result to system (3.25), it follows that the equilibria of $E_1(u_*)$ are also nonlinearly unstable. Note that while y decreases in Model I, the dynamics on center manifold W^c show that both y and u increase in Model II when the slower reactions start impacting the dynamics. Because the Model II rate constants are $\mathcal{O}(10^{-4})$ and the dynamics on a center manifold (3.30) are quadratic, the growth in y occurs on a time scale $\mathcal{O}(10^{-8})$. This manifests as the delayed initiation phase observed in UDAR trials.

The only other equilibria in the system (3.25) is the set $E_2(y_*)$. When $y_* = 0$, this equilibria is an element of the set of equilibria $E_1(1)$ and obeys the center manifold behavior described above. For other values, we have the following result.

Corollary 6.2. *Consider the reduced system (3.29). The Jacobian matrix at an equilibrium $x \in \xi_2(y_*)$ is*

$$\mathcal{J}(x) = \begin{bmatrix} 0 & 2y_*^2 + 2\alpha + \beta & 2y_*^2 + \gamma & 2y_*^2 & 2y_*^2 \\ 0 & -y_*^2 - \alpha - \beta & -y_*^2 & -y_*^2 & -y_*^2 \\ 0 & \beta & -\gamma - \lambda & \delta & 0 \\ 0 & 0 & \gamma & -\delta & 0 \\ 0 & 0 & \lambda & 0 & 0 \end{bmatrix}$$

which has a zero eigenvalue with eigenvector $\vec{e}_y$ along the y axis. The rest of the

eigenvalues are negative,

$$\chi_{1,2} = -\frac{1}{2}\left(y_*^2 + \alpha + \beta \pm \sqrt{(y_*^2 + \alpha + \beta)^2 - 4\beta y_*^2}\right)$$
$$\chi_{3,4} = -\frac{1}{2}\left(\gamma + \delta + \lambda \pm \sqrt{(\gamma + \delta + \lambda)^2 - 4\delta\lambda}\right)$$

Therefore the manifold of equilibria $\xi_2(y^*)$ (and therefore the set $E_2(y_*)$), with $y_* \neq 0$ is locally asymptotically stable.

Together, Corollaries 6.1 and 6.2 indicate solutions repelled by an unstable equilibrium in $E_1(u_*)$ along a center manifold will eventually converge to a stable equilibrium in $E_2(y_*)$. This process allows y to grow larger than 10, forcing us to revisit the standing assumptions of this section.

3.2.3 Analysis for $y \geq 10$

As noted before, when the concentration of Y increases after the plateau, $P \approx P_0$ becomes an inappropriate assumption. However, in §3.2.1 we determined that these same simulations indicate the amount of free polymerase decreases by at most one order of magnitude. Thus for the primary amplification and plateau phases where $Y \in [10, 100]$ and $J < 1$ (Figure 3.15), we see that $P \sim \mathcal{O}\left(10^{-4}\right)$. Since coefficients β, δ and ζ are functions of P, we change from the previous assumptions (3.19), and now assume

$$\begin{aligned} &\theta \sim \mathcal{O}\left(10^2\right), \quad \alpha \sim \mathcal{O}(1), \quad \beta, \delta, \gamma \sim \mathcal{O}\left(10^{-2}\right), \\ &\eta \sim \mathcal{O}\left(10^{-3}\right), \quad \lambda \sim \mathcal{O}\left(10^{-4}\right), \quad \zeta \sim \mathcal{O}\left(10^{-8}\right) \end{aligned} \tag{3.31}$$

Next, we consider the reaction rates for the two remaining mechanisms, recycling and dimerization. Because $y > 10$, we see that the terms y^4 and y^2, present in the

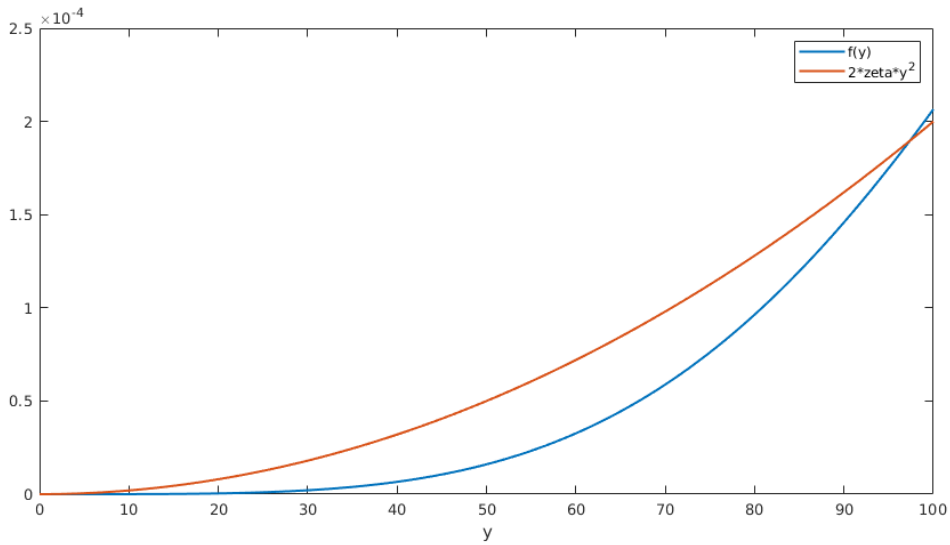

Figure 3.18: Approximate reaction rates for the recycling and dimerization functions as y ranges through the values under which P is lowered by one order of magnitude.

recycling and dimerization terms respectively, will change dynamically as simulated in Figure 3.18. When y is on the lower end, less than 30 or so, we see the dimerization reaction is faster than the recycling reaction. However, as y passes 40, it becomes clear that these reactions are of the same order until overtaking the constraints of the $P \sim \mathcal{O}\left(10^{-4}\right)$ assumption. Therefore, the best option to analyze the system after $y > 10$, due to the rapid change through this period of secondary amplification, is to simply analyze the full model as we have done in §3.1.5. As before, when we scale the system we'll find three partial equilibria: one satisfying the $y < 10$ assumptions along the unstable manifold where $y_* = 0$, one saddle where y_* is relatively small that strongly attracts trajectories before slowly pushing them away, and one sink where y_* is relatively large to which the active components of the system (y, t, z, w, v, u, and j) will converge.

While the long term behavior analysis identified the key mechanisms behind the biphasic behavior, the regular perturbation analysis shed light on the persistent

degenerate manifold of equilibria when

$$y(\tau) = Y(\mathfrak{t}) = 0$$

and the mechanisms required to enter into the primary amplification phase. We hope that these insights will guide rational design of UDAR templates to behave more predictably and consistently.

CHAPTER FOUR

PROOFS

4.1 Proofs for Partial Model Equilibrium Analysis

Here we present technical proofs for the results in §3.1. For all of these proofs, we use the standing assumption that functions will either converge to a finite value or diverge to infinity but never oscillate indefinitely. When referring to a component of the systems (3.1), (3.6), (3.11), or (3.14) we use the notation Ω, i.e., $\Omega = Y,\ T,\ Z,\ W, ...$ Recall that when a limit at infinity is known or assumed to exist, we use the notation

$$\Omega_\infty := \lim_{t\to\infty} \Omega$$

and instead of using (3.3) to compute P, we use the simplified form (3.5). This introductory section presents preliminary lemmas for use in the subsequent proofs of §3.1. Then we present the proof of Theorems 1, 2, 3, and 4 from §§3.1.2, 3.1.3, 3.1.4, and 3.1.5 respectively.

4.1.1 Preliminary results

Lemma 4.1. *Let $\Omega \geq 0$ be a component function of (3.1), (3.6), (3.11), or (3.14). If*

$$\dot{\Omega}_\infty \textit{ exists and is finite,}$$

then

$$\dot{\Omega}_\infty \geq 0.$$

Proof. We prove this by contradiction by assuming $\dot{\Omega}_\infty < 0$. This means that for any

$\delta > 0$, there's a δ-dependent time τ_δ such that for $t > \tau_\delta$,

$$\dot{\Omega} < -\delta.$$

We define the function

$$f(t) := \int_{\tau_\delta}^{t} -\dot{\Omega}(s)ds$$

over the domain $t > \tau_\delta$. Since $\dot{\Omega} < -\delta$ on this domain, it's true that

$$f(t) \geq \int_{\tau_\delta}^{t} \delta ds = (t - \tau_\delta)\delta.$$

and consequently $f(t)$ will diverge to infinity as $t \to \infty$. Because

1. f is continuous,
2. $f(\tau_\delta) = 0$,
3. $f \geq 0$ for all $t > \tau_\delta$ by our assumption,
4. and f will diverge to infinity as $t \to \infty$,

the Intermediate Value Theorem implies there exists a $\tau^* > \tau_\delta$ such that

$$f(\tau^*) = \Omega(\tau_\delta).$$

Then $\Omega(\tau^*)$ can be written equivalently as

$$\Omega(\tau^*) = \Omega(\tau_\delta) + \int_{\tau_\delta}^{\tau^*} \dot{\Omega}(s)ds$$

and

$$\Omega(\tau^*) = \Omega(\tau_\delta) - f(\tau^*) = 0$$

By construction, f is monotonically increasing for $t > \tau^*$ and the assumption that $\dot{\Omega}_\infty < 0$ for $t > \tau_\delta$ requires that $\dot{\Omega}$ decreases for $t > \tau^*$. Finally, because $\Omega(\tau^*) = 0$, it must be that $\Omega < 0$ for $t > \tau^*$ which contradicts the assumption that $\Omega \geq 0$ for all t. This contradiction shows that, indeed, the assumptions imply that

$$\dot{\Omega}_\infty \geq 0.$$

□

Lemma 4.2. *Let $\Omega \geq 0$ be a component function of (3.1), (3.6), (3.11), or (3.14). If*

1. *$\dot{\Omega}_\infty$ exists and is finite*
2. *and $\dot{\Omega}_\infty > 0$,*

then

$$\Omega \textit{ diverges to infinity.}$$

Proof. By assumption (2), for any $\delta > 0$, there's a δ-dependent time τ_δ such that for all $t > \tau_\delta$,

$$\dot{\Omega} > \delta.$$

We define the function

$$f(t) := \int_{\tau_\delta}^{t} \dot{\Omega}(s) ds$$

over the domain $t > \tau_\delta$. Since $\dot{\Omega} > \delta$ on this domain,

$$f(t) \geq \int_{\tau_\delta}^{t} \delta ds = (t - \tau_\delta)\delta$$

and f diverges to infinity as t grows. Then for any $t > \tau_\delta$,

$$\Omega = \Omega(\tau_\delta) + \int_{\tau_\delta}^{t} \dot{\Omega}(s)ds$$

$$\lim_{t\to\infty} \Omega = \Omega(\tau_\delta) + \lim_{t\to\infty} f(t)$$

Since $\Omega(\tau_\delta) \geq 0$ by the initial conditions, $\lim_{t\to\infty} \Omega$ will diverge to infinity, too. □

Corollary 4.2.1. *Let $\Omega \geq 0$ be a component function of (3.1), (3.6), (3.11), or (3.14). If*

1. *$\dot{\Omega}_\infty$ exists and is finite*
2. *and Ω is bounded,*

then

$$\dot{\Omega}_\infty = 0 \text{ and } \Omega_\infty \text{ exists and is finite.}$$

Lemma 4.3. *Assume*

$$\dot{T}_\infty,\ \dot{Z}_\infty,\ \dot{W}_\infty,\ \dot{V}_\infty,\ \dot{Y}_\infty \text{ (and when appropriate } \dot{W}^*_\infty) \text{ exist and are finite,}$$

then

1. *Y is bounded for systems (3.1), (3.6), (3.11), and (3.14)*
2. *J is bounded for system (3.1),*
3. *and P is bounded away from zero in systems (3.1), (3.6), and (3.11).*

Proof. We consider first the special case of system (3.14) where $P = P_0$ is constant. By Lemma 4.1, it must be that $\dot{Y}_\infty \geq 0$ so

$$\lim_{t\to\infty} \big(-2k_+TY^2 + 2k_-Z + k_1ZP_0 + k_2W - k_6YP_0(2Y + J)\big) \geq 0$$

Because the system is subject to the conservation law (3.4),

$$T + Z + W + V + W^* = T_0,$$

the positive terms are bounded by the conservation law,

$$2k_- Z + k_1 Z P_0 + k_2 W \leq T_0(2k_- + k_1 P_0 + k_2).$$

Thus it must be that

$$\lim_{t\to\infty} - \left(2k_+ T Y^2 + k_6 Y P_0 (2Y + J)\right) + T_0(2k_- + k_1 P_0 + k_2) \geq 0$$

and

$$T_0(2k_- + k_1 P_0 + k_2) \geq \lim_{t\to\infty} \left(2k_+ T Y^2 + 2k_6 Y^2 P_0 + k_6 Y J P_0\right)$$

for all t. Because the terms on the right hand side are all nonnegative, the term $2k_6 Y^2 P_0$ implies there's an upper bound on Y which, by Corollary 4.2.1, implies Y_∞ exists and is finite.

Next we consider the cases where P is represented by equation (3.5),

$$P = \frac{P_0}{1 + \frac{Z+V+\kappa_2(Y^2+YJ)}{\kappa_1}}.$$

In systems (3.1), (3.6), and (3.11), we have the equations

$$\begin{aligned}
\dot{Y} &= -2k_+ T Y^2 + 2k_- Z + k_1 Z P + k_2 W - k_6 Y P (2Y + J) \\
\dot{Z} &= k_+ T Y^2 - k_- Z - k_1 Z P \\
\dot{V} &= k_2 W - k_3 V P
\end{aligned}$$

Seeking contradiction, assume that either J diverges, Y diverges, or both. From equation (3.5), this implies $P_\infty = 0$. Because Z and V are bounded by conservation law (3.26),

$$\lim_{t\to\infty} k_1 ZP = \lim_{t\to\infty} k_3 VP = 0.$$

By Corollary 4.2.1, we then have

$$\dot{Z} + k_1 ZP = k_+ TY^2 - k_- Z$$
$$\lim_{t\to\infty} \left(\dot{Z} + k_1 ZP\right) = 0 = \lim_{t\to\infty} \left(k_+ TY^2 - k_- Z\right)$$

and

$$\dot{V} + k_3 VP = k_2 W$$
$$\lim_{t\to\infty} \left(\dot{V} + k_3 VP\right) = 0 = \lim_{t\to\infty} k_2 W$$

Using both of these results with the fact that $\lim_{t\to\infty} k_1 ZP = 0$ in the $\dot{Y}$ equation, we have

$$\begin{aligned}
\dot{Y} - 2\left(-k_+ TY^2 + k_- Z\right) + k_1 ZP + k_2 W \\
&= -k_6 YP(2Y + J) \\
\lim_{t\to\infty} \left(\dot{Y} - 2\left(-k_+ TY^2 + k_- Z\right) + k_1 ZP + k_2 W\right) \\
&= -\lim_{t\to\infty} k_6 YP(2Y + J) \\
\dot{Y}_\infty &= -k_6 P_0 \lim_{t\to\infty} \frac{Y(2Y + J)}{1 + \frac{Z+V+\kappa_2(Y^2+JY)}{\kappa_1}}
\end{aligned}$$

If Y diverges at the same rate or faster than J diverges (or Y diverges and J doesn't),

there's a nonnegative constant $\mathcal{C} \geq 0$ such that

$$\lim_{t\to\infty} \frac{J}{Y} := \mathcal{C}.$$

We divide both numerator and denominator on the right hand side by Y^2, and compute the limit

$$\begin{aligned}
\dot{Y}_\infty &= -k_6\kappa_1 P_0 \lim_{t\to\infty} \left(\frac{2 + \frac{J}{Y}}{\frac{\kappa_1+Z+V}{Y^2} + \kappa_2\left(1 + \frac{J}{Y}\right)} \right) \\
\dot{Y}_\infty &= \frac{-k_6\kappa_1 P_0}{\kappa_2} \left(\frac{2+\mathcal{C}}{1+\mathcal{C}} \right).
\end{aligned}$$

Since the right hand side is a negative constant this contradicts Lemma 4.1. Thus Y can't diverge to infinity at the same rate or faster than J.

We now assume that if J diverges to infinity faster than Y (or J diverges to infinity and Y doesn't). This means

$$\lim_{t\to\infty} \frac{Y}{J} = 0$$

We divide both numerator and denominator on the right hand side by YJ and compute the limit

$$\begin{aligned}
\dot{Y}_\infty &= -k_6\kappa_1 P_0 \lim_{t\to\infty} \left(\frac{2\left(\frac{Y}{J}\right) + 1}{\frac{\kappa_1+Z+V}{YJ} + \kappa_2\left(\frac{Y}{J} + 1\right)} \right) \\
\dot{Y}_\infty &= \frac{-k_6 P_0 \kappa_1}{\kappa_2}
\end{aligned}$$

The right hand side is again a negative constant which contradicts Lemma 4.1. These two contradictions show that neither Y nor J can diverge to infinity in systems (3.1), (3.6), and (3.11).

Finally, because Z and V are bounded above by conservation law (3.4), equation (3.5) shows that P is uniformly bound away from zero at all times in systems (3.1), (3.6), and (3.11). □

4.1.2 Proof of Theorem 1 for Model 1

In this section we prove the results regarding the partial model with no deactivation or recycling of amplifiers. Recall that system (3.6) is

$$\dot{Y} = -2k_+TY^2 + 2k_-Z + k_1ZP + k_2W - 2k_6Y^2P \tag{4.1}$$

$$\dot{T} = -k_+TY^2 + k_-Z \tag{4.2}$$

$$\dot{Z} = k_+TY^2 - k_-Z - k_1ZP \tag{4.3}$$

$$\dot{W} = k_1ZP - k_2W + k_3VP \tag{4.4}$$

$$\dot{V} = k_2W - k_3VP \tag{4.5}$$

$$\dot{D} = k_6Y^2P \tag{4.6}$$

with initial conditions (3.7),

$$(Y(0), T(0), Z(0), W(0), V(0), D(0)) = (Y_0, T_0, 0, 0, 0, 0)$$

and where P is given by

$$P := \frac{P_0}{1 + \frac{Z+V+\kappa_2Y^2}{\kappa_1}}.$$

Equations (4.2)-(4.5) admit conservation law (3.8),

$$T + Z + W + V = T_0$$

so the component functions are therefore bounded in the interval $[0, T_0]$ for all t.

Lemma 4.4. *In system (3.6) with initial conditions (3.7), if*

1. $\dot{T}_\infty,\ \dot{Z}_\infty,\ \dot{W}_\infty,\ \dot{V}_\infty,\ \dot{Y}_\infty$ *exist and are finite*

2. *and* $Y_\infty = 0$,

then

$$\lim_{t\to\infty}(Y, T, Z, W, V, D, P) = (0, T_0, 0, 0, 0, D_\infty, P_0)$$

where

$$D_\infty := \lim_{t\to\infty} k_6 \int_0^t \frac{\kappa_1 P_0 [Y(\tau)]^2}{\kappa_1 + Z(\tau) + V(\tau) + \kappa_2 [Y(\tau)]^2} d\tau$$

may be infinite.

Proof. The first assumption satisfies the hypotheses of Lemma 4.3, so it follows that P is uniformly bound away from zero. Additionally, both assumptions with conservation law (3.8) are sufficient to meet the conditions of Corollary 4.2.1 for functions $Y,\ T,\ Z,\ W,\ V$. Therefore

$$\dot{Y}_\infty = \dot{T}_\infty = \dot{Z}_\infty = \dot{W}_\infty = \dot{V}_\infty = 0$$

and $T_\infty,\ Z_\infty,\ W_\infty,\ V_\infty$ exist and are finite. This further implies that P_∞ exists. Using assumption (2) in equation (4.2) with the fact that these limits exist, we see

$$\begin{aligned}
\lim_{t\to\infty} \dot{T} &= \lim_{t\to\infty} \left(-k_+ T Y^2 + k_- Z\right) \\
0 &= -k_+ T_\infty \cdot 0^2 + k_- Z_\infty \\
0 &= k_- Z_\infty
\end{aligned}$$

and it must be that $Z_\infty = 0$. Using this result with assumption (2) and the fact that

P_∞ and T_∞ exist and are bounded, we determine that

$$\begin{aligned}
\lim_{t\to\infty} \dot{Y} &= \lim_{t\to\infty}(-2k_+TY^2 + 2k_-Z + k_1ZP + k_2W - 2k_6Y^2P) \\
0 &= -2k_+T_\infty \cdot 0^2 + 2k_- \cdot 0 + k_1 \cdot 0 \cdot P_\infty + k_2W_\infty - 2k_6 \cdot 0^2 \cdot P_\infty \\
0 &= k_2W_\infty
\end{aligned}$$

so $W_\infty = 0$ as well. Now this result in equation (4.5) shows that

$$\begin{aligned}
\lim_{t\to\infty} \dot{V} &= \lim_{t\to\infty}(k_2W - k_3VP) \\
0 &= k_2 \cdot 0 - k_3V_\infty P_\infty \\
0 &= -k_3V_\infty P_\infty
\end{aligned}$$

Again because P is uniformly bounded away from zero, it must be that $V_\infty = 0$. Finally, since $Z_\infty = W_\infty = V_\infty = 0$, conservation law (3.8) implies

$$\lim_{t\to\infty}(T + Z + W + V) = T_\infty = T_0.$$

The only remaining equation, D, can be evaluated using formula for P,

$$D_\infty = \lim_{t\to\infty} k_6 \int_0^t \frac{\kappa_1 P_0[Y(\tau)]^2}{\kappa_1 + Z(\tau) + V(\tau) + \kappa_2[Y(\tau)]^2} d\tau.$$

Note that D may diverge to infinity based on how quickly Y converges. □

Lemma 4.5. *In system (3.6) with initial conditions (3.7), if*

1. $\dot{T}_\infty,\ \dot{Z}_\infty,\ \dot{W}_\infty,\ \dot{V}_\infty,\ \dot{Y}_\infty$ *exist and are finite*

2. *and* $Y_\infty \neq 0$,

then

$$\lim_{t\to\infty}(Y,T,Z,W,V,P) = (Y_\infty, 0, 0, W_\infty, V_\infty^+, P_\infty)$$

where V_∞^+ *is the positive root of*

$$k_2(2k_6+\kappa_2 k_3)V_\infty^2 + \left(2\kappa_1 k_6(k_2+k_3P_0) - k_2T_0(2k_6+\kappa_2k_3)\right)V_\infty - 2\kappa_1k_2k_6T_0 = 0,$$

the remaining functions converge to

$$\begin{aligned} Y_\infty &= \sqrt{\frac{k_3V_\infty^+}{2k_6}}, \\ P_\infty &= \frac{2\kappa_1k_6P_0}{2\kappa_1k_6 + (2k_6+\kappa_2k_3)V_\infty^+}, \\ W_\infty &= \frac{2\kappa_1k_3k_6P_0V_\infty^+}{k_2\left(2\kappa_1k_6 + (2k_6+\kappa_2k_3)V_\infty^+\right)}, \end{aligned}$$

and D *diverges to infinity.*

Proof. The first assumption satisfies the hypotheses of Lemma 4.3, so it follows that P is uniformly bounded away from zero and Y is bounded. Additionally, this assumption and conservation law (3.8) satisfy the conditions of Corollary 4.2.1 for functions $Y,\ T,\ Z,\ W,\ V$. Therefore

$$\dot{Y}_\infty = \dot{T}_\infty = \dot{Z}_\infty = \dot{W}_\infty = \dot{V}_\infty = 0$$

and $Y_\infty,\ T_\infty,\ Z_\infty,\ W_\infty,\ V_\infty$ exist and are finite. This further implies that P_∞ exists. Now from equation (4.2) we know that

$$\begin{aligned} \lim_{t\to\infty}\dot{T} &= \lim_{t\to\infty}\left(-k_+TY^2 + k_-Z\right) \\ 0 &= -k_+T_\infty Y_\infty^2 + k_-Z_\infty \end{aligned} \tag{4.7}$$

Using this result in equation (4.3), we determine that

$$\begin{aligned}
\lim_{t\to\infty} \dot{Z} &= \lim_{t\to\infty} \left(-k_+ T Y^2 + k_- Z - k_1 Z P\right) \\
0 &= \left(-k_+ T_\infty Y_\infty^2 + k_- Z_\infty\right) - k_1 Z_\infty P_\infty \\
0 &= -k_1 Z_\infty P_\infty
\end{aligned}$$

Because P is uniformly bounded away from zero, it must be that $Z_\infty = 0$. Using this now in the relation (4.7) shows that

$$\begin{aligned}
0 &= -k_+ T_\infty Y_\infty^2 + k_- \cdot 0 \\
0 &= -\lim_{t\to\infty} k_+ T_\infty Y_\infty^2
\end{aligned}$$

Since we assume $Y_\infty \neq 0$, it must be that $T_\infty = 0$. Now from equation (4.1) we compute

$$\begin{aligned}
\lim_{t\to\infty} \dot{Y} &= \lim_{t\to\infty} (-2k_+ T Y^2 + 2k_- Z + k_1 Z P + k_2 W - 2k_6 Y^2 P) \\
0 &= -2k_+ \cdot 0 \cdot Y_\infty^2 + 2k_- \cdot 0 + k_1 \cdot 0 \cdot P_\infty + k_2 W_\infty - 2k_6 Y_\infty^2 P_\infty \\
0 &= k_2 W_\infty - 2k_6 Y_\infty^2 P_\infty \\
2k_6 Y_\infty^2 P_\infty &= k_2 W_\infty \qquad (4.8)
\end{aligned}$$

Similarly from equation (4.5), we can determine a relation between V_∞ and W_∞,

$$\begin{aligned}
\lim_{t\to\infty} \dot{V} &= \lim_{t\to\infty} (k_2 W - k_3 V P) \\
0 &= k_2 W_\infty - k_3 V_\infty P_\infty \\
k_2 W_\infty &= k_3 V_\infty P_\infty \qquad (4.9)
\end{aligned}$$

Now because P is uniformly bounded away from zero, W_∞ and V_∞ are either both zero or both nonzero. If we let t go to infinity, conservation law (3.8) shows that

$$\lim_{t\to\infty}(T+Z+W+V) = W_\infty + V_\infty = T_0 \tag{4.10}$$

so neither can be zero. Using the equivalent values for $k_2 W_\infty$ in (4.8) and (4.9) we compute,

$$\begin{aligned} 2k_6 Y_\infty^2 P_\infty &= k_3 V_\infty P_\infty \\ Y_\infty &= \sqrt{\frac{k_3 V_\infty}{2k_6}} \end{aligned}$$

Also from (4.9), we have the relation

$$W_\infty = \frac{k_3}{k_2} V_\infty P_\infty.$$

Expanding the P equation, this becomes

$$\begin{aligned} W_\infty &= \frac{k_3}{k_2} V_\infty \left(\frac{P_0}{1 + \frac{V_\infty}{\kappa_1} + \frac{\kappa_2}{\kappa_1}\left(Y_\infty^2\right)} \right) \\ &= \frac{k_3}{k_2} V_\infty \left(\frac{P_0}{1 + \frac{V_\infty}{\kappa_1} + \frac{\kappa_2}{\kappa_1}\left(\frac{k_3 V_\infty}{2k_6}\right)} \right) \\ &= \frac{k_3}{k_2} \left(\frac{2\kappa_1 k_6 P_0 V_\infty}{2\kappa_1 k_6 + (2k_6 + \kappa_2 k_3) V_\infty} \right) \end{aligned}$$

This formulation of W_∞, substituted into (4.10), creates a function of V_∞,

$$\frac{2\kappa_1 k_3 k_6 P_0 V_\infty}{k_2\left(2\kappa_1 k_6 + (2k_6 + \kappa_2 k_3) V_\infty\right)} + V_\infty = T_0 \tag{4.11}$$

that can be expressed as a quadratic polynomial (see Appendix A.1),

$$k_2(2k_6 + \kappa_2 k_3)V_\infty^2 + (2k_6\kappa_1(k_2 + k_3P_0) - k_2T_0(2k_6 + \kappa_2 k_3))\, V_\infty - 2\kappa_1 k_2 k_6 T_0 = 0$$

This describes an upward open parabola in variable V_∞ with a negative value at $V_\infty = 0$. It follows that this expression has one negative root V_∞^- and one positive root V_∞^+. As we require that V be non-negative, we only need to consider V_∞^+. This value can be used to compute the remaining nonzero values,

$$\begin{aligned} P_\infty &= \frac{2\kappa_1 k_6 P_0}{2\kappa_1 k_6 + (2k_6 + \kappa_2 k_3)V_\infty^+} \\ W_\infty &= \frac{2\kappa_1 k_3 k_6 P_0 V_\infty^+}{k_2\left(2\kappa_1 k_6 + (2k_6 + \kappa_2 k_3)V_\infty^+\right)}. \end{aligned}$$

Finally, because we assume $Y_\infty > 0$ and have concluded that $P_\infty \neq 0$, it follows from equation (4.6) that $\dot{D}_\infty > 0$ which implies D diverges to infinity by Lemma 4.2. □

Proof of Theorem 1 In all cases, either Lemma 4.4 or Lemma 4.5 is satisfied. These two then lead to the dichotomy that is the conclusion of Theorem 1. ■

4.1.3 Proof of Theorem 2 for Model 2

In this section, we prove the results regarding the partial model with deactivation but no recycling. Recall that system (3.11) is

$$\dot{Y} = -2k_+TY^2 + 2k_-Z + k_1ZP + k_2W - 2k_6Y^2P \tag{4.12}$$

$$\dot{T} = -k_+TY^2 + k_-Z \tag{4.13}$$

$$\dot{Z} = k_+TY^2 - k_-Z - k_1ZP \tag{4.14}$$

$$\dot{W} = k_1ZP - k_2W + k_3VP - k_4W \tag{4.15}$$

$$\dot{V} = k_2W - k_3VP \tag{4.16}$$

$$\dot{W}^* = k_4W \tag{4.17}$$

$$\dot{D} = k_6Y^2P \tag{4.18}$$

with initial conditions (3.12),

$$(Y(0), T(0), Z(0), W(0), V(0), W^*(0), D(0)) = (Y_0, T_0, 0, 0, 0, 0, 0)$$

and where

$$P := \frac{P_0}{1 + \frac{Z+V+\kappa_2Y^2}{\kappa_1}}.$$

Equations (4.13)-(4.17) admit the conservation law (3.4),

$$T + Z + W + V + W^* = T_0$$

so the component functions are bounded in $[0, T_0]$ for all t.

Proof of Theorem 2 The assumptions of this theorem satisfy the hypotheses of Lemma 4.3, so we know P is uniformly bounded away from 0 and that Y

is bounded. With conservation law (3.4), Corollary 4.2.1 holds for the functions $Y,\ T,\ Z,\ W,\ V,\ W^*$, so

$$\dot{Y}_\infty = \dot{T}_\infty = \dot{Z}_\infty = \dot{W}_\infty = \dot{V}_\infty = W^*_\infty = 0$$

and $Y_\infty,\ T_\infty,\ Z_\infty,\ W_\infty,\ V_\infty,\ W^*_\infty$ exist and are finite. Thus from equation (4.13) we know that

$$\begin{aligned} \lim_{t\to\infty} \dot{T} &= \lim_{t\to\infty} \left(-k_+ T Y^2 + k_- Z\right) \\ 0 &= -k_+ T_\infty Y_\infty^2 + k_- Z_\infty. \end{aligned}$$

Using this fact in equation (4.14) shows that

$$\begin{aligned} \lim_{t\to\infty} \dot{Z} &= \lim_{t\to\infty} \left(-k_+ T Y^2 + k_- Z - k_1 Z P\right) \\ 0 &= 0 - k_1 Z_\infty P_\infty. \end{aligned}$$

Because P is uniformly bounded away from zero, it must be that $Z_\infty = 0$. We can also sum equations (4.15) and (4.16) to produce the relation

$$\dot{W} + \dot{V} = k_1 Z P - k_4 W$$

Then letting t approach infinity, we see that

$$\begin{aligned} \lim_{t\to\infty} \left(\dot{W} + \dot{V}\right) &= \lim_{t\to\infty} \left(k_1 Z P - k_4 W\right) \\ 0 &= -k_4 W_\infty, \end{aligned}$$

which means $W_\infty = 0$. Using these facts in equation (4.15), we see that

$$\begin{aligned}
\lim_{t\to\infty} \dot{W} &= \lim_{t\to\infty} (k_1 ZP - k_2 W + k_3 VP - k_4 W) \\
0 &= k_1 \cdot 0 \cdot P_\infty - k_2 \cdot 0 + k_3 V_\infty P_\infty - k_4 \cdot 0 \\
0 &= k_3 V_\infty P_\infty.
\end{aligned}$$

Since P is uniformly bounded away from zero, we conclude it must be that $V_\infty = 0$. Continuing on, we use these results in equation (4.12), to find that

$$\begin{aligned}
\lim_{t\to\infty} \dot{Y} &= \lim_{t\to\infty} (-2k_+ TY^2 + 2k_- Z + k_1 ZP + k_2 W - 2k_6 Y^2 P) \\
0 &= 0 + k_1 \cdot 0 \cdot P_\infty + k_2 \cdot 0 - 2k_6 Y_\infty^2 P_\infty \\
0 &= -2k_6 Y_\infty^2 P_\infty
\end{aligned}$$

Expanding the equation for P_∞, we have

$$0 = -2k_6 Y_\infty^2 \left(\frac{P_0}{1 + \frac{0}{\kappa_1} + \frac{\kappa_2 Y_\infty^2}{\kappa_1}} \right) = \frac{-2\kappa_1 k_6 P_0 Y_\infty^2}{\kappa_1 + \kappa_2 Y_\infty^2}$$

which is only true if $Y_\infty = 0$. Because equations (4.13) and (4.15) are first order, linear, variable coefficient ODEs, they have closed form solutions

$$\begin{aligned}
T &= \frac{\int_0^t e^{\int_0^\tau k_+ [Y(s)]^2 ds} k_- Z(\tau) d\tau + T_0}{e^{\int_0^t k_+ Y^2 d\tau}} \\
W &= \frac{\int_0^t e^{(k_2+k_4)\tau} [k_1 Z(\tau) + k_3 V(\tau)] P(\tau) d\tau}{e^{(k_2+k_4)t}}
\end{aligned}$$

which implies

$$T_\infty = \lim_{t\to\infty} \frac{\int_0^t e^{\int_0^\tau k_+[Y(s)]^2 ds} k_- Z(\tau) d\tau + T_0}{e^{\int_0^t k_+[Y(\tau)]^2 d\tau}}$$
$$W_\infty^* = \lim_{t\to\infty} \int_0^t \frac{k_4 \int_0^\tau e^{(k_2+k_4)s}[k_1 Z(s) + k_3 V(s)]P(s) ds}{e^{(k_2+k_4)\tau}} d\tau$$

Because $Z_\infty = W_\infty = V_\infty = 0$, conservation law (3.4) now requires that

$$T_\infty + W_\infty^* = T_0.$$

Finally, we can compute

$$D_\infty := \lim_{t\to\infty} k_6 \int_0^t \frac{\kappa_1 P_0 [Y(\tau)]^2}{\kappa_1 + Z(\tau) + V(\tau) + \kappa_2 [Y(\tau)]^2} d\tau$$

numerically, though it may diverge to infinity. ■

4.1.4 Proof of Theorem 3 for Model 3

In this section we analyze the full model under the assumption that the polymerase is needed for the reactions, but that it isn't sequestered by these reactions.

Recall that system (3.14) is

$$\dot{Y} = -2k_+TY^2 + 2k_-Z + k_1ZP_0 + k_2W - k_6YP_0(2Y + J) \tag{4.19}$$

$$\dot{T} = -k_+TY^2 + k_-Z + k_5f(Y)(W + W^*) \tag{4.20}$$

$$\dot{Z} = k_+TY^2 - k_-Z - k_1ZP_0 \tag{4.21}$$

$$\dot{W} = k_1ZP_0 - k_2W + k_3VP_0 - k_4W - k_5f(Y)W \tag{4.22}$$

$$\dot{V} = k_2W - k_3VP_0 \tag{4.23}$$

$$\dot{W}^* = k_4W - k_5f(Y)W^* \tag{4.24}$$

$$\dot{J} = k_5f(Y)(W + W^*) - k_6JYP_0 \tag{4.25}$$

$$\dot{G} = k_6JYP_0 \tag{4.26}$$

$$\dot{D} = k_6Y^2P_0 \tag{4.27}$$

with initial conditions (3.2),

$$(Y(0), T(0), Z(0), W(0), V(0), W^*(0), J(0), G(0), D(0)) = (Y_0, T_0, 0, 0, 0, 0, 0, 0, 0)$$

and where

$$f(Y) := \frac{Y^4}{\kappa_R^4 + Y^4}.$$

Equations (4.20)-(4.24) admit conservation law (3.4), so the the component functions are bounded in $[0, T_0]$ for all t.

Lemma 4.6. *In the system (4.19)-(4.27) with initial conditions (3.2), if*

1. $\dot{T}_\infty$, $\dot{Z}_\infty$, $\dot{W}_\infty$, $\dot{V}_\infty$, $\dot{W}^*_\infty$, $\dot{J}_\infty$, $\dot{Y}_\infty$ *exist and are finite*

2. *and* $Y_\infty = 0$,

then

$$\lim_{t\to\infty}(Y,T,Z,W,V,W^*,J,G,D) = (0,T_\infty,0,0,0,W^*_\infty,J_\infty,G_\infty,D_\infty)$$

where

$$\begin{aligned}
T_\infty &= \lim_{t\to\infty} \frac{\int_0^t e^{\int_0^s k_+[Y(\tau)]^2 d\tau}(k_- Z(s) + k_5 h(Y(s))[W(s)+W^*(s)])ds + T_0}{e^{\int_0^t k_+[Y(\tau)]^2 d\tau}} \\
W^*_\infty &= \lim_{t\to\infty} \frac{\int_0^t e^{\int_0^s k_5 h(Y(\tau))d\tau} k_4 W(s)ds}{e^{\int_0^t k_5 h(Y(\tau))d\tau}} \\
J_\infty &= \lim_{t\to\infty} \frac{\int_0^t e^{\int_0^s k_6 P_0 Y(\tau)d\tau} k_5 h(Y(s))[W(s)+W^*(s)]ds}{e^{\int_0^t k_6 P_0 Y(\tau)d\tau}} \\
G_\infty &= \lim_{t\to\infty} k_6 P_0 \int_0^t J(\tau)Y(\tau)d\tau \\
D_\infty &= \lim_{t\to\infty} k_6 P_0 \int_0^t [Y(\tau)]^2 d\tau
\end{aligned}$$

and $T_\infty + W^*_\infty = T_0$. J_∞, G_∞, *and* D_∞ *may diverge to infinity.*

Proof. The assumptions satisfy the hypotheses of Lemma 4.3, so P is uniformly bounded away from zero. With conservation law (3.4), the hypotheses of Corollary 4.2.1 are satisfied for functions Y, T, Z, W, V, W^*, so

$$\dot{Y}_\infty = \dot{T}_\infty = \dot{Z}_\infty = \dot{W}_\infty = \dot{V}_\infty = W^*_\infty = 0$$

and T_∞, Z_∞, W_∞, V_∞, W^*_∞ exist and are finite. With the second assumption and the fact that T is bounded, we see from equation (4.21) that

$$\begin{aligned}
\lim_{t\to\infty} \dot{Z} &= \lim_{t\to\infty} \left(k_+ T Y^2 - k_- Z + k_1 P_0 Z\right) \\
0 &= k_+ T_\infty \cdot 0^2 + k_- Z_\infty + k_1 P_0 Z_\infty \\
0 &= Z_\infty(k_- + k_1 P_0)
\end{aligned}$$

which means $Z_\infty = 0$. Using the second assumption and the fact that W^* is a bounded function, equation (4.24) shows that

$$\begin{aligned}
\lim_{t\to\infty} \dot{W}^* &= \lim_{t\to\infty} (k_4 W - k_5 f(Y) W^*) \\
0 &= k_4 W_\infty - k_5 f(0) W^*_\infty \\
0 &= k_4 W_\infty
\end{aligned}$$

and $W_\infty = 0$ as well. Now from equation (4.23),

$$\begin{aligned}
\lim_{t\to\infty} \dot{V} &= \lim_{t\to\infty} (k_2 W - k_3 V P_0) \\
0 &= k_2 \cdot 0 - k_3 V_\infty P_0 \\
0 &= -k_3 V_\infty P_0
\end{aligned}$$

so $V_\infty = 0$. Finally we can compute T, W^*, and J as first order, variable coefficient ODEs,

$$\begin{aligned}
T_\infty &= \lim_{t\to\infty} \frac{\int_0^t e^{\int_0^s k_+ [Y(\tau)]^2 d\tau} (k_- Z(s) + k_5 h(Y(s))[W(s) + W^*(s)]) ds + T_0}{e^{\int_0^t k_+ [Y(\tau)]^2 d\tau}} \\
W^*_\infty &= \lim_{t\to\infty} \frac{\int_0^t e^{\int_0^s k_5 h(Y(\tau)) d\tau} k_4 W(s) ds}{e^{\int_0^t k_5 h(Y(\tau)) d\tau}} \\
J_\infty &= \lim_{t\to\infty} \frac{\int_0^t e^{\int_0^s k_6 P_0 Y(\tau) d\tau} k_5 h(Y(s))[W(s) + W^*(s)] ds}{e^{\int_0^t k_6 P_0 Y(\tau) d\tau}}
\end{aligned}$$

and the remaining values numerically,

$$\begin{aligned}
G_\infty &= \lim_{t\to\infty} k_6 P_0 \int_0^t J(\tau) Y(\tau) d\tau \\
D_\infty &= \lim_{t\to\infty} k_6 P_0 \int_0^t [Y(\tau)]^2 d\tau
\end{aligned}$$

Because $Z_\infty = W_\infty = V_\infty$, conservation law (3.4) requires that

$$T_\infty + W^*_\infty = T_0.$$

However J, G, and D may diverge to infinity. □

Lemma 4.7. *In the system (4.19)-(4.27) with initial conditions (3.2), if*

1. $\dot{T}_\infty,\ \dot{Z}_\infty,\ \dot{W}_\infty,\ \dot{V}_\infty,\ \dot{W}^*_\infty,\ \dot{J}_\infty,\ \dot{Y}_\infty$ *exist and are finite*

2. *and* $Y_\infty \neq 0$,

then there's a fourth order polynomial $\mathcal{P}\left(Y^2\right)$ *such that* Y_∞ *can correspond to up to four positive, real roots of* $\mathcal{P}\left(Y^2_\infty\right) = 0$. *Furthermore, if any real values for* Y_∞ *exist, there are rational functions* $\mathcal{T}(Y),\ \mathcal{Z}(Y),\ \mathcal{W}(Y),\ \mathcal{V}(Y)$, $\mathcal{W}^*(Y)$, *and* $\mathcal{J}(Y)$ *such that*

$$T_\infty = \mathcal{T}(Y_\infty),\ Z_\infty = \mathcal{Z}(Y_\infty),\ W_\infty = \mathcal{W}(Y_\infty),$$

$$V_\infty = \mathcal{V}(Y_\infty),\ W^*_\infty = \mathcal{W}^*(Y_\infty),\ J_\infty = \mathcal{J}(Y_\infty)$$

and D, G *will diverge to infinity.*

Proof. Because of conservation law (3.4) and the fact that $f(Y)$ is bound above by one, we know that

$$k_5 f(Y)(W + W^*) \leq k_5 T_0.$$

Then

$$\lim_{t\to\infty} \dot{J} = \lim_{t\to\infty} \left(k_5 f(Y)(W + W^*) - k_6 P_0 Y J\right)$$
$$\lim_{t\to\infty} \dot{J} \leq \lim_{t\to\infty} \left(k_5 T_0 - k_6 P_0 Y_\infty J\right)$$

Lemma 4.1 applies here, so $\lim_{t\to\infty} \dot{J} \geq 0$. For this to be true, it must also be that

$$\begin{aligned} k_5 T_0 - k_6 P_0 Y_\infty \lim_{t\to\infty} J &\geq 0 \\ \frac{k_5 T_0}{k_6 P_0 Y_\infty} &\geq \lim_{t\to\infty} J \end{aligned}$$

which means there's an upper bound on $\lim_{t\to\infty} J$ and therefore J is a bounded function. With this result, our assumptions, and conservation law (3.4), the hypotheses of Corollary 4.2.1 hold for the functions Y, T, Z, W, W^*, V, J, so

$$\dot{Y}_\infty = \dot{T}_\infty = \dot{Z}_\infty = \dot{W}_\infty = \dot{W}^*_\infty = \dot{V}_\infty = \dot{J}_\infty = 0$$

and $Y_\infty,\ T_\infty,\ Z_\infty,\ W_\infty,\ W^*_\infty,\ V_\infty,\ J_\infty$ exist and are finite.

We now use the conservation law (3.4) to construct a polynomial in the variable Y_∞. Starting with equation (4.25), we compute

$$\begin{aligned} \lim_{t\to\infty} \dot{J} &= \lim_{t\to\infty} \left(k_5 f(Y)(W + W^*) - k_6 J Y P_0\right) \\ 0 &= k_5 f(Y_\infty)(W_\infty + W^*_\infty) - k_6 P_0 J_\infty Y_\infty \\ k_6 P_0 J_\infty Y_\infty &= k_5 f(Y_\infty)(W_\infty + W^*_\infty) \end{aligned}$$

Next we consider equation (4.20) to show that

$$\begin{aligned} \lim_{t\to\infty} \dot{T} &= \lim_{t\to\infty} \left(-k_+ T Y^2 + k_- Z + k_5 f(Y)(W + W^*)\right) \\ 0 &= -k_+ T_\infty Y_\infty^2 + k_- Z_\infty + k_5 f(Y_\infty)(W_\infty + W_\infty) \\ k_+ T_\infty Y_\infty^2 - k_- Z_\infty &= k_5 f(Y_\infty)(W_\infty + W_\infty) \end{aligned}$$

and from equation (4.21), it's also true that

$$\begin{aligned}
\lim_{t\to\infty} \dot{Z} &= \left(k_+ T Y^2 - k_- Z - k_1 Z P_0\right) \\
0 &= k_+ T_\infty Y_\infty^2 - k_- Z_\infty - k_1 P_0 Z_\infty \qquad (4.28) \\
k_+ T_\infty Y_\infty^2 - k_- Z_\infty &= k_1 P_0 Z_\infty
\end{aligned}$$

Linking together these equivalent expressions, we have that

$$k_+ T_\infty Y_\infty^2 - k_- Z_\infty = k_1 P_0 Z_\infty = k_5 f(Y_\infty)(W_\infty + W_\infty^*) = k_6 P_0 J_\infty Y_\infty \qquad (4.29)$$

By rearranging, we can compute some values in terms of Z_∞ and Y_∞,

$$W_\infty + W_\infty^* = \frac{k_1 P_0 Z_\infty}{k_5 f(Y_\infty)} \qquad (4.30)$$

$$T_\infty = \frac{(k_- + k_1 P_0) Z_\infty}{k_+ Y_\infty^2} \qquad (4.31)$$

Continuing on, equation (4.23) shows the relation

$$\begin{aligned}
\lim_{t\to\infty} \dot{V} &= \lim_{t\to\infty} \left(k_2 W - k_3 V P_0\right) \\
0 &= k_2 W_\infty - k_3 P_0 V_\infty \\
k_2 W_\infty &= k_3 P_0 V_\infty \qquad (4.32)
\end{aligned}$$

which can be used to simplify the relation from equation (4.22),

$$\begin{aligned}
\lim_{t\to\infty} \dot{W} &= \lim_{t\to\infty} (k_1 Z P_0 - k_2 W + k_3 V P_0 - k_4 W - k_5 f(Y) W) \\
0 &= k_1 P_0 Z_\infty - k_2 W_\infty + k_3 P_0 V_\infty - k_4 W_\infty - k_5 f(Y_\infty) W_\infty \\
0 &= k_1 P_0 Z_\infty - k_4 W_\infty - k_5 f(Y_\infty) W_\infty \\
W_\infty &= \frac{k_1 P_0 Z_\infty}{k_4 + k_5 f(Y_\infty)}. \qquad (4.33)
\end{aligned}$$

Using (4.32) again, we also can express V_∞ in terms of Z_∞ and Y_∞,

$$\begin{aligned}
k_3 P_0 V_\infty = k_2 W_\infty &= \frac{k_1 k_2 P_0 Z_\infty}{k_4 + k_5 f(Y_\infty)} \\
V_\infty &= \frac{k_1 k_2 Z_\infty}{k_3 (k_4 + k_5 f(Y_\infty))}. \qquad (4.34)
\end{aligned}$$

Finally, we have all the necessary functions expressed in terms of Z_∞ and Y_∞. Furthermore, we can compute Z_∞ entirely in terms of Y_∞. From (4.28) we know

$$-k_+ T_\infty Y_\infty^2 + k_- Z_\infty + k_1 P_0 Z_\infty = 0.$$

Using this in equation (4.19),

$$\begin{aligned}
\lim_{t\to\infty} \dot{Y} &= \lim_{t\to\infty} (-2k_+ T Y^2 + 2k_- Z + k_1 Z P_0 + k_2 W - k_6 Y P_0 (2Y + J)) \\
0 &= -2k_+ T_\infty Y_\infty^2 + 2k_- Z_\infty + k_1 P_0 Z_\infty + k_2 W_\infty - 2k_6 P_0 Y_\infty^2 - k_6 P_0 Y_\infty J_\infty \\
0 &= -k_+ T_\infty Y_\infty^2 + k_- Z_\infty + k_2 W_\infty - 2k_6 P_0 Y_\infty^2 - k_6 P_0 Y_\infty J_\infty \qquad (4.35)
\end{aligned}$$

Recalling from (4.29) that

$$-k_+ T_\infty Y_\infty^2 + k_- Z_\infty = -k_6 P_0 J_\infty Y_\infty,$$

we use this substitution in (4.35) to further simplify and determine

$$0 = k_2 W_\infty - 2k_6 P_0 Y_\infty^2$$
$$k_2 W_\infty = 2k_6 P_0 Y_\infty^2$$

Using this result with (4.33), we compute

$$\frac{k_1 k_2 P_0 Z_\infty}{k_4 + k_5 f(Y_\infty)} = 2k_6 P_0 Y_\infty^2$$
$$Z_\infty = \frac{2k_6 Y_\infty^2 (k_4 + k_5 f(Y_\infty))}{k_1 k_2}$$

Finally, using the relations (4.30), (4.31), and (4.34) in conservation law (3.4) we have

$$\begin{aligned} T_\infty + Z_\infty + V_\infty + W_\infty + W_\infty^* &= T_0 \\ Z_\infty \left(\frac{k_- + k_1 P_0}{k_+ Y_\infty^2} + 1 + \frac{k_1 k_2}{k_3 (k_4 + k_5 f(Y_\infty))} + \frac{k_1 P_0}{k_5 f(Y_\infty)} \right) &= T_0 \\ \left(\frac{2k_6 Y_\infty^2 (k_4 + k_5 f(Y_\infty))}{k_1 k_2} \right) \left(\frac{k_- + k_1 P_0}{k_+ Y_\infty^2} + 1 + \frac{k_1 k_2}{k_3 (k_4 + k_5 f(Y_\infty))} + \frac{k_1 P_0}{k_5 f(Y_\infty)} \right) &= T_0 \end{aligned} \tag{4.36}$$

Expanding $f(Y)$ (see Appendix A.3) produces a fourth order polynomial, $\mathcal{P}\left(Y_\infty^2\right)$. This means that roots of $\mathcal{P}$ come in pairs $\pm Y_\infty$. In the context of our problem, we only consider the positive roots. Noting that the Y-intercept is positive,

$$\mathcal{P}(0) = 2\kappa_R^8 k_+ k_1 k_3 k_4 k_6 P_0$$

there can be up to 4 nonzero, positive, real roots. Furthermore, the leading coefficient is positive (see Appendix A.3), so it's possible that no real roots exist. When real, nonzero roots do exist, every such solution will determine a unique set of limiting

values for the other components, T_∞, Z_∞, V_∞, W_∞, W^*_∞, J_∞. Finally, from equations (4.27) and (4.26) we can compute

$$D_\infty = \lim_{t\to\infty} k_6 P_0 \int_0^t [Y(\tau)]^2 d\tau$$
$$G_\infty = \lim_{t\to\infty} k_6 P_0 \int_0^t J(\tau)Y(\tau) d\tau$$

Because we assume $Y_\infty > 0$, it follows that $J_\infty \neq 0$ and the integrals will diverge. □

Proof of Theorem 3 In all cases, either Lemma 4.6 or Lemma 4.7 is satisfied. These results create the dichotomy that is the conclusion of Theorem 3. ■

4.1.5 Proof of Theorem 4 for Model 4 *(Full Model)*

In this section we prove the results for the full model. Recall system (3.1) is

$$\dot{Y} = -2k_+TY^2 + 2k_-Z + k_1ZP + k_2W - k_6YP(2Y + J) \tag{4.37}$$
$$\dot{T} = -k_+TY^2 + k_-Z + k_5f(Y)(W + W^*) \tag{4.38}$$
$$\dot{Z} = k_+TY^2 - k_-Z - k_1ZP \tag{4.39}$$
$$\dot{W} = k_1ZP - k_2W + k_3VP - k_4W - k_5f(Y)W \tag{4.40}$$
$$\dot{V} = k_2W - k_3VP \tag{4.41}$$
$$\dot{W}^* = k_4W - k_5f(Y)W^* \tag{4.42}$$
$$\dot{J} = k_5f(Y)(W + W^*) - k_6JYP \tag{4.43}$$
$$\dot{G} = k_6JYP \tag{4.44}$$
$$\dot{D} = k_6Y^2P \tag{4.45}$$

with initial conditions (3.2),

$$(Y(0), T(0), Z(0), W(0), V(0), W^*(0), J(0), G(0), D(0)) = (Y_0, T_0, 0, 0, 0, 0, 0, 0, 0)$$

and where

$$f(Y) := \frac{Y^4}{\kappa_R^4 + Y^4},$$

$$P := \frac{P_0}{1 + \frac{Z+V+\kappa_2(Y^2+JY)}{\kappa_1}}.$$

Equations (4.38)-(4.42) admit conservation law (3.4),

$$T + Z + W + V + W^* = T_0$$

so the component functions are bounded in $[0, T_0]$ for all t.

Lemma 4.8. *In the system (3.1) with initial conditions (3.2), if*

1. $\dot{T}_\infty,\ \dot{Z}_\infty,\ \dot{W}_\infty,\ \dot{V}_\infty,\ \dot{W}^*_\infty,\ \dot{J}_\infty,\ \dot{Y}_\infty$ *exist and are finite*

2. *and* $Y_\infty = 0$,

then

$$\lim_{t\to\infty}(Y, T, Z, W, V, W^*, J, G, D, P) = (0, T_\infty, 0, 0, 0, W^*_\infty, 0, G_\infty, D_\infty, P_0)$$

where

$$\begin{aligned}
T_\infty &= \lim_{t\to\infty} \frac{\int_0^t e^{\int_0^s k_+[Y(\tau)]^2 d\tau}(k_- Z(s) + k_5 h(Y(s))[W(s) + W^*(s)])ds + T_0}{e^{\int_0^t k_+[Y(\tau)]^2 d\tau}} \\
W^*_\infty &= \lim_{t\to\infty} \frac{\int_0^t e^{\int_0^s k_5 h(Y(\tau))d\tau} k_4 W(s) ds}{e^{\int_0^t k_5 h(Y(\tau))d\tau}} \\
G_\infty &= \lim_{t\to\infty} k_6 \int_0^t \frac{\kappa_1 P_0 J(\tau) Y(\tau)}{\kappa_1 + Z(\tau) + V(\tau) + \kappa_2 \left(J(\tau)Y(\tau) + [Y(\tau)]^2\right)} d\tau \\
D_\infty &= \lim_{t\to\infty} k_6 \int_0^t \frac{\kappa_1 P_0 [Y(\tau)]^2}{\kappa_1 + Z(\tau) + V(\tau) + \kappa_2 \left(J(\tau)Y(\tau) + [Y(\tau)]^2\right)} d\tau
\end{aligned}$$

and $T_\infty + W^*_\infty = T_0$. G_∞ *and* D_∞ *may diverge to infinity.*

Proof. The assumptions satisfy the hypotheses of Lemma 4.3, so we know J is bounded and P is uniformly bounded away from zero. With conservation law (3.4), the hypotheses of Corollary 4.2.1 are satisfied for functions $Y,\ T,\ Z,\ W,\ V,\ W^*$, and J, so

$$\dot{Y}_\infty = \dot{T}_\infty = \dot{Z}_\infty = \dot{W}_\infty = \dot{V}_\infty = W^*_\infty = J_\infty = 0$$

and $T_\infty,\ Z_\infty,\ W_\infty,\ V_\infty,\ W^*_\infty$ and J_∞ exist and are finite. Now using the second assumption and the fact that T is bounded, we see from equation (4.39) that

$$\begin{aligned}
\lim_{t\to\infty} \dot{Z} &= \lim_{t\to\infty} \left(k_+ T Y^2 - k_- Z + k_1 Z P)\right) \\
0 &= k_+ T_\infty \cdot 0^2 - k_- Z_\infty - k_1 Z_\infty P_\infty \\
0 &= Z_\infty (k_- + k_1 P_\infty)
\end{aligned}$$

so it must be that $Z_\infty = 0$. Since also $\dot{J}_\infty = 0$, we can compute

$$\begin{aligned}
\lim_{t\to\infty} \dot{J} &= \lim_{t\to\infty} \left(k_5 f(Y)(W + W^*) - k_6 Y J P\right) \\
0 &= k_5 f(Y_\infty)(W_\infty + W^*_\infty) - k_6 Y_\infty J_\infty P_\infty \\
k_5 f(Y_\infty)(W_\infty + W^*_\infty) &= k_6 Y_\infty J_\infty P_\infty
\end{aligned}$$

Before evaluating Y_∞, however, we expand the $f(Y)$ and P functions to obtain

$$\frac{Y_\infty^4 (W_\infty + W^*_\infty)}{\kappa_R^4 + Y_\infty^4} = \frac{\kappa_1 k_6 P_0 Y_\infty J_\infty}{\kappa_1 + Z_\infty + V_\infty + \kappa_2 \left(Y_\infty J_\infty + Y_\infty^2\right)}$$

and cross multiply to find that

$$Y_\infty^4 (W_\infty + W^*_\infty) \left(\kappa_1 + Z_\infty + V_\infty + \kappa_2 \left(Y_\infty J_\infty + Y_\infty^2\right)\right) = \kappa_1 k_6 P_0 Y_\infty J_\infty \left(\kappa_R^4 + Y_\infty^4\right).$$

Dividing each side by Y_∞ and noting that $Y_\infty = 0$ is a known solution, we have

$$Y_\infty^3(W_\infty + W_\infty^*)\left(\kappa_1 + Z_\infty + V_\infty + \kappa_2\left(Y_\infty J_\infty + Y_\infty^2\right)\right) = \kappa_1 k_6 P_0 J_\infty\left(\kappa_R^4 + Y_\infty^4\right).$$

Finally substituting in the assumed value $Y_\infty = 0$, we see

$$0 = \kappa_1 \kappa_R^4 k_6 P_0 J_\infty$$

which implies that $J_\infty = 0$ as well.

Now considering equation (4.40), we have the result that

$$\begin{aligned}
\lim_{t\to\infty} \dot{W} &= \lim_{t\to\infty} (k_1 ZP - k_2 W + k_3 VP - k_4 W - k_5 f(Y)W) \\
0 &= k_1 \cdot P_\infty - k_2 W_\infty + k_3 V_\infty P_\infty - k_4 W_\infty - k_5 f(0) W_\infty \\
0 &= -(k_2 + k_4)W_\infty + k_3 V_\infty P_\infty \\
(k_2 + k_4)W_\infty &= k_3 V_\infty P_\infty \qquad (4.46)
\end{aligned}$$

Similarly for equation (4.41),

$$\begin{aligned}
\lim_{t\to\infty} \dot{V} &= \lim_{t\to\infty} (k_2 W - k_3 VP) \\
0 &= k_2 W_\infty - k_3 V_\infty P_\infty \\
k_2 W_\infty &= k_3 V_\infty P_\infty \qquad (4.47)
\end{aligned}$$

Putting together results (4.46) and (4.47), we observe that

$$k_3 V_\infty P_\infty = k_2 W_\infty = (k_2 + k_4) W_\infty.$$

Clearly we conclude that $W_\infty = 0$. Furthermore, because J is bounded, Lemma

4.3 tells us that P is bounded away from zero. Thus this relation also implies that $V_\infty = 0$. Finally, using these results in (3.5), we conclude that

$$P_\infty = \frac{P_0}{1 + \frac{Z_\infty + V_\infty + \kappa_2(Y_\infty^2 + Y_\infty J_\infty)}{\kappa_1}} = P_0$$

Because equations (4.38) and (4.42) are first order, linear, variable coefficient ODEs, they have closed form solutions

$$T = \frac{\int_0^t e^{\int_0^s k_+[Y(\tau)]^2 d\tau}(k_- Z(s) + k_5 h(Y(s))[W(s) + W^*(s)])ds + T_0}{e^{\int_0^t k_+[Y(\tau)]^2 d\tau}}$$
$$W^* = \frac{\int_0^t e^{\int_0^s k_5 h(Y(\tau))d\tau} k_4 W(s) ds}{e^{\int_0^t k_5 h(Y(\tau))d\tau}}$$

which lead to expressions

$$T_\infty = \lim_{t\to\infty} \frac{\int_0^t e^{\int_0^s k_+[Y(\tau)]^2 d\tau}(k_- Z(s) + k_5 h(Y(s))[W(s) + W^*(s)])ds + T_0}{e^{\int_0^t k_+[Y(\tau)]^2 d\tau}}$$
$$W^*_\infty = \lim_{t\to\infty} \frac{\int_0^t e^{\int_0^s k_5 h(Y(\tau))d\tau} k_4 W(s) ds}{e^{\int_0^t k_5 h(Y(\tau))d\tau}}.$$

Because $Z_\infty = W_\infty = V_\infty = 0$, conservation law (3.4) requires that $T_\infty + W^*_\infty = T_0$. Finally, we can also numerically compute

$$G_\infty = \lim_{t\to\infty} k_6 \int_0^t \frac{\kappa_1 P_0 J(\tau) Y(\tau)}{\kappa_1 + Z(\tau) + V(\tau) + \kappa_2 \left(J(\tau)Y(\tau) + [Y(\tau)]^2\right)} d\tau$$
$$D_\infty = \lim_{t\to\infty} k_6 \int_0^t \frac{\kappa_1 P_0 [Y(\tau)]^2}{\kappa_1 + Z(\tau) + V(\tau) + \kappa_2 \left(J(\tau)Y(\tau) + [Y(\tau)]^2\right)} d\tau$$

where G_∞ and D_∞ may diverge to infinity. □

Lemma 4.9. *In the system (3.1) with initial conditions (3.2), if*

1. $\dot{T}_\infty,\ \dot{Z}_\infty,\ \dot{W}_\infty,\ \dot{V}_\infty,\ \dot{W}^*_\infty,\ \dot{Y}_\infty$ *exist and are finite*

2. $Y_\infty \neq 0$

then there's a seventh order polynomial $\mathcal{P}\left(Y^2\right)$ *such that* Y_∞ *can correspond to up to seven positive, real roots of* $\mathcal{P}\left(Y_\infty^2\right) = 0$*. Furthermore, if any real values for* Y_∞ *exist, then there are rational functions* $\mathcal{T}(Y),\ \mathcal{Z}(Y),\ \mathcal{W}(Y),\ \mathcal{V}(Y), \mathcal{W}^*(Y)$*, and* $\mathcal{J}(Y)$ *such that*

$$T_\infty = \mathcal{T}(Y_\infty),\ Z_\infty = \mathcal{Z}(Y_\infty),\ W_\infty = \mathcal{W}(Y_\infty),$$

$$V_\infty = \mathcal{V}(Y_\infty),\ W_\infty^* = \mathcal{W}^*(Y_\infty),\ J_\infty = \mathcal{J}(Y_\infty),$$

and $D,\ G$ *will diverge to infinity.*

Proof. The assumptions satisfy the hypotheses of Lemma 4.3, so we know P is uniformly bounded away from zero and that Y is bounded. With conservation law (3.4), the hypotheses of Corollary 4.2.1 are satisfied for the functions $Y,\ T,\ Z,\ W,\ V,\ W^*$, so

$$\dot{Y}_\infty = \dot{T}_\infty = \dot{Z}_\infty = \dot{W}_\infty = \dot{V}_\infty = W_\infty^* = 0$$

and $Y_\infty,\ T_\infty,\ Z_\infty,\ W_\infty,\ V_\infty,\ W_\infty^*$ exist and are finite. Using the relationships that form as a consequence of these results and the conservation law (3.4), we will construct a function of Y_∞ exclusively. Starting with equation (4.39), we compute

$$\begin{aligned}
\lim_{t\to\infty} \dot{Z} &= \lim_{t\to\infty} \left(k_+ T Y^2 - k_- Z - k_1 Z P\right) \\
0 &= k_+ T_\infty Y_\infty^2 - k_- Z_\infty - k_1 Z_\infty P_\infty \\
T_\infty &= \frac{(k_- + k_1 P_\infty) Z_\infty}{k_+ Y_\infty^2}.
\end{aligned} \tag{4.48}$$

Noting that equations (4.40) and (4.41) sum to

$$\dot{W} + \dot{V} = k_1 Z P - k_4 W - k_5 f(Y) W,$$

we compute

$$\begin{aligned}
\lim_{t\to\infty}(\dot{W}+\dot{V}) &= \lim_{t\to\infty}(k_1ZP - k_4W - k_5f(Y)W) \\
0 &= k_1Z_\infty P_\infty - k_4W_\infty - k_5f(Y_\infty)W_\infty \\
W_\infty &= \frac{k_1Z_\infty P_\infty}{k_4 + k_5f(Y_\infty)}. \qquad (4.49)
\end{aligned}$$

Similarly for equation (4.41),

$$\begin{aligned}
\lim_{t\to\infty}\dot{V} &= \lim_{t\to\infty}(k_2W - k_3VP) \\
0 &= k_2W_\infty - k_3V_\infty P_\infty \\
V_\infty &= \frac{k_2W_\infty}{k_3P_\infty}
\end{aligned}$$

and with relation (4.49), we have that

$$V_\infty = \frac{k_1k_2Z_\infty}{k_3(k_4 + k_5f(Y_\infty))}. \qquad (4.50)$$

Now summing equations (4.38) and (4.39) we see that

$$\dot{T} + \dot{Z} = k_5f(Y)(W + W^*) - k_1ZP$$

and we can compute

$$\begin{aligned}
\lim_{t\to\infty}(\dot{T}+\dot{Z}) &= \lim_{t\to\infty}(k_5f(Y)(W+W^*) - k_1ZP) \\
0 &= k_5f(Y_\infty)(W_\infty + W^*_\infty) - k_1Z_\infty P_\infty \\
W_\infty + W^*_\infty &= \frac{k_1Z_\infty P_\infty}{k_5f(Y_\infty)}. \qquad (4.51)
\end{aligned}$$

At this point, we have values for every component of conservation law (3.4) in terms

of Z_∞, Y_∞, and P_∞. Because P is a function of J, we next consider J_∞. By Lemma 4.3, we know that J is bounded and P is uniformly bounded away from zero. First Corollary 4.2.1 implies that J_∞ exists and is finite. Then equation (4.43) shows that

$$\begin{aligned}
\lim_{t\to\infty} \dot{J} &= \lim_{t\to\infty} (k_5 f(Y)(W + W^*) - k_6 JYP) \\
0 &= k_5 f(Y_\infty)(W_\infty + W^*_\infty) - k_6 J_\infty Y_\infty P_\infty \\
k_6 J_\infty Y_\infty P_\infty &= k_5 f(Y_\infty)(W_\infty + W^*_\infty). \qquad (4.52)
\end{aligned}$$

Combining (4.51) and (4.52) we get

$$k_6 J_\infty Y_\infty P_\infty = k_5 f(Y_\infty)(W_\infty + W^*_\infty) = k_1 Z_\infty P_\infty \qquad (4.53)$$

and since $P_\infty \neq 0$,

$$J_\infty = \frac{k_1 Z_\infty}{k_6 Y_\infty}$$

Now we have all components of conservation law (3.4) in terms of Z_∞ and Y_∞. Because we haven't used (4.37) yet, we can solve for Z_∞ in terms of Y_∞. Using the outside equivalencies on relation (4.53) in equation (4.37), we see that

$$\begin{aligned}
\lim_{t\to\infty} \dot{Y} &= \lim_{t\to\infty} (-2k_+ TY^2 + 2k_- Z + k_1 ZP + k_2 W - k_6 YP(2Y + J)) \\
0 &= -2k_+ T_\infty Y_\infty^2 + 2k_- Z_\infty + k_1 Z_\infty P_\infty + k_2 W_\infty - 2k_6 Y_\infty^2 P_\infty - k_6 J_\infty P_\infty Y_\infty
\end{aligned}$$

reduces to

$$\begin{aligned}
0 &= -2k_+ T_\infty Y_\infty^2 + 2k_- Z_\infty + k_2 W_\infty - 2k_6 Y_\infty^2 P_\infty \\
2Y_\infty^2 (k_+ T_\infty + k_6 P_\infty) &= 2k_- Z_\infty + k_2 W_\infty.
\end{aligned}$$

Substituting relation (4.48) for T_∞ and (4.49) for W_∞, we have

$$2Y_\infty^2\left(\frac{k_+(k_- + k_1P_\infty)Z_\infty}{k_+Y_\infty^2} + k_6P_\infty\right) = 2k_-Z_\infty + k_2\left(\frac{k_1Z_\infty P_\infty}{k_4 + k_5f(Y_\infty)}\right)$$

which simplifies to

$$2k_-Z_\infty + 2k_1P_\infty Z_\infty + 2k_6P_\infty Y_\infty^2 = 2k_-Z_\infty + \frac{k_1k_2Z_\infty P_\infty}{k_4 + k_5f(Y_\infty)}.$$

Subtracting $2k_-Z_\infty$ and then dividing P_∞ from both sides, we have

$$2k_1Z_\infty + 2k_6Y_\infty^2 = \frac{k_1k_2Z_\infty}{k_4 + k_5f(Y_\infty)}$$

and we can collect the Z_∞ terms on the right side,

$$2k_6Y_\infty^2 = Z_\infty\left(\frac{k_1k_2}{k_4 + k_5f(Y_\infty)} - 2k_1\right)$$

to solve for Z_∞ in terms of Y_∞,

$$Z_\infty = \frac{2k_6}{k_1}\left(\frac{k_4 + k_5f(Y_\infty)}{k_2 - 2(k_4 + k_5f(Y_\infty))}\right)Y_\infty^2 \tag{4.54}$$

Finally, we can use relations (4.48), (4.50), and (4.51) in the conservation law (3.4) to construct an equation in Y_∞,

$$T_\infty + Z_\infty + W_\infty + W_\infty^* + V_\infty = T_0$$

$$Z_\infty\left(\frac{k_- + k_1P_\infty}{k_+Y_\infty^2} + 1 + \frac{k_1P_\infty}{k_5f(Y_\infty)} + \frac{k_1k_2}{k_3(k_4 + k_5f(Y_\infty))}\right) = T_0 \tag{4.55}$$

where Z_∞ and P_∞ can be expressed in terms of Y_∞. Expanding Z_∞, P_∞ and $f(Y_\infty)$ in this function (see Appendix A.4) produces a seventh order polynomial, $\mathcal{P}\left(Y_\infty^2\right)$.

This means that reals roots come in pairs $\pm Y_\infty$. In the context of our problem, we only consider the positive roots. Noting that

$$\mathcal{P}(0) = 2\kappa_1\kappa_R^{12}k_+k_1^2k_3^2k_4k_6P_0(2k_4 - k_2),$$

there can be up to 7 positive real roots if $k_2 \neq 2k_4$. Furthermore, the leading coefficient is negative so when $k_2 > 2k_4$ (as generally is expected for this system), it's possible that no real nonzero roots exist. When real, nonzero roots do exist, every such solution will determine a unique set of limiting values for the other components T_∞, Z_∞, V_∞, W_∞, W_∞^*, P_∞, J_∞. Finally, from equations (4.45) and (4.44), we can compute

$$\begin{aligned} D_\infty &= \lim_{t\to\infty} k_6 \int_0^t \frac{\kappa_1 P_0[Y(\tau)]^2}{\kappa_1 + Z(\tau) + V(\tau) + \kappa_2\left(J(\tau)Y(\tau) + [Y(\tau)]^2\right)} d\tau \\ G_\infty &= \lim_{t\to\infty} k_6 \int_0^t \frac{\kappa_1 P_0 J(\tau)Y(\tau)}{\kappa_1 + Z(\tau) + V(\tau) + \kappa_2\left(J(\tau)Y(\tau) + [Y(\tau)]^2\right)} d\tau \end{aligned}$$

Because we assume $Y_\infty > 0$, we have $P_\infty,\ J_\infty > 0$ and these integrals diverge. □

Proof of Theorem 4 In all cases, either Lemma 4.8 or Lemma 4.9 is satisfied. These two then lead to the dichotomy that is the conclusion of Theorem 4. ■

4.2 Proofs for Multiple Time Scale Analysis

4.2.1 Proof of Theorem 5 for Model I

In this section, we prove the results regarding the $\mathcal{O}(1)$ reactions. Recall that system (3.20) is

$$y' = -2ty^2 + 2\alpha z \tag{4.56}$$

$$t' = -ty^2 + \alpha z \tag{4.57}$$

$$z' = ty^2 - \alpha z \tag{4.58}$$

$$w' = 0 \tag{4.59}$$

$$v' = 0 \tag{4.60}$$

$$u' = 0 \tag{4.61}$$

$$j' = 0 \tag{4.62}$$

with initial conditions (3.23)

$$(y_0, t_0, z_0, w_0, v_0, u_0, j_0) = (\varepsilon, 1, 0, 0, 0, 0, 0).$$

and conservation laws (3.21)-(3.22),

$$2z + y = \varepsilon$$

$$z + t = 1$$

Using the initial conditions, we explicitly solve (4.59)-(4.62)

$$w(\tau) \equiv 0, \qquad v(\tau) \equiv 0, \qquad u(\tau) \equiv 0, \qquad j(\tau) \equiv 0$$

and consider the remaining equations, (4.56)-(4.58). From conservation law (3.22) we have $t = 1 - z$ and from conservation law (3.21) we have $y = \varepsilon - 2z$. Using these expressions in equation (4.58), we can construct a single, dimensionless ODE to interpret the dynamics of system (4.56)-(4.58),

$$z' = (1 - z)(\varepsilon - 2z)^2 - \alpha z =: g(z). \tag{4.63}$$

The cubic term $(1-z)(\varepsilon-2z)^2$ has a double root at $z = \frac{\varepsilon}{2}$ and a simple root at $z = 1$. First we note that because

$$g(0) = \varepsilon^2 > 0$$

and

$$g\left(\frac{\varepsilon}{2}\right) = -\frac{\alpha\varepsilon}{2} < 0,$$

the Intermediate Value Theorem implies there's a value $z_* \in \left[0, \frac{\varepsilon}{2}\right]$ such that $g(z_*) = 0$. Then because $(1-z)(\varepsilon-2z)^2$ is monotonically decreasing and αz is monotonically increasing on $[0, \frac{\varepsilon}{2}]$, we have

$$g'(z) > 0 \text{ for } z \in \left[0, \frac{\varepsilon}{2}\right].$$

Thus by the Mean Value Theorem, the solution z_* of $g(z_*) = 0$ is unique. Since $z_* \in \left[0, \frac{\varepsilon}{2}\right]$ we also have an upper bound on z_*,

$$z_* \leq \frac{\varepsilon}{2} \sim \mathcal{O}(\varepsilon) = \mathcal{O}\left(10^{-4}\right).$$

Finally, with the initial condition $z(0) = 0$ and because (4.63) is a scalar differential equation, it follows that

$$\lim_{\tau\to\infty} z = z^*$$

and this equilibrium is stable. Therefore this system has one stable equilibrium,

$$(y_*, t_*, z_*, w_*, v_*, u_*, j_*) = (\varepsilon - 2z_*, 1 - z_*, z_*, 0, 0, 0, 0)$$

where $t \sim \mathcal{O}(1)$ and $y, z < \mathcal{O}\left(10^{-4}\right)$. ■

4.2.2 Proof of Theorem 6 for Model II

In this section, we prove the results regarding the $\mathcal{O}\left(10^{-4}\right)$ reactions when $y < 10$. Recall system (3.25) is

$$\begin{aligned}
y' &= -2ty^2 + (2\alpha + \beta)z + \gamma w \\
t' &= -ty^2 + \alpha z \\
z' &= ty^2 - (\alpha + \beta)z \\
w' &= \beta z + \delta v - (\gamma + \lambda)w \\
v' &= -\delta v + \gamma w \\
u' &= \lambda w \\
j' &= 0
\end{aligned}$$

with initial conditions in the neighborhood of (3.24) at a time τ_1,

$$(y_{\tau_1}, t_{\tau_1}, z_{\tau_1}, w_{\tau_1}, v_{\tau_1}, u_{\tau_1}, j_{\tau_1}) = (\varepsilon - 2z_*, 1 - z_*, z_*, 0, 0, 0, 0),$$

and has conservation law (3.26),

$$t + z + w + v + u = 1.$$

Using this law in the form $t \equiv 1 - z - w - v - u$, we can eliminate the t' equation from the system. Solving the last equation explicitly with initial condition $j(\tau_1) = 0$ from (3.24), we have

$$j(\tau) \equiv 0.$$

Thus the solutions of (3.25) can be obtained by solving the reduced system

$$y' = -2(1 - z - w - v - u)y^2 + (2\alpha + \beta)z + \gamma w \tag{4.64}$$

$$z' = (1 - z - w - v - u)y^2 - (\alpha + \beta)z \tag{4.65}$$

$$w' = \beta z + \delta v - (\gamma + \lambda)w \tag{4.66}$$

$$v' = -\delta v + \gamma w \tag{4.67}$$

$$u' = \lambda w \tag{4.68}$$

and pairing the results with

$$t \equiv 1 - z - w - v - u, \qquad j \equiv 0$$

to fully solve the system. We reduce the initial conditions approximation (3.24) to

$$(y_{\tau_1}, z_{\tau_1}, w_{\tau_1}, v_{\tau_1}, u_{\tau_1}) = (\varepsilon - 2z_*, z_*, 0, 0, 0).$$

Using the assumptions of the theorem, we seek equilibria for the reduced system (4.64)-(4.68). First observe from equation (4.68) that $w_* = 0$. With equation (4.67), this implies $v_* = 0$ and with equation (4.66), these results imply that $z_* = 0$. Finally, equations (4.64) and (4.65) are satisfied if and only if

$$(1 - u_*)y_*^2 = 0.$$

The solutions of the reduced system form two one dimensional manifolds of equilibria,

$$\xi_1(u_*) = (0, 0, 0, 0, u_*), \qquad u_* \in [0, 1]$$
$$\xi_2(y_*) = (y_*, 0, 0, 0, 1), \qquad y_* \in [0, \infty)$$

where the limit on u_* follows from conservation law (3.26). Because $j(\tau) \equiv 0$, this corresponds to one dimensional manifolds of equilibria of the full system,

$$E_1(u_*) = (y_*, t_*, z_*, w_*, v_*, u_*, j_*) = (0, 1 - u_*, 0, 0, 0, u_*, 0), \qquad u_* \in [0, 1]$$
$$E_2(y_*) = (y_*, t_*, z_*, w_*, v_*, u_*, j_*) = (y_*, 0, 0, 0, 0, 1, 0), \qquad y_* \in [0, \infty).$$

■

4.2.3 Center Manifold Dynamics for Model II

In this section we compute a center manifold W^c for an arbitrary $x \in \xi_1$. Because there are three negative eigenvalues for $\mathcal{J}(x)$, there's a three dimensional stable manifold where the functions not in the span of the zero eigenspace, z, w, and v, exponentially converge to W^c. To examine the higher order dynamics of (3.29) near x, we approximate the second order behavior of the functions y and u on a center manifold W^c [49].

We first define a change of variables $\nu = u_* - u$ to move x to the origin so all linear terms will have coefficient zero. Then we approximate the second order

behavior of z, w, and v near the shifted equilibrium with

$$\begin{aligned} z &= f(y,\nu) = a_1y^2 + b_1y\nu + c_1\nu^2 \\ w &= g(y,\nu) = a_2y^2 + b_2y\nu + c_2\nu^2 \\ v &= h(y,\nu) = a_3y^2 + b_3y\nu + c_3\nu^2. \end{aligned} \tag{4.69}$$

These approximations have derivatives

$$\begin{aligned} z' &= y'(2a_1y + b_1\nu) + \nu'(b_1y + 2c_1\nu) \\ w' &= y'(2a_2y + b_2\nu) + \nu'(b_2y + 2c_2\nu) \\ v' &= y'(2a_3y + b_3\nu) + \nu'(b_3y + 2c_3\nu). \end{aligned} \tag{4.70}$$

Substituting expressions (4.69) for z, w, v into equations (4.64)-(4.68), the system can be expressed in terms of y and ν

$$\begin{aligned} y' = &-2[1 - (a_1 + a_2 + a_3)y^2 - (b_1 + b_2 + b_3)y\nu - (c_1 + c_2 + c_3)\nu^2 - \nu]y^2 \\ &+ (2\alpha + \beta)(a_1y^2 + b_1y\nu + c_1\nu^2) + \gamma(a_2y^2 + b_2y\nu + c_2\nu^2) \end{aligned} \tag{4.71}$$

$$\begin{aligned} z' = &[1 - (a_1 + a_2 + a_3)y^2 - (b_1 + b_2 + b_3)y\nu - (c_1 + c_2 + c_3)\nu^2 - \nu]y^2 \\ &- (\alpha + \beta)(a_1y^2 + b_1y\nu + c_1\nu^2) \end{aligned} \tag{4.72}$$

$$w' = \beta(a_1y^2 + b_1y\nu + c_1\nu^2) + \delta(a_3y^2 + b_3y\nu + c_3\nu^2) - (\gamma + \lambda)(a_2y^2 + b_2y\nu + c_2\nu^2) \tag{4.73}$$

$$v' = -\delta(a_3y^2 + b_3y\nu + c_3\nu^2) + \gamma(a_2y^2 + b_2y\nu + c_2\nu^2) \tag{4.74}$$

$$\nu' = \lambda(a_2y^2 + b_2y\nu + c_2\nu^2) \tag{4.75}$$

By plugging (4.71) and (4.75) into the derivatives of the approximation (4.70), we have equations for z', w', and v' that can be solved with (4.72), (4.73), and (4.74)

respectively to solve for the unknown coefficients, a_1, a_2, a_3, b_1, b_2, b_3, c_1, c_2, c_3. We simplify these expressions with Mathematica in Appendix A.5 and collect the coefficients of the leading order terms, y^2, ν^2, and $y\nu$. Comparing (4.70) with equation (4.72), we find the coefficients

$$a_1(\alpha+\beta) = 1, \quad b_1(\alpha+\beta) = 0, \quad c_1(\alpha+\beta) = 0$$

so

$$a_1 = \frac{1}{\alpha+\beta}, \qquad b_1 = 0, \qquad c_1 = 0.$$

Comparing equations (4.70) and (4.73), we have coefficients

$$a_2(\gamma+\lambda) = a_1\beta + a_3\delta, \quad b_2(\gamma+\lambda) = b_1\beta + b_3\delta, \quad c_2(\gamma+\lambda) = c_1\beta + c_3\delta$$

and comparing equations (4.70) and (4.74), we have coefficients

$$a_3\delta = a_2\gamma, \quad b_3\delta = b_2\gamma, \quad c_3\delta = c_2\gamma.$$

This implies that

$$\begin{aligned} a_2 &= \frac{\beta}{\lambda(\alpha+\beta)}, \qquad b_2 = 0, \qquad c_2 = 0 \\ a_3 &= \frac{\beta\gamma}{\delta\lambda(\alpha+\beta)}, \qquad b_3 = 0, \qquad c_3 = 0 \end{aligned}$$

and the second order approximation of $W^c(x)$ is

$$z = \left(\frac{1}{\alpha+\beta}\right) y^2, \qquad w = \left(\frac{\beta}{\lambda(\alpha+\beta)}\right) y^2, \qquad v = \left(\frac{\beta\gamma}{\delta\lambda(\alpha+\beta)}\right) y^2.$$

These parameterizations, substituted into equations (4.71) and (4.74), approximate

the second order, nonlinear dynamics of y and ν on a center manifold W^c near x,

$$
\begin{aligned}
y' &= y^2 \left[2\nu + \left(\frac{2(\delta\lambda + \beta\delta + \beta\gamma)}{\delta\lambda(\alpha+\beta)} \right) y^2 + \frac{\beta(\gamma-\lambda)}{\lambda(\alpha+\beta)} \right] \\
\nu' &= \left(\frac{\beta}{\alpha+\beta} \right) y^2.
\end{aligned}
$$

Because $\nu' = u'$, in the original variables we have the flow

$$
\begin{aligned}
y' &= y^2 \left[2(u_* - u) + \left(\frac{2(\delta\lambda + \beta\delta + \beta\gamma)}{\delta\lambda(\alpha+\beta)} \right) y^2 + \frac{\beta(\gamma-\lambda)}{\lambda(\alpha+\beta)} \right] \\
u' &= \left(\frac{\beta}{\alpha+\beta} \right) y^2.
\end{aligned}
$$

CHAPTER FIVE

CONCLUSION

Clear and accurate microRNA (miRNA) expression profiles have the potential to paint precise pictures of the latent biological processes behind disease and injury. Aberrant miRNA expression has been shown to indicate heart disease, neurological diseases, autoimmune diseases, infectious diseases, and even acute physical injuries. The challenge remains to develop an effective measuring protocol in the presence of the key challenges of high sequence homology and low concentrations of circulating miRNA. While PCR can successfully and reliably identify miRNAs, the technology requires rigorous attention to detail (highly trained personnel) to work with such small DNA strands and expensive equipment. Isothermal amplification is a less intensive technique that's shown great promise but still requires significant improvement to increase its specificity. In this work, we explore one such technique: Ultrasensitive DNA Amplification Reaction (UDAR). This technique is particularly suitable for mathematical investigation due to its distinctive biphasic amplification pattern. Besides UDAR, most isothermal amplification techniques show a relatively short initiation period followed by a single amplification period that quickly levels off the for the remaining experimental run time. UDAR has a slightly extended initiation period that gives way to two distinct amplification periods with different growth rates and separated by a plateau of slow growth, all occurring within one hour. The distinct growth rates, how much amplification occurs in those periods, and the length of the intermittent slow growth phases are all features that need to be explored, understood, and hopefully someday rationally tuned.

In this work, we determined the key mechanisms required to reproduce biphasic

amplification, (1) the deactivation of amplifying complexes and (2) the subsequent recycling of the deactivated amplifying complexes. This recycling of templates is facilitated by the UDAR's distinct recurrence of the target palindromic sequence in both templates and triggers, allowing the triggers to restart deactivated amplifiers when present in sufficient concentrations. Recycling then promotes unprecedented levels of DNA amplification compared to other isothermal amplification techniques. Together, these features create conditions that cause the reaction to level off as enzyme indeed becomes limiting. However, counter to initial suspicions, polymerase is the limiting enzyme and it's unavailable rather than depleted. In sufficient concentrations, the replicated palindromic triggers have an affinity to bind to each other and call on the polymerase enzyme to extend over the toehold regions. But when too many binding events demand polymerase synthesis, the availability of polymerase decreases, slowing the extension rate and thereby slowing the amplification rate.

Analyzing mathematical models for DNA amplification is largely unprecedented, so results presented here are the first attempt to understand the mechanisms behind the experiments of Özay et al. [26] and other researchers in the field [24, 36, 40]. We used numerical simulation, equilibrium analysis, and perturbation theory to isolate key features and examine their effects on the UDAR reaction. Using the first two approaches, we determined that deactivation and recycling are required to create two distinct amplification phases. With deactivation but not recycling, the equilibrium analysis gives ambiguous answers but numerical simulation shows the system behaves like another popular isothermal amplification reaction, EXPonential Amplification Reaction (EXPAR). This indicates EXPAR templates do in fact become deactivated before depleting the nicking enzyme. This is important because it shows the potential to design even stronger isothermal DNA amplification assays.

Perturbation theory shed light on the mechanisms behind the delayed initiation

phase. We found that the low initial concentration of trigger binds to a few templates and starts replicating a very small amount of trigger. This replication is so slow that the overall trigger concentration attempts to converge to zero. But, as the initiation term in the model is of the third order (TY^2), the zero equilibrium for trigger is actually nonlinearly unstable. When the trigger concentration is extremely small, it begins to increase. Eventually, through this process, the trigger attains the critical concentration needed for amplification to begin and rapidly enters the primary amplification phase.

Finally, we find that the solution trajectories first approach an unstable partial equilibrium with a very small positive eigenvalue and temporarily slow down, which manifests as the experimentally observed plateau. Once past the neighborhood of the unstable partial equilibrium, solutions proceed to converge to a second, stable partial equilibrium. If we assume the supply of polymerase is unlimited, long term behavior predicts the active reaction components: triggers, templates, and amplifier forms, will eventually equilibrate to a partial equilibrium value for the system. Because these components converge to nonzero values, inactive byproducts continue to form indefinitely. Finally, taking into account that polymerase is a finite resource that's sequestered by the demand of too many extension processes, we arrive at our full model. Here, numerical simulation shows the growth of inactive byproduct slows dramatically after about 30 minutes. The equilibrium analysis results in a seventh order polynomial whose positive real roots are in one-to-one correspondence with the partial equilibria of the full system. For the simulated rate parameters that reproduce experimental data, there are two satisfactory partial equilibria. As before, the smaller value is a saddle partial equilibrium that causes an amplification plateau and the larger value is a stable partial equilibrium near the final amplification level. This model accurately replicates all the distinctive characteristics of UDAR.

The presented work is a promising first step into modeling DNA amplification and a decisive step toward the rational design of effective techniques to quantify miRNA expression. These results can be adapted to help design molecular diagnostics, DNA circuits, and other synthetic biology applications. While the analysis techniques are general, our focus was firmly on one specific type of template, the UDAR Type II template. Fitting this model structure to a wide variety of template designs can help identify the important rate parameters. This knowledge could be used to design UDAR templates that produce a more precise signal. In addition, since we used several simplifications and experimentally unverified mechanisms in this work, there are several rate parameters that require further experimental investigation.

Combined with the modeling effort presented here, our results can guide the process of creating rationally designed isothermal DNA amplification reactions that will lead to clear and accurate readings of miRNA expression profiles.

REFERENCES CITED

[1] S. Ohno, "So much 'junk' in our genome," *Evolution of Genetic Systems*, pp. 366–372, 1972.

[2] J. Brosius and S. J. Gould, "On "genomenclature": A comprehensive (and respectful) taxonomy for pseudogenese and other "junk dna"," *Proceedings of the National Academy of Sciences*, vol. 89, no. 22, pp. 10706–10710, 1992.

[3] D. P. Bartel, "Genomics, biogenesis, mechanism, and function," *Cell*, vol. 116, no. 2, pp. 281–297, 2004.

[4] R. Deng, K. Zhang, and J. Li, "Isothermal amplification for microrna detection: From the test tube to the cell," *Accounts of Chemical Research*, vol. 50, no. 4, pp. 1059–1068, 2017.

[5] J. Wang, O. W. Liew, A. M. Richards, and Y.-T. Chen, "Overview of micrornas in cardiac hypertrophy, fibrosis, and apoptosis," *International Journal of Molecular Sciences*, vol. 17, no. 5, p. 749, 2016.

[6] E. Sun and Y. Shi, "Micrornas: Small molecules with big roles in neurodevelopment and diseases," *Experimental Neurology*, vol. 268, pp. 46–53, 2015.

[7] N. Baulina, O. Kulakova, and O. Favorova, "Micrornas: The role in autoimmune inflammation," *Acta naturae*, vol. 8, no. 1, pp. 21–33, 2016.

[8] J. Hayes, P. P. Peruzzi, and S. Lawler, "Micrornas in cancer: biomarkers, functions and therapy," *Trends in Molecular Medicine*, vol. 20, no. 8, pp. 460–469, 2014.

[9] K. Strimbu and J. A. Tavel, "What are biomarkers?," *Wolters Kluwer*, vol. 5, no. 6, pp. 463–466, 2010.

[10] Y.-K. Kim, "Extracellular micrornas as biomarkers in human disease," *Chonnam National University Medical School*, vol. 51, no. 2, pp. 51–57, 2015.

[11] K. Toffolo, J. Osei, W. Kelly, A. Poulsen, K. Donahue, J. Wang, M. Hunter, J. Bard, J. Wang, and D. Poulsen, "Circulating micrornas as biomarkers in traumatic brain injury," *Elsevier*, vol. 145, no. B, pp. 199–208, 2019.

[12] A. Liu and X. Xu, *MicroRNA Isolation from Formalin-Fixed, Paraffin-Embedded Tissues*, pp. 259–267. Totowa, NJ: Humana Press, 2011.

[13] P. S. Mitchell, R. K. Parkin, E. M. Kroh, B. R. Fritz, S. K. Wyman, E. L. Pogosova-Agadjanyan, A. Peterson, J. Noteboom, K. C. Briant, A. Allen, D. W. Lin, N. Urban, C. W. Drescher, B. S. Knudsen, D. L. Stirewalt, R. Gentleman, R. L. Vessella, P. S. Nelson, D. B. Martin, and M. Tewari, "Circulating micrornas as stable blood-based markers for cancer detection," *Proceedings of the National Academy of Sciences*, vol. 105, no. 30, pp. 10513–10518, 2008.

[14] A. Gallo, M. Tandon, I. Alevizos, and G. G. Illei, "The majority of micrornas detectable in serum and saliva is concentrated in exosomes," *PLoS One*, vol. 7, no. 3, p. e30679, 2012.

[15] P. Rao, E. Benito, and A. Fischer, "Micrornas as biomarkers for cns disease," *Frontiers in Molecular Neuroscience*, vol. 6, p. 39, 2013.

[16] R. Navickas, D. Gal, A. Laucevicius, A. Taparauskaite, M. Zdanyte, and P. Holvoet, "Identifying circulating micrornas as biomarkers of cardiovascular disease: a systematic review," *Cardiovascular Research*, vol. 111, no. 4, pp. 322–337, 2012.

[17] J. Ward, C. Kanchagar, I. Veksler-Lublinsky, R. C. Lee, M. R. McGill, H. Jaeschke, S. C. Curry, and V. R. Ambros, "Circulating microrna profiles in human patiences with acetaminophen hepatotoxicity or ischemic hepatitis," *Proceedings of the National Academy of Sciences*, vol. 111, no. 33, pp. 12169–12174, 2014.

[18] S. Taheri, F. Tanriverdi, G. Zarasiz, G. Elbuken, Z. Karaca, A. Selcuklu, K. Unluhizarci, K. Tanriverdi, and F. Kelestimur, "Circulating micrornas as potential biomarkers for traumatic brain injury-induved hypopituitarism," *Journal of Neurotrauma*, vol. 33, no. 20, pp. 1818–1825, 2016.

[19] C. N. Correia, N. C. Nalpas, K. E. McLoughlin, J. A. Browne, S. V. Gordon, D. E. MacHugh, and R. G. Shaughnessy, "Circulating micrornas as potential biomarkers of infectious disease," *Frontiers in Immunology*, vol. 8, p. 118, 2017.

[20] I. Lee, S. S. Ajay, H. Chen, A. Maruyama, N. Wang, M. G. McInnis, and B. D. Athey, "Discriminating single-base difference mirna expressions using microarray probe design guru (prodeg)," *Oxford University Press*, vol. 36, no. 5, p. e27, 2008.

[21] C. Chen, R. Tan, L. Wong, R. Fekete, and J. Halsey, *Quantitation of MicroRNAs by Real-Time RT-qPCR*, pp. 113–134. Totowa, NJ: Humana Press, 2011.

[22] S. E. McCalla and A. Tripathi, "Microfluidic reactors for diagnostics applications," *Annual Review of Biomedical Engineering*, vol. 13, no. 1, pp. 321–343, 2011.

[23] W. Zhou, L. Hu, L. Ying, P. K. Chu, and X.-F. Yu, "A crisprcas9-triggered strand displacement amplification method for ultrasensitive dna detection," *Natureresearch*, vol. 9, no. 5012, 2018.

[24] J. Van Ness, L. K. Van Ness, and D. J. Galas, "Isothermal reactions for the amplification of oligonucleotides," *Proceedings of the National Academy of Sciences*, vol. 100, no. 8, pp. 4504–4509, 2003.

[25] E. Tan, B. Erwin, S. Dames, T. Ferguson, M. Buechel, B. Irvine, K. Voelkerding, and A. Niemz, "Specific versus nonspecific isothermal dna amplification through thermophilic polymerase and nicking enzyme activities," *Biochemistry*, vol. 47, no. 38, pp. 9987–9999, 2008.

[26] B. Ozay, C. M. Robertus, J. L. Negri, and S. E. McCalla, "First characterization of a biphasic, switch-like DNA amplification," *Analyst*, vol. 143, pp. 1820–1828, 2018.

[27] D. Y. Zhang and E. Winfree, "Control of DNA strand displacement kinetics using toehold exchange," *Journal of the American Chemical Society*, vol. 131, no. 47, pp. 17303–17314, 2009.

[28] A. Baccouche, K. Montagne, A. Padirac, T. Fujii, and Y. Rondelez, "Dynamic DNA-toolbox reaction circuits: a walkthrough," *Methods*, vol. 67, no. 2, pp. 234–249, 2014.

[29] P. LaBarre, K. R. Hawkins, J. Gerlach, J. Wilmoth, A. Beddoe, J. Singleton, D. Boyle, and B. Weigl, "A simple, inexpensive device for nucleic acid amplification without electricitytoward instrument-free molecular diagnostics in low-resource settings," *PloS one*, vol. 6, no. 5, p. e19738, 2011.

[30] Z.-z. Zhang and C.-y. Zhang, "Highly sensitive detection of protein with aptamer-based target-triggering two-stage amplification," *Analytical Chemistry*, vol. 84, no. 3, pp. 1623–1629, 2012.

[31] W. Tang, T. Zhang, Q. Li, H. Wang, H. Wang, and Z. Li, "Sensitive detection of tumor cells based on aptamer recognition and isothermal exponential amplification," *RSC Adv.*, vol. 6, pp. 89888–89894, 2016.

[32] X. Zhang, C. Liu, L. Sun, X. Duan, and Z. Li, "Lab on a single microbead: an ultrasensitive detection strategy enabling microrna analysis at the single-molecule level," *Chem. Sci.*, vol. 6, pp. 6213–6218, 2015.

[33] E. Tan, B. Erwin, S. Dames, K. Voelkerding, and A. Niemz, "Isothermal dna amplification with gold nanosphere-based visual colorimetric readout for herpes simplex virus detection," *Clinical Chemistry*, vol. 53, no. 11, pp. 2017–2020, 2007.

[34] K. Roskos, A. I. Hickerson, H.-W. Lu, T. M. Ferguson, D. N. Shinde, Y. Klaue, and A. Niemz, "Simple system for isothermal dna amplification coupled to lateral flow detection," *PLoS One*, vol. 8, no. 7, p. e69355, 2013.

[35] Y. Zhao, L. Zhou, and Z. Tang, "Cleavage-based signal amplification of rna," *Nature communications*, vol. 4, p. 1493, 2013.

[36] K. Montagne, G. Gines, T. Fujii, and Y. Rondelez, "Boosting functionality of synthetic DNA circuits with tailored deactivation," *Nature Communications*, vol. 7, p. 13474, 2016.

[37] J. Qian, T. M. Ferguson, D. N. Shinde, A. J. Ramírez-Borrero, A. Hintze, C. Adami, and A. Niemz, "Sequence dependence of isothermal dna amplification via expar," *Nucleic acids research*, vol. 40, no. 11, pp. e87–e87, 2012.

[38] S. J. Green, D. Lubrich, and A. J. Turberfield, "Dna hairpins: fuel for autonomous dna devices," *Biophysical journal*, vol. 91, no. 8, pp. 2966–2975, 2006.

[39] T. Fujii and Y. Rondelez, "Predator–prey molecular ecosystems," *ACS nano*, vol. 7, no. 1, pp. 27–34, 2012.

[40] C. M. Nycz, C. H. Dean, P. D. Haaland, C. A. Spargo, and G. T. Walker, "Quantitative reverse transcription strand displacement amplification: quantitation of nucleic acids using an isothermal amplification technique," *Analytical biochemistry*, vol. 259, no. 2, pp. 226–234, 1998.

[41] L. E. Morrison and L. M. Stols, "Sensitive fluorescence-based thermodynamic and kinetic measurements of DNA hybridization in solution," *Biochemistry*, vol. 32, no. 12, pp. 3095–3104, 1993.

[42] R. D. Kuchta, V. Mizrahi, P. A. Benkovic, K. A. Johnson, and S. J. Benkovic, "Kinetic mechanism of DNA polymerase I (Klenow)," *Biochemistry*, vol. 26, no. 25, pp. 8410–8417, 1987.

[43] G. Nevinsky, A. Nemudraya, A. Levina, and V. Khomov, "The algorithm of estimation of the k m values for primers of various structure and length in the polymerization reaction catalyzed by klenow fragment of dna polymerase i from e. coli," *FEBS letters*, vol. 258, no. 1, pp. 166–170, 1989.

[44] F. R. Bryant, K. A. Johnson, and S. J. Benkovic, "Elementary steps in the DNA polymerase I reaction pathway," *Biochemistry*, vol. 22, no. 15, pp. 3537–3546, 1983.

[45] N. R. Markham and M. Zuker, "DINAMelt web server for nucleic acid melting prediction," *Nucleic acids research*, vol. 33, no. suppl_2, pp. W577–W581, 2005.

[46] A. Goldbeter and D. E. Koshland, "An amplified sensitivity arising from covalent modification in biological systems," *Proceedings of the National Academy of Sciences*, vol. 78, no. 11, pp. 6840–6844, 1981.

[47] I. S. Bukhrashvili, D. Z. Chinchaladze, O. I. Lavrik, A. S. Levina, G. A. Nevinsky, and D. A. Prangishvili, "Comparison of initiating abilities of primers

of different length in polymerization reactions catalyzed by dna polymerases from thermoacidophilic archaebacteria," *Biochimica et Biophysica Acta (BBA)-Gene Structure and Expression*, vol. 1008, no. 1, pp. 102–107, 1989.

[48] R. C. Robinson, *An Introduction to Dynamical Systems: Continuous and Discrete*. Providence, Rhode Island: American Mathematical Society, second ed., 2012.

[49] J. Guckenheimer and P. Holmes, *Nonlinear Oscillations, Dynamical Systems, and Bifurcation of Vector Fields*. Springer New York, 1983.

APPENDICES

APPENDIX A

MATHEMATICA CODE

This section contains Wolfram Language that was used throughout this work to illuminate results through symbolic simplifications and computations.

A.1 Model 1

In Lemma 4.5, we want to write equation (4.11) as a polynomial in V_∞. This was done with Wolfram Language

```
Collect[2*\[Kappa]1*k3*k6*P0*V - k2*(2*\[Kappa]1*k6 + 2*k6*V + \[Kappa]2*k3
    ↪ *V)*(T0 - V), V]
```

The output reported in Lemma 4.5 and Theorem 1 is

```
-2 k2 k6 T0 \[Kappa]1 + V^2 (2 k2 k6 + k2 k3 \[Kappa]2) + V (-2 k2 k6 T0 +
    ↪ 2 k2 k6 \[Kappa]1 + 2 k3 k6 P0 \[Kappa]1 - k2 k3 T0 \[Kappa]2)
```

The Jacobian for system (3.10) was determined using Wolfram Language

```
yd = -2*kon*(T0 - Z - W - V)*Y^2 + 2*koff*Z + k1*Z*P + k2*W - 2*k6*P*Y^2;
zd = kon*(T0 - Z - W - V)*Y^2 - koff*Z - k1*Z*P;
wd = k1*Z*P - k2*W + k3*V*P;
vd = k2*W - k3*V*P;

JacMat = D[{yd, zd, wd, vd}, {{Y, Z, W, V}}];
MatrixForm[JacMat]
```

The eigenvalues and eigenvectors for Corollary 1.1 were computed by appending

```
Y = 0; Z = 0; W = 0; V = 0;
Eigensystem[JacMat]
```

to the previous language. This produces the result

```
{{0, 0, -koff - k1 P, -k2 - k3 P},
       {{1, 0, 0, 0}, {0, 0, 0, 0},
       {(k3 (2 koff + k1 P))/(k1 (koff + k1 P)) + ((2 k2 - 2 koff - k1 P) (
           ↪ koff + k1 P - k3 P))/(k1 k2 P), -(k3/k1) + ((-k2 + koff + k1
           ↪ P) (koff + k1 P - k3 P))/(k1 k2 P), -((koff + k1 P - k3 P)/k2
           ↪ ), 1},
       {k2/(k2 + k3 P), 0, -1, 1}}}
```

where `{0, 0, -koff - k1 P, -k2 - k3 P}` is the list of eigenvalues and the subsequent lists are the eigenvectors corresponding to those eigenvalues. The second zero eigenvalue corresponds to a zero vector, meaning it has multiplicity two. To compute a generalized eigenvector, append the Wolfram Language

```
LinearSolve[JacMat,{1,0,0,0}]
```

which produces the generalized vector

```
{0, 0, 1/k2, 1/(k3 P)}
```

With the vector $(1, 0, 0, 0)$, this spans the zero eigenspace.

For Corollary 1.2, we seek the eigenvalues and eigenvectors of the Jacobian for system (3.10) when $Y_\infty \neq 0$. We assign a parameter set (here we use simulation values *(Table 2.1)* with $k_4 = k_5 = 0$) and obtain numerical solutions for the other limit values using the code above. Then we compute the numerical eigenvalues for our parameter set. The Wolfram Language used for this work was

```
yd = -2*kon*(T0 - Z - W - V)*Y^2 + 2*koff*Z + k1*Z*P + k2*W - 2*k6*P*Y^2;
zd = kon*(T0 - Z - W - V)*Y^2 - koff*Z - k1*Z*P;
wd = k1*Z*P - k2*W + k3*V*P;
vd = k2*W - k3*V*P;

JacMat = D[{yd, zd, wd, vd}, {{Y, Z, W, V}}];

kon = 2000; koff = 45; k1 = 400; k2 = 0.625; k3 = 800; k4 = 0.013; k5 =
    ↪ 0.1; k6 = 0.01;
\[Kappa]r = 14; kp1 = 0.015; kp2 = 0.225; ka = 0.0075;
T0 = 0.1; P0 = 0.005; \[Kappa]1 = kp1; \[Kappa]2 = (kp1*ka)/kp2;

Z=0;
vlist = V /. Solve[2*\[Kappa]1*k3*k6*P0*V - k2*(2*\[Kappa]1*k6 + 2*k6*V +
    ↪ \[Kappa]2*k3*V)*(T0 - V) == 0 && V > 0, V];
V = vlist[[1]]
Y = Sqrt[k3*V/(2*k6)]
P = (2*\[Kappa]1*k6*P0)/(2*\[Kappa]1*k6 + (2*k6 + \[Kappa]2*k3)*V)
W = (k3/k2)*P*V

Eigensystem[JacMat]
```

which produces limit values

$$
\begin{aligned}
V_\infty &= 0.0954625,\\
Y_\infty &= 61.794,\\
P_\infty &= 0.000037134,\\
W_\infty &= 0.00453748.
\end{aligned}
$$

The eigenvalues are all negative,

```
{{-7.63705*10^6, -0.654707, -0.0148535, -0.0000917863},
       {{0.894427, -0.447214, 8.69804*10^-10, -7.11829*10^-17},
       {-0.973974, -7.12097*10^-17, -0.160272, 0.160272},
       {0.99999, 0.00320695, -0.0000744472, -0.00313252},
       {-1., -6.98203*10^-22, 5.11172*10^-21, 1.07877*10^-19}}}
```

A.2 Model 2

The Jacobian for system (3.13) was determined using Wolfram Language

```
yd = -2*kon*(T0 - Z - W - V - WS)*Y^2 + 2*koff*Z + k1*Z*P + k2*W - 2*k6*P*Y
    ↪ ^2;
zd = kon*(T0 - Z - W - V - WS)*Y^2 - koff*Z - k1*Z*P;
wd = k1*Z*P - k2*W + k3*V*P - k4*W;
vd = k2*W - k3*V*P;
wsd = k4*W;

JacMat = D[{yd, zd, wd, vd, wsd}, {{Y, Z, W, V, WS}}];
MatrixForm[JacMat]
```

The eigenvalues for Corollary 2.1 were computed by appending

```
Y = 0; Z = 0; W = 0; V = 0;
Eigenvalues[JacMat]
```

to the previous language. This produces the result

```
{{0, 0, -koff - k1 P, 1/2 (-k2 - k4 - k3 P - Sqrt[-4 k3 k4 P + (k2 + k4 +
    ↪ k3 P)^2]), 1/2 (-k2 - k4 - k3 P + Sqrt[-4 k3 k4 P + (k2 + k4 + k3 P)
    ↪ ^2])},
       {{0, 0, 0, 0, 1}, {1, 0, 0, 0, 0},
       {-((k3 (2 koff + k1 P) (-k2 koff - k1 k2 P))/(k1 k4 (koff + k1 P) (
           ↪ koff + k1 P - k3 P))) - (-2 k2 koff - 2 k4 koff + 2 koff^2 -
           ↪ 2 k1 k2 P - k1 k4 P + 3 k1 koff P + k1^2 P^2)/(k1 k4 P), ((
           ↪ koff + k1 P) (-k2 - k4 + koff + k1 P))/(k1 k4 P) + (k3 (-k2
           ↪ koff - k1 k2 P))/(k1 k4 (koff + k1 P - k3 P)), -((koff + k1 P
           ↪ )/k4), -((-k2 koff - k1 k2 P)/(k4 (koff + k1 P - k3 P))), 1},
       {k2/k4, 0, -((k2 + k4 + k3 P + Sqrt[k2^2 + 2 k2 k4 + k4^2 + 2 k2 k3
           ↪ P - 2 k3 k4 P + k3^2 P^2])/(2 k4)), -((-k2^2 - k2 k4 - 2 k2
           ↪ k3 P + k3 k4 P - k3^2 P^2 - k2 Sqrt[k2^2 + 2 k2 k4 + k4^2 + 2
           ↪  k2 k3 P - 2 k3 k4 P + k3^2 P^2] - k3 P Sqrt[k2^2 + 2 k2 k4 +
           ↪  k4^2 + 2 k2 k3 P - 2 k3 k4 P + k3^2 P^2])/(k4 (k2 + k4 + k3
           ↪ P + Sqrt[k2^2 + 2 k2 k4 + k4^2 + 2 k2 k3 P - 2 k3 k4 P + k3^2
           ↪  P^2]))), 1},
       {k2/k4, 0, -((k2 + k4 + k3 P - Sqrt[k2^2 + 2 k2 k4 + k4^2 + 2 k2 k3
           ↪ P - 2 k3 k4 P + k3^2 P^2])/(2 k4)), -((k2^2 + k2 k4 + 2 k2 k3
           ↪  P - k3 k4 P + k3^2 P^2 - k2 Sqrt[k2^2 + 2 k2 k4 + k4^2 + 2
           ↪ k2 k3 P - 2 k3 k4 P + k3^2 P^2] - k3 P Sqrt[k2^2 + 2 k2 k4 +
           ↪ k4^2 + 2 k2 k3 P - 2 k3 k4 P + k3^2 P^2])/(k4 (-k2 - k4 - k3
           ↪ P + Sqrt[k2^2 + 2 k2 k4 + k4^2 + 2 k2 k3 P - 2 k3 k4 P + k3^2
           ↪  P^2]))), 1}}}
```

where

```
{0, 0, -koff - k1 P, 1/2 (-k2 - k4 - k3 P - Sqrt[-4 k3 k4 P + (k2 + k4 + k3
    ↪  P)^2]), 1/2 (-k2 - k4 - k3 P + Sqrt[-4 k3 k4 P + (k2 + k4 + k3 P)
    ↪ ^2])}
```

is the list of eigenvalues and the subsequent lists are the eigenvectors corresponding to those eigenvalues.

A.3 Model 3

For Lemma 4.7, we want to write equation (4.36) as a polynomial in Y_∞. This was done with Wolfram Language

```
f[y_] := y^4/(\[Kappa]r^4 + y^4);
Z = (2*k6*Y^2*(k4 + k5*f[Y]))/(k1*k2);
X = Together[Z*((koff + k1*P)/(kon*Y^2) + 1 + (k1*P)/(k5*f[Y]) + (k1*k2)/(
    ↪ k3*(k4 + k5*f[Y])))];
Q = Collect[Numerator[X] - T0*Denominator[X], Y]
```

which produces the output

```
(2 k3 k4 k5 k6 koff + 2 k3 k5^2 k6 koff + 2 k1 k3 k4 k5 k6 P + 2 k1 k3 k5^2
    ↪  k6 P - k1 k2 k3 k5 kon T0) Y^6
       + (2 k1 k2 k5 k6 kon + 2 k3 k4 k5 k6 kon + 2 k3 k5^2 k6 kon + 2 k1
           ↪ k3 k4 k6 kon P + 2 k1 k3 k5 k6 kon P) Y^8
       + 2 k1 k3 k4 k6 kon P \[Kappa]r^8
       + Y^4 (2 k1 k2 k5 k6 kon \[Kappa]r^4 + 2 k3 k4 k5 k6 kon \[Kappa]r^4
           ↪  + 4 k1 k3 k4 k6 kon P \[Kappa]r^4 + 2 k1 k3 k5 k6 kon P \[
           ↪ Kappa]r^4)
       + Y^2 (2 k3 k4 k5 k6 koff \[Kappa]r^4 + 2 k1 k3 k4 k5 k6 P \[Kappa]r
           ↪ ^4 - k1 k2 k3 k5 kon T0 \[Kappa]r^4)
```

and shows the result is a fourth order polynomial of Y_∞^2. The Wolfram Language

```
Simplify[Coefficient[Q, Y, 0]]
```

isolates the constant term

```
2 k1 k3 k4 k6 kon P \[Kappa]r^8
```

and the Wolfram Language

```
Simplify[Coefficient[Q, Y, 8]]
```

isolates the leading term

```
2 k6 kon (k1 k2 k5 + k3 k5 (k4 + k5) + k1 k3 (k4 + k5) P)
```

The Jacobian for system (3.15) was determined with Wolfram Language

```
P = P0;
yd = -2*kon*(T0 - Z - W - V - WS)*Y^2 + 2*koff*Z + k1*Z*P + k2*W - k6*P*Y
    ↪ *(2*Y + J);
zd = kon*(T0 - Z - W - V - WS)*Y^2 - koff*Z - k1*Z*P;
wd = k1*Z*P - k2*W + k3*V*P - k4*W - k5*W*f[Y];
vd = k2*W - k3*V*P;
wsd = k4*W - k5*WS*f[Y];
jd = k5*(W + WS)*f[Y] - k6*P*J*Y;

JacMat = D[{yd, zd, wd, vd, wsd, jd}, {{Y, Z, W, V, WS, J}}];
MatrixForm[JacMat]
```

The eigenvalues and eigenvectors for Corollary 3.1 were computed by appending

```
Y = 0; Z = 0; W = 0; V = 0;
f[y_] := y^4/(\[Kappa]r^4 + y^4);
Eigensystem[JacMat]
```

to the previous language. This produces the result

```
{{0, 0, -J k6 P0, -koff - k1 P0, 1/2 (-k2 - k4 - k3 P0 - Sqrt[-4 k3 k4 P0 +
    ↪  (k2 + k4 + k3 P0)^2]), 1/2 (-k2 - k4 - k3 P0 + Sqrt[-4 k3 k4 P0 + (
    ↪ k2 + k4 + k3 P0)^2])},
       {{0, 0, 0, 0, 0, 1}, {0, 0, 0, 0, 1, 0}, {1, 0, 0, 0, 0, 1},
       {-((-koff - k1 P0)/(J k6 P0)), ((-koff - k1 P0 + J k6 P0) (-k2 koff
           ↪ ^2 - k4 koff^2 + koff^3 - 2 k1 k2 koff P0 - 2 k1 k4 koff P0 +
           ↪  k3 k4 koff P0 + 3 k1 koff^2 P0 - k3 koff^2 P0 - k1^2 k2 P0^2
           ↪  - k1^2 k4 P0^2 + k1 k3 k4 P0^2 + 3 k1^2 koff P0^2 - 2 k1 k3
           ↪ koff P0^2 + k1^3 P0^3 - k1^2 k3 P0^3))/(J k6 P0 (-2 k2 koff^2
           ↪  - 2 k4 koff^2 + 2 koff^3 - 4 k1 k2 koff P0 - 3 k1 k4 koff P0
           ↪  + 2 k3 k4 koff P0 + 5 k1 koff^2 P0 - 2 k3 koff^2 P0 - 2 k1^2
           ↪  k2 P0^2 + k1 k2 k3 P0^2 - k1^2 k4 P0^2 + k1 k3 k4 P0^2 + 4
           ↪ k1^2 koff P0^2 - 3 k1 k3 koff P0^2 + k1^3 P0^3 - k1^2 k3 P0
           ↪ ^3)), ((koff + k1 P0) (-k1 koff^2 - 2 k1^2 koff P0 + k1 k3
           ↪ koff P0 + J k1 k6 koff P0 - k1^3 P0^2 + k1^2 k3 P0^2 + J k1^2
           ↪  k6 P0^2 - J k1 k3 k6 P0^2))/(J k6 (2 k2 koff^2 + 2 k4 koff^2
           ↪  - 2 koff^3 + 4 k1 k2 koff P0 + 3 k1 k4 koff P0 - 2 k3 k4
           ↪ koff P0 - 5 k1 koff^2 P0 + 2 k3 koff^2 P0 + 2 k1^2 k2 P0^2 -
           ↪ k1 k2 k3 P0^2 + k1^2 k4 P0^2 - k1 k3 k4 P0^2 - 4 k1^2 koff P0
           ↪ ^2 + 3 k1 k3 koff P0^2 - k1^3 P0^3 + k1^2 k3 P0^3)), -(((k2
           ↪ koff + k1 k2 P0) (-k1 koff - k1^2 P0 + J k1 k6 P0))/(J k6 (2
           ↪ k2 koff^2 + 2 k4 koff^2 - 2 koff^3 + 4 k1 k2 koff P0 + 3 k1
           ↪ k4 koff P0 - 2 k3 k4 koff P0 - 5 k1 koff^2 P0 + 2 k3 koff^2
           ↪ P0 + 2 k1^2 k2 P0^2 - k1 k2 k3 P0^2 + k1^2 k4 P0^2 - k1 k3 k4
           ↪  P0^2 - 4 k1^2 koff P0^2 + 3 k1 k3 koff P0^2 - k1^3 P0^3 + k1
           ↪ ^2 k3 P0^3))), (k1 k4 koff^2 + 2 k1^2 k4 koff P0 - k1 k3 k4
           ↪ koff P0 - J k1 k4 k6 koff P0 + k1^3 k4 P0^2 - k1^2 k3 k4 P0^2
```

```
        ↪  - J k1^2 k4 k6 P0^2 + J k1 k3 k4 k6 P0^2)/(J k6 (2 k2 koff^2
        ↪  + 2 k4 koff^2 - 2 koff^3 + 4 k1 k2 koff P0 + 3 k1 k4 koff P0
        ↪  - 2 k3 k4 koff P0 - 5 k1 koff^2 P0 + 2 k3 koff^2 P0 + 2 k1^2
        ↪  k2 P0^2 - k1 k2 k3 P0^2 + k1^2 k4 P0^2 - k1 k3 k4 P0^2 - 4
        ↪ k1^2 koff P0^2 + 3 k1 k3 koff P0^2 - k1^3 P0^3 + k1^2 k3 P0
        ↪ ^3)), 1},
{-((-k2 - k4 - k3 P0 - Sqrt[k2^2 + 2 k2 k4 + k4^2 + 2 k2 k3 P0 - 2 k3 k4
    ↪  P0 + k3^2 P0^2])/(2 J k6 P0)), 0, -(1/(2 J k2 k6 P0))(k2^2 + 2 k2
    ↪  k4 + k4^2 + 2 k2 k3 P0 - J k2 k6 P0 - J k4 k6 P0 + k3^2 P0^2 - J
    ↪ k3 k6 P0^2 + k2 Sqrt[k2^2 + 2 k2 k4 + k4^2 + 2 k2 k3 P0 - 2 k3 k4
    ↪ P0 + k3^2 P0^2] + k4 Sqrt[k2^2 + 2 k2 k4 + k4^2 + 2 k2 k3 P0 - 2
    ↪ k3 k4 P0 + k3^2 P0^2] + k3 P0 Sqrt[k2^2 + 2 k2 k4 + k4^2 + 2 k2 k3
    ↪  P0 - 2 k3 k4 P0 + k3^2 P0^2] - J k6 P0 Sqrt[k2^2 + 2 k2 k4 + k4^2
    ↪  + 2 k2 k3 P0 - 2 k3 k4 P0 + k3^2 P0^2]), -(1/(2 J k2 k6 P0))(-k2
    ↪ ^2 - k2 k4 - 2 k2 k3 P0 + k3 k4 P0 + J k2 k6 P0 - J k4 k6 P0 - k3
    ↪ ^2 P0^2 + J k3 k6 P0^2 - k2 Sqrt[k2^2 + 2 k2 k4 + k4^2 + 2 k2 k3
    ↪ P0 - 2 k3 k4 P0 + k3^2 P0^2] - k3 P0 Sqrt[k2^2 + 2 k2 k4 + k4^2 +
    ↪ 2 k2 k3 P0 - 2 k3 k4 P0 + k3^2 P0^2] + J k6 P0 Sqrt[k2^2 + 2 k2 k4
    ↪  + k4^2 + 2 k2 k3 P0 - 2 k3 k4 P0 + k3^2 P0^2]), -((-k2^2 k4 - 2
    ↪ k2 k4^2 - k4^3 - 2 k2 k3 k4 P0 + J k2 k4 k6 P0 + J k4^2 k6 P0 - k3
    ↪ ^2 k4 P0^2 + J k3 k4 k6 P0^2 - k2 k4 Sqrt[k2^2 + 2 k2 k4 + k4^2 +
    ↪ 2 k2 k3 P0 - 2 k3 k4 P0 + k3^2 P0^2] - k4^2 Sqrt[k2^2 + 2 k2 k4 +
    ↪ k4^2 + 2 k2 k3 P0 - 2 k3 k4 P0 + k3^2 P0^2] - k3 k4 P0 Sqrt[k2^2 +
    ↪  2 k2 k4 + k4^2 + 2 k2 k3 P0 - 2 k3 k4 P0 + k3^2 P0^2] + J k4 k6
    ↪ P0 Sqrt[k2^2 + 2 k2 k4 + k4^2 + 2 k2 k3 P0 - 2 k3 k4 P0 + k3^2 P0
    ↪ ^2])/(J k2 k6 P0 (k2 + k4 + k3 P0 + Sqrt[k2^2 + 2 k2 k4 + k4^2 + 2
    ↪  k2 k3 P0 - 2 k3 k4 P0 + k3^2 P0^2]))), 1},
{-((-k2 - k4 - k3 P0 + Sqrt[k2^2 + 2 k2 k4 + k4^2 + 2 k2 k3 P0 - 2 k3 k4
    ↪  P0 + k3^2 P0^2])/(2 J k6 P0)), 0, -(1/(2 J k2 k6 P0))(k2^2 + 2 k2
    ↪  k4 + k4^2 + 2 k2 k3 P0 - J k2 k6 P0 - J k4 k6 P0 + k3^2 P0^2 - J
    ↪ k3 k6 P0^2 - k2 Sqrt[k2^2 + 2 k2 k4 + k4^2 + 2 k2 k3 P0 - 2 k3 k4
    ↪ P0 + k3^2 P0^2] - k4 Sqrt[k2^2 + 2 k2 k4 + k4^2 + 2 k2 k3 P0 - 2
    ↪ k3 k4 P0 + k3^2 P0^2] - k3 P0 Sqrt[k2^2 + 2 k2 k4 + k4^2 + 2 k2 k3
    ↪  P0 - 2 k3 k4 P0 + k3^2 P0^2] + J k6 P0 Sqrt[k2^2 + 2 k2 k4 + k4^2
    ↪  + 2 k2 k3 P0 - 2 k3 k4 P0 + k3^2 P0^2]), -(1/(2 J k2 k6 P0))(-k2
    ↪ ^2 - k2 k4 - 2 k2 k3 P0 + k3 k4 P0 + J k2 k6 P0 - J k4 k6 P0 - k3
    ↪ ^2 P0^2 + J k3 k6 P0^2 + k2 Sqrt[k2^2 + 2 k2 k4 + k4^2 + 2 k2 k3
    ↪ P0 - 2 k3 k4 P0 + k3^2 P0^2] + k3 P0 Sqrt[k2^2 + 2 k2 k4 + k4^2 +
    ↪ 2 k2 k3 P0 - 2 k3 k4 P0 + k3^2 P0^2] - J k6 P0 Sqrt[k2^2 + 2 k2 k4
    ↪  + k4^2 + 2 k2 k3 P0 - 2 k3 k4 P0 + k3^2 P0^2]), -((k2^2 k4 + 2 k2
    ↪  k4^2 + k4^3 + 2 k2 k3 k4 P0 - J k2 k4 k6 P0 - J k4^2 k6 P0 + k3^2
    ↪  k4 P0^2 - J k3 k4 k6 P0^2 - k2 k4 Sqrt[k2^2 + 2 k2 k4 + k4^2 + 2
    ↪ k2 k3 P0 - 2 k3 k4 P0 + k3^2 P0^2] - k4^2 Sqrt[k2^2 + 2 k2 k4 + k4
    ↪ ^2 + 2 k2 k3 P0 - 2 k3 k4 P0 + k3^2 P0^2] - k3 k4 P0 Sqrt[k2^2 + 2
    ↪  k2 k4 + k4^2 + 2 k2 k3 P0 - 2 k3 k4 P0 + k3^2 P0^2] + J k4 k6 P0
```

```
↪ Sqrt[k2^2 + 2 k2 k4 + k4^2 + 2 k2 k3 P0 - 2 k3 k4 P0 + k3^2 P0^2])
↪ /(J k2 k6 P0 (-k2 - k4 - k3 P0 + Sqrt[k2^2 + 2 k2 k4 + k4^2 + 2 k2
↪  k3 P0 - 2 k3 k4 P0 + k3^2 P0^2]))), 1}}}
```

where

```
{0, 0, -J k6 P0, -koff - k1 P0, 1/2 (-k2 - k4 - k3 P0 - Sqrt[-4 k3 k4 P0 +
    ↪ (k2 + k4 + k3 P0)^2]), 1/2 (-k2 - k4 - k3 P0 + Sqrt[-4 k3 k4 P0 + (
    ↪ k2 + k4 + k3 P0)^2])}
```

is the list of eigenvalues and the subsequent lists are the eigenvectors corresponding to those eigenvalues. Here again we have two zero eigenvalues, now corresponding to linearly independent eigenvectors

$$\vec{v}_1 = (0, 0, 0, 0, 0, 1), \quad \vec{v}_2 = (0, 0, 0, 0, 1, 0).$$

To compute the viable Y_∞ values for a given parameter set, assign the parameter values (here we use simulation values *(Table 2.1)*) and use the Wolfram Language:

```
kon = 2000; koff = 45; k1 = 400; k2 = 0.625; k3 = 800; k4 = 0.013; k5 =
    ↪ 0.1; k6 = 0.01;
\[Kappa]r = 14; kp1 = 0.015; kp2 = 0.225; ka = 0.0075;
T0 = 0.1; P0 = 0.005; \[Kappa]1 = kp1; \[Kappa]2 = (kp1*ka)/kp2;

P = P0;
f[y_] := y^4/(\[Kappa]r^4 + y^4);
Z = (2*k6*Y^2*(k4 + k5*f[Y]))/(k1*k2);

ylist = Y /. Solve[Z*((koff + k1*P)/(kon*Y^2) + 1 + (k1*P)/(k5*f[Y]) + (k1*
    ↪ k2)/(k3*(k4 + k5*f[Y]))) == T0 && Y > 0, Y, Reals]
```

This produces results $Y_{\infty_1} = 2.85082$ and $Y_{\infty_2} = 21.4478$. To compute the remaining values, append the Wolfram Language

```
Y = ylist[[which]];
f[y_] := y^4/(\[Kappa]r^4 + y^4);
Z = (2*k6*Y^2*(k4 + k5*f[Y]))/(k1*k2);
V = (k1*k2*Z)/(k3*(k4 + k5*f[Y]));
J = (k1*Z)/(k6*Y);
T = ((koff + k1*P)*Z)/(kon*Y^2);
W = (k3*P*V)/k2;
WS = (k1*Z*P)/(k5*f[Y]) - W;
```

where `which` is the desired Y_∞ value. Because this parameter set has two real, positive solutions for Y_∞, in this case `which` can either be `1` or `2`. The results of this language are found in Table A.1.

For Corollary 3.2, we seek the eigenvalues and eigenvectors of the Jacobian for system (3.15) when $Y_\infty \neq 0$. We assign a parameter set (here we use simulation

	Y = ylist[[1]] = 2.85082	Y = ylist[[2]] = 21.4478
T_∞	2.47627*10^-8	1.83554*10^-7
Z_∞	8.56384*10^-6	0.00359304
W_∞	0.00130035	0.0736014
V_∞	0.000203179	0.0115002
W^*_∞	0.0984879	0.0113052
J_∞	0.12016	6.70099

Table A.1: Mathematica output for Model 3 nonzero limit values with simulation values *(Table 2.1)*

values *(Table 2.1)*) and obtain numerical solutions for the other limit values using the code above. Then we compute the numerical eigenvalues for our parameter set. The Wolfram Language used for this work was

```
P = P0;
yd = -2*kon*(T0 - Z - W - V - WS)*Y^2 + 2*koff*Z + k1*Z*P + k2*W - k6*P*Y
    ↪ *(2*Y + J);
zd = kon*(T0 - Z - W - V - WS)*Y^2 - koff*Z - k1*Z*P;
wd = k1*Z*P - k2*W + k3*V*P - k4*W - k5*W*f[Y];
vd = k2*W - k3*V*P;
wsd = k4*W - k5*WS*f[Y];
jd = k5*(W + WS)*f[Y] - k6*P*J*Y;

JacMat = D[{yd, zd, wd, vd, wsd, jd}, {{Y, Z, W, V, WS, J}}];

kon = 2000; koff = 45; k1 = 400; k2 = 0.625; k3 = 800; k4 = 0.013; k5 =
    ↪ 0.1; k6 = 0.01;
\[Kappa]r = 14; kp1 = 0.015; kp2 = 0.225; ka = 0.0075;
T0 = 0.1; P0 = 0.005; \[Kappa]1 = kp1; \[Kappa]2 = (kp1*ka)/kp2;

P=P0;
f[y_] := y^4/(\[Kappa]r^4 + y^4);
Z = (2*k6*Y^2*(k4 + k5*f[Y]))/(k1*k2);

ylist = Y /. Solve[Z*((koff + k1*P)/(kon*Y^2) + 1 + (k1*P)/(k5*f[Y]) + (k1*
    ↪ k2)/(k3*(k4 + k5*f[Y]))) == T0 && Y > 0, Y, Reals];

Y = ylist[[which]];
Z = (2*k6*Y^2*(k4 + k5*f[Y]))/(k1*k2);
V = (k1*k2*Z)/(k3*(k4 + k5*f[Y]));
J = (k1*Z)/(k6*Y);
T = ((koff + k1*P)*Z)/(kon*Y^2);
W = (k3*P*V)/k2;
```

```
WS = (k1*Z*P)/(k5*f[Y]) - W;

Eigenvalues[JacMat]
```

Then for Y_{∞_1} = `ylist[[1]] = 2.85082` we have

```
{-16299.3, -4.6268, -1.99463, -0.0124928, 0.000472093, -0.000138747}
```

and for Y_{∞_2} = `ylist[[2]] = 21.4478` we have

```
{-920062., -4.64748, -2.06395, -0.0960804, -0.00474393, -0.00103166}
```

which implies Y_{∞_1} is a saddle point and Y_{∞_2} is stable.

A.4 Model 4 *(Full Model)*

For Lemma 4.9, we want to write equation (4.55) as a polynomial in Y_∞. This was done with Wolfram Language

```
f[y_] := y^4/(\[Kappa]r^4 + y^4);
Z = (2*k6*Y^2*(k4 + k5*f[Y]))/(k1*(k2 - 2*(k4 + k5*f[Y])));
V = (k1*k2*Z)/(k3*(k4 + k5*f[Y]));
J = (k1*Z)/(k6*Y);
P = P0/(1 + (Z + V + \[Kappa]2*(Y^2 + J*Y))/\[Kappa]1);
X = Together[Z*((koff + k1*P)/(kon*Y^2) + 1 + (k1*P)/(k5*f[Y]) + (k1*k2)/(
    ↪ k3*(k4 + k5*f[Y])))];
Q = Collect[Numerator[X] - T0*Denominator[X], Y];
```

which produces the output

```
Y^14 (-4 k1^2 k2^2 k5 k6^2 kon - 8 k1 k2 k3 k4 k5 k6^2 kon - 4 k3^2 k4^2 k5
    ↪  k6^2 kon - 8 k1 k2 k3 k5^2 k6^2 kon - 8 k3^2 k4 k5^2 k6^2 kon - 4
    ↪ k3^2 k5^3 k6^2 kon - 2 k1^2 k2^2 k3 k5 k6 kon \[Kappa]2 - 2 k1 k2 k3
    ↪ ^2 k4 k5 k6 kon \[Kappa]2 - 2 k1 k2 k3^2 k5^2 k6 kon \[Kappa]2) +
       Y^12 (-4 k1 k2 k3 k4 k5 k6^2 koff - 4 k3^2 k4^2 k5 k6^2 koff - 4 k1
           ↪ k2 k3 k5^2 k6^2 koff - 8 k3^2 k4 k5^2 k6^2 koff - 4 k3^2 k5^3
           ↪  k6^2 koff + 2 k1^2 k2^2 k3 k5 k6 kon T0 - 4 k1^2 k2 k3 k4 k5
           ↪  k6 kon T0 + 2 k1 k2 k3^2 k4 k5 k6 kon T0 -4 k1 k3^2 k4^2 k5
           ↪ k6 kon T0 - 4 k1^2 k2 k3 k5^2 k6 kon T0 + 2 k1 k2 k3^2 k5^2
           ↪ k6 kon T0 - 8 k1 k3^2 k4 k5^2 k6 kon T0 - 4 k1 k3^2 k5^3 k6
           ↪ kon T0 - 2 k1^2 k2^2 k3 k5 k6 kon \[Kappa]1 + 4 k1^2 k2 k3 k4
           ↪  k5 k6 kon \[Kappa]1 - 2 k1 k2 k3^2 k4 k5 k6 kon \[Kappa]1 +
           ↪ 4 k1 k3^2 k4^2 k5 k6 kon \[Kappa]1 + 4 k1^2 k2 k3 k5^2 k6 kon
           ↪  \[Kappa]1 - 2 k1 k2 k3^2 k5^2 k6 kon \[Kappa]1 + 8 k1 k3^2
           ↪ k4 k5^2 k6 kon \[Kappa]1 + 4 k1 k3^2 k5^3 k6 kon \[Kappa]1 -
           ↪ 2 k1^2 k2 k3^2 k4 k6 kon P0 \[Kappa]1 + 4 k1^2 k3^2 k4^2 k6
           ↪ kon P0 \[Kappa]1 - 2 k1^2 k2 k3^2 k5 k6 kon P0 \[Kappa]1 + 8
           ↪ k1^2 k3^2 k4 k5 k6 kon P0 \[Kappa]1 + 4 k1^2 k3^2 k5^2 k6 kon
```

```
    ↪  P0 \[Kappa]1 - 2 k1 k2 k3^2 k4 k5 k6 koff \[Kappa]2 - 2 k1
    ↪ k2 k3^2 k5^2 k6 koff \[Kappa]2 + k1^2 k2^2 k3^2 k5 kon T0 \[
    ↪ Kappa]2 - 2 k1^2 k2 k3^2 k4 k5 kon T0 \[Kappa]2 - 2 k1^2 k2
    ↪ k3^2 k5^2 kon T0 \[Kappa]2)
- 2 k1^2 k2 k3^2 k4 k6 kon P0 \[Kappa]1 \[Kappa]r^12 + 4 k1^2 k3^2
    ↪ k4^2 k6 kon P0 \[Kappa]1 \[Kappa]r^12
+ Y^10 (-2 k1 k2 k3^2 k4 k5 k6 koff \[Kappa]1 + 4 k1 k3^2 k4^2 k5 k6
    ↪  koff \[Kappa]1 - 2 k1 k2 k3^2 k5^2 k6 koff \[Kappa]1 + 8 k1
    ↪ k3^2 k4 k5^2 k6 koff \[Kappa]1 + 4 k1 k3^2 k5^3 k6 koff \[
    ↪ Kappa]1 - 2 k1^2 k2 k3^2 k4 k5 k6 P0 \[Kappa]1 + 4 k1^2 k3^2
    ↪ k4^2 k5 k6 P0 \[Kappa]1 - 2 k1^2 k2 k3^2 k5^2 k6 P0 \[Kappa]1
    ↪  + 8 k1^2 k3^2 k4 k5^2 k6 P0 \[Kappa]1 + 4 k1^2 k3^2 k5^3 k6
    ↪ P0 \[Kappa]1 + k1^2 k2^2 k3^2 k5 kon T0 \[Kappa]1 - 4 k1^2 k2
    ↪  k3^2 k4 k5 kon T0 \[Kappa]1 + 4 k1^2 k3^2 k4^2 k5 kon T0 \[
    ↪ Kappa]1 - 4 k1^2 k2 k3^2 k5^2 kon T0 \[Kappa]1 + 8 k1^2 k3^2
    ↪ k4 k5^2 kon T0 \[Kappa]1 + 4 k1^2 k3^2 k5^3 kon T0 \[Kappa]1
    ↪ - 8 k1^2 k2^2 k5 k6^2 kon \[Kappa]r^4 - 16 k1 k2 k3 k4 k5 k6
    ↪ ^2 kon \[Kappa]r^4 - 8 k3^2 k4^2 k5 k6^2 kon \[Kappa]r^4 - 8
    ↪ k1 k2 k3 k5^2 k6^2 kon \[Kappa]r^4 - 8 k3^2 k4 k5^2 k6^2 kon
    ↪ \[Kappa]r^4 - 4 k1^2 k2^2 k3 k5 k6 kon \[Kappa]2 \[Kappa]r^4
    ↪ - 4 k1 k2 k3^2 k4 k5 k6 kon \[Kappa]2 \[Kappa]r^4 - 2 k1 k2
    ↪ k3^2 k5^2 k6 kon \[Kappa]2 \[Kappa]r^4)
+ Y^8 (-8 k1 k2 k3 k4 k5 k6^2 koff \[Kappa]r^4 - 8 k3^2 k4^2 k5 k6^2
    ↪  koff \[Kappa]r^4 - 4 k1 k2 k3 k5^2 k6^2 koff \[Kappa]r^4 - 8
    ↪  k3^2 k4 k5^2 k6^2 koff \[Kappa]r^4 + 4 k1^2 k2^2 k3 k5 k6
    ↪ kon T0 \[Kappa]r^4 - 8 k1^2 k2 k3 k4 k5 k6 kon T0 \[Kappa]r^4
    ↪  + 4 k1 k2 k3^2 k4 k5 k6 kon T0 \[Kappa]r^4 - 8 k1 k3^2 k4^2
    ↪ k5 k6 kon T0 \[Kappa]r^4 - 4 k1^2 k2 k3 k5^2 k6 kon T0 \[
    ↪ Kappa]r^4 + 2 k1 k2 k3^2 k5^2 k6 kon T0 \[Kappa]r^4 - 8 k1 k3
    ↪ ^2 k4 k5^2 k6 kon T0 \[Kappa]r^4 - 4 k1^2 k2^2 k3 k5 k6 kon
    ↪ \[Kappa]1 \[Kappa]r^4 + 8 k1^2 k2 k3 k4 k5 k6 kon \[Kappa]1
    ↪ \[Kappa]r^4 - 4 k1 k2 k3^2 k4 k5 k6 kon \[Kappa]1 \[Kappa]r^4
    ↪  + 8 k1 k3^2 k4^2 k5 k6 kon \[Kappa]1 \[Kappa]r^4 + 4 k1^2 k2
    ↪  k3 k5^2 k6 kon \[Kappa]1 \[Kappa]r^4 - 2 k1 k2 k3^2 k5^2 k6
    ↪ kon \[Kappa]1 \[Kappa]r^4 + 8 k1 k3^2 k4 k5^2 k6 kon \[Kappa
    ↪ ]1 \[Kappa]r^4 - 6 k1^2 k2 k3^2 k4 k6 kon P0 \[Kappa]1 \[
    ↪ Kappa]r^4 + 12 k1^2 k3^2 k4^2 k6 kon P0 \[Kappa]1 \[Kappa]r^4
    ↪  - 4 k1^2 k2 k3^2 k5 k6 kon P0 \[Kappa]1 \[Kappa]r^4 + 16 k1
    ↪ ^2 k3^2 k4 k5 k6 kon P0 \[Kappa]1 \[Kappa]r^4 + 4 k1^2 k3^2
    ↪ k5^2 k6 kon P0 \[Kappa]1 \[Kappa]r^4 - 4 k1 k2 k3^2 k4 k5 k6
    ↪ koff \[Kappa]2 \[Kappa]r^4 - 2 k1 k2 k3^2 k5^2 k6 koff \[
    ↪ Kappa]2 \[Kappa]r^4 + 2 k1^2 k2^2 k3^2 k5 kon T0 \[Kappa]2 \[
    ↪ Kappa]r^4 - 4 k1^2 k2 k3^2 k4 k5 kon T0 \[Kappa]2 \[Kappa]r^4
    ↪  - 2 k1^2 k2 k3^2 k5^2 kon T0 \[Kappa]2 \[Kappa]r^4)
+ Y^2 (-2 k1 k2 k3^2 k4 k5 k6 koff \[Kappa]1 \[Kappa]r^8 + 4 k1 k3^2
```

```
        ↪  k4^2 k5 k6 koff \[Kappa]1 \[Kappa]r^8 - 2 k1^2 k2 k3^2 k4 k5
        ↪  k6 P0 \[Kappa]1 \[Kappa]r^8 + 4 k1^2 k3^2 k4^2 k5 k6 P0 \[
        ↪ Kappa]1 \[Kappa]r^8 + k1^2 k2^2 k3^2 k5 kon T0 \[Kappa]1 \[
        ↪ Kappa]r^8 - 4 k1^2 k2 k3^2 k4 k5 kon T0 \[Kappa]1 \[Kappa]r^8
        ↪  + 4 k1^2 k3^2 k4^2 k5 kon T0 \[Kappa]1 \[Kappa]r^8)
    + Y^6 (-4 k1 k2 k3^2 k4 k5 k6 koff \[Kappa]1 \[Kappa]r^4 + 8 k1 k3^2
        ↪  k4^2 k5 k6 koff \[Kappa]1 \[Kappa]r^4 - 2 k1 k2 k3^2 k5^2 k6
        ↪  koff \[Kappa]1 \[Kappa]r^4 + 8 k1 k3^2 k4 k5^2 k6 koff \[
        ↪ Kappa]1 \[Kappa]r^4 - 4 k1^2 k2 k3^2 k4 k5 k6 P0 \[Kappa]1 \[
        ↪ Kappa]r^4 + 8 k1^2 k3^2 k4^2 k5 k6 P0 \[Kappa]1 \[Kappa]r^4 -
        ↪  2 k1^2 k2 k3^2 k5^2 k6 P0 \[Kappa]1 \[Kappa]r^4 + 8 k1^2 k3
        ↪ ^2 k4 k5^2 k6 P0 \[Kappa]1 \[Kappa]r^4 + 2 k1^2 k2^2 k3^2 k5
        ↪ kon T0 \[Kappa]1 \[Kappa]r^4 - 8 k1^2 k2 k3^2 k4 k5 kon T0 \[
        ↪ Kappa]1 \[Kappa]r^4 + 8 k1^2 k3^2 k4^2 k5 kon T0 \[Kappa]1 \[
        ↪ Kappa]r^4 - 4 k1^2 k2 k3^2 k5^2 kon T0 \[Kappa]1 \[Kappa]r^4
        ↪ + 8 k1^2 k3^2 k4 k5^2 kon T0 \[Kappa]1 \[Kappa]r^4 - 4 k1^2
        ↪ k2^2 k5 k6^2 kon \[Kappa]r^8 - 8 k1 k2 k3 k4 k5 k6^2 kon \[
        ↪ Kappa]r^8 - 4 k3^2 k4^2 k5 k6^2 kon \[Kappa]r^8 - 2 k1^2 k2^2
        ↪  k3 k5 k6 kon \[Kappa]2 \[Kappa]r^8 - 2 k1 k2 k3^2 k4 k5 k6
        ↪ kon \[Kappa]2 \[Kappa]r^8)
    + Y^4 (-4 k1 k2 k3 k4 k5 k6^2 koff \[Kappa]r^8 - 4 k3^2 k4^2 k5 k6^2
        ↪  koff \[Kappa]r^8 + 2 k1^2 k2^2 k3 k5 k6 kon T0 \[Kappa]r^8 -
        ↪  4 k1^2 k2 k3 k4 k5 k6 kon T0 \[Kappa]r^8 + 2 k1 k2 k3^2 k4
        ↪ k5 k6 kon T0 \[Kappa]r^8 - 4 k1 k3^2 k4^2 k5 k6 kon T0 \[
        ↪ Kappa]r^8 - 2 k1^2 k2^2 k3 k5 k6 kon \[Kappa]1 \[Kappa]r^8 +
        ↪ 4 k1^2 k2 k3 k4 k5 k6 kon \[Kappa]1 \[Kappa]r^8 - 2 k1 k2 k3
        ↪ ^2 k4 k5 k6 kon \[Kappa]1 \[Kappa]r^8 + 4 k1 k3^2 k4^2 k5 k6
        ↪ kon \[Kappa]1 \[Kappa]r^8 - 6 k1^2 k2 k3^2 k4 k6 kon P0 \[
        ↪ Kappa]1 \[Kappa]r^8 + 12 k1^2 k3^2 k4^2 k6 kon P0 \[Kappa]1
        ↪ \[Kappa]r^8 - 2 k1^2 k2 k3^2 k5 k6 kon P0 \[Kappa]1 \[Kappa]r
        ↪ ^8 + 8 k1^2 k3^2 k4 k5 k6 kon P0 \[Kappa]1 \[Kappa]r^8 - 2 k1
        ↪  k2 k3^2 k4 k5 k6 koff \[Kappa]2 \[Kappa]r^8 + k1^2 k2^2 k3^2
        ↪  k5 kon T0 \[Kappa]2 \[Kappa]r^8 - 2 k1^2 k2 k3^2 k4 k5 kon
        ↪ T0 \[Kappa]2 \[Kappa]r^8)
```

and shows the result is a seventh order polynomial of Y_∞^2. The Wolfram Language

```
Simplify[Coefficient[Q, Y, 0]]
```

isolates the constant term

```
2 k1^2 k3^2 k4 (-k2 + 2 k4) k6 kon P0 \[Kappa]1 \[Kappa]r^12
```

and the Wolfram Language

```
Simplify[Coefficient[Q, Y, 14]]
```

isolates the leading term

```
-2 k5 (k1 k2 + k3 (k4 + k5)) k6 kon (2 k3 (k4 + k5) k6 + k1 k2 (2 k6 + k3
    ↪ \[Kappa]2))
```

where we see that the leading term is always negative and the constant term can change signs depending on the choice of parameters. However, Table 2.1 indicates this term generally will be negative for physically plausible parameter sets.

The Jacobian Matrix of the reduced system (3.16) is determined with the Wolfram Language

```
yd = -2*kon*(T0 - Z - W - V - WS)*Y^2 + 2*koff*Z + k1*Z*P + k2*W - k6*P*Y
    ↪ *(2*Y + J);
zd = kon*(T0 - Z - W - V - WS)*Y^2 - koff*Z - k1*Z*P;
wd = k1*Z*P - k2*W + k3*V*P - k4*W - k5*W*f[Y];
vd = k2*W - k3*V*P;
wsd = k4*W - k5*WS*f[Y];
jd = k5*(W + WS)*f[Y] - k6*P*J*Y;

JacMat = D[{yd, zd, wd, vd, wsd, jd}, {{Y, Z, W, V, WS, J}}];
MatrixForm[JacMat]
```

The eigenvalues and eigenvectors for Corollary 4.1 are computed by appending

```
Y = 0; Z = 0; W = 0; V = 0; J = 0;
f[y_] := y^4/(\[Kappa]r^4 + y^4);
Eigensystem[JacMat]
```

to the previous language. This produces the result

```
{{0, 0, 0, -koff - k1 P, 1/2 (-k2 - k4 - k3 P - Sqrt[-4 k3 k4 P + (k2 + k4
    ↪ + k3 P)^2]), 1/2 (-k2 - k4 - k3 P + Sqrt[-4 k3 k4 P + (k2 + k4 + k3
    ↪ P)^2])},
       {{0, 0, 0, 0, 0, 1}, {0, 0, 0, 0, 1, 0}, {1, 0, 0, 0, 0, 0},
       {-((k3 (2 koff + k1 P) (-k2 koff - k1 k2 P))/(k1 k4 (koff + k1 P) (
           ↪ koff + k1 P - k3 P))) - (-2 k2 koff - 2 k4 koff + 2 koff^2 -
           ↪ 2 k1 k2 P - k1 k4 P + 3 k1 koff P + k1^2 P^2)/(k1 k4 P), ((
           ↪ koff + k1 P) (-k2 - k4 + koff + k1 P))/(k1 k4 P) + (k3 (-k2
           ↪ koff - k1 k2 P))/(k1 k4 (koff + k1 P - k3 P)), -((koff + k1 P
           ↪ )/k4), -((-k2 koff - k1 k2 P)/(k4 (koff + k1 P - k3 P))), 1,
           ↪ 0},
       {k2/k4, 0, -((k2 + k4 + k3 P + Sqrt[k2^2 + 2 k2 k4 + k4^2 + 2 k2 k3
           ↪ P - 2 k3 k4 P + k3^2 P^2])/(2 k4)), -((-k2^2 - k2 k4 - 2 k2
           ↪ k3 P + k3 k4 P - k3^2 P^2 - k2 Sqrt[k2^2 + 2 k2 k4 + k4^2 + 2
           ↪  k2 k3 P - 2 k3 k4 P + k3^2 P^2] - k3 P Sqrt[k2^2 + 2 k2 k4 +
           ↪  k4^2 + 2 k2 k3 P - 2 k3 k4 P + k3^2 P^2])/(k4 (k2 + k4 + k3
           ↪ P + Sqrt[k2^2 + 2 k2 k4 + k4^2 + 2 k2 k3 P - 2 k3 k4 P + k3^2
           ↪  P^2]))), 1, 0},
```

```
{k2/k4, 0, -((k2 + k4 + k3 P - Sqrt[k2^2 + 2 k2 k4 + k4^2 + 2 k2 k3
    ↪ P - 2 k3 k4 P + k3^2 P^2])/(2 k4)), -((k2^2 + k2 k4 + 2 k2 k3
    ↪  P - k3 k4 P + k3^2 P^2 - k2 Sqrt[k2^2 + 2 k2 k4 + k4^2 + 2
    ↪ k2 k3 P - 2 k3 k4 P + k3^2 P^2] - k3 P Sqrt[k2^2 + 2 k2 k4 +
    ↪ k4^2 + 2 k2 k3 P - 2 k3 k4 P + k3^2 P^2])/(k4 (-k2 - k4 - k3
    ↪ P + Sqrt[k2^2 + 2 k2 k4 + k4^2 + 2 k2 k3 P - 2 k3 k4 P + k3^2
    ↪  P^2]))), 1, 0}}}
```

where

```
{0, 0, 0, -koff - k1 P, 1/2 (-k2 - k4 - k3 P - Sqrt[-4 k3 k4 P + (k2 + k4 +
    ↪  k3 P)^2]), 1/2 (-k2 - k4 - k3 P + Sqrt[-4 k3 k4 P + (k2 + k4 + k3 P
    ↪ )^2])}
```

is the list of eigenvalues and the other lists are the eigenvectors corresponding to those eigenvalues. Here the three zero eigenvalues correspond to linearly independent eigenvectors

$$\vec{v}_1 = (0,0,0,0,0,1), \quad \vec{v}_2 = (0,0,0,0,1,0), \quad \vec{v}_3 = (1,0,0,0,0,0).$$

To compute the viable Y_∞ values for a given parameter set, assign the parameter values (here we use simulation values *(Table 2.1)*) and create a list of viable solutions using the following Wolfram Language:

```
kon = 2000; koff = 45; k1 = 400; k2 = 0.625; k3 = 800; k4 = 0.013; k5 =
    ↪ 0.1; k6 = 0.01;
\[Kappa]r = 14; kp1 = 0.015; kp2 = 0.225; ka = 0.0075;
T0 = 0.1; P0 = 0.005; \[Kappa]1 = kp1; \[Kappa]2 = (kp1*ka)/kp2;

f[y_] := y^4/(\[Kappa]r^4 + y^4);
Z = ((2*k6)/k1)*Y^2*((k4 + k5*f[Y])/(k2 - 2*(k4 + k5*f[Y])));
V = (k1*k2*Z)/(k3*(k4 + k5*f[Y]));
J = (k1*Z)/(k6*Y);
P = P0/(1 + ((Z + V) + \[Kappa]2*(Y^2 + Y*J))/\[Kappa]1);

ylist = Y /. Solve[Z*((koff + k1*P)/(kon*Y^2) + 1 + (k1*P)/(k5*f[Y]) + (k1*
    ↪ k2)/(k3*(k4 + k5*f[Y]))) == T0 && Y > 0, Y, Reals]
```

Then we have $Y_{\infty_1} = 2.60126$ and $Y_{\infty_2} = 42.3847$. To compute the nonzero values for $T_{\infty_{1,2}}$, $Z_{\infty_{1,2}}$, $W_{\infty_{1,2}}$, $V_{\infty_{1,2}}$, $W^*_{\infty_{1,2}}$, and $J_{\infty_{1,2}}$, append the Wolfram Language

```
Y = ylist[[which]];
Z = ((2*k6)/k1)*Y^2*((k4 + k5*f[Y])/(k2 - 2*(k4 + k5*f[Y])));
V = (k1*k2*Z)/(k3*(k4 + k5*f[Y]));
J = (k1*Z)/(k6*Y);
P = p0/(1 + ((Z + V) + \[Kappa]2*(Y^2 + Y*J))/\[Kappa]1);
T = ((koff + k1*P)*Z)/(kon*Y^2);
W = (k3*P*V)/k2;
```

```
WS = (k1*Z*P)/(k5*f[Y]) - W;
```

where `which` assigns which Y_∞ value to pull from the list. Because this parameter set has two real, positive solutions for Y_∞, `which` can either be `1` or `2`. The results of this language are found in Table A.2.

	Y = ylist[[1]] = 2.60126	Y = ylist[[2]] = 42.3847
T_∞	2.55271*10^-8	3.13583*10^-7
Z_∞	7.41284*10^-6	0.0250263
W_∞	0.000905737	0.00445015
V_∞	0.000176576	0.0699379
W^*_∞	0.0989102	0.000585406
J_∞	0.113989	23.6182
P_∞	0.00400737	0.000049711

Table A.2: Mathematica output for Full Model limit values with simulation values *(Table 2.1)*

For Corollary 4.2, we seek the eigenvalues and eigenvectors of the Jacobian for system (3.16) when $Y_\infty \neq 0$. We assign a parameter set (here we use simulation values *(Table 2.1)*) and obtain numerical solutions for the other limit values using the code above. Then we compute the numerical eigenvalues for our parameter set. The Wolfram Language used for this work was

```
yd = -2*kon*(T0 - Z - W - V - WS)*Y^2 + 2*koff*Z + k1*Z*P + k2*W - k6*P*Y
    ↪ *(2*Y + J);
zd = kon*(T0 - Z - W - V - WS)*Y^2 - koff*Z - k1*Z*P;
wd = k1*Z*P - k2*W + k3*V*P - k4*W - k5*W*f[Y];
vd = k2*W - k3*V*P;
wsd = k4*W - k5*WS*f[Y];
jd = k5*(W + WS)*f[Y] - k6*P*J*Y;

JacMat = D[{yd, zd, wd, vd, wsd, jd}, {{Y, Z, W, V, WS, J}}];

kon = 2000; koff = 45; k1 = 400; k2 = 0.625; k3 = 800; k4 = 0.013; k5 =
    ↪ 0.1; k6 = 0.01;
\[Kappa]r = 14; kp1 = 0.015; kp2 = 0.225; ka = 0.0075;
T0 = 0.1; P0 = 0.005; \[Kappa]1 = kp1; \[Kappa]2 = (kp1*ka)/kp2;

f[y_] := y^4/(\[Kappa]r^4 + y^4);
Z = ((2*k6)/k1)*Y^2*((k4 + k5*f[Y])/(k2 - 2*(k4 + k5*f[Y])));
V = (k1*k2*Z)/(k3*(k4 + k5*f[Y]));
J = (k1*Z)/(k6*Y);
P = P0/(1 + ((Z + V) + \[Kappa]2*(Y^2 + Y*J))/\[Kappa]1);
```

```
ylist = Y /. Solve[Z*((koff + k1*P)/(kon*Y^2) + 1 + (k1*P)/(k5*f[Y]) + (k1*
    ↪ k2)/(k3*(k4 + k5*f[Y]))) == T0 && Y > 0, Y, Reals];

Y = ylist[[which]];
Z = ((2*k6)/k1)*Y^2*((k4 + k5*f[Y])/(k2 - 2*(k4 + k5*f[Y])));
V = (k1*k2*Z)/(k3*(k4 + k5*f[Y]));
J = (k1*Z)/(k6*Y);
P = P0/(1 + ((Z + V) + \[Kappa]2*(Y^2 + Y*J))/\[Kappa]1);
T = ((koff + k1*P)*Z)/(kon*Y^2);
W = (k3*P*V)/k2;
WS = (k1*Z*P)/(k5*f[Y]) - W;

Eigenvalues[JacMat]
```

Then for Y_{∞_1} = `ylist[[1]] = 2.60126`, we have eigenvalues

```
{-13578.1, -3.83306, -1.59773, -0.011828, 0.000387824, -0.000101557}
```

and for Y_{∞_2} = `ylist[[2]] = 42.3847`, we have eigenvalues

```
{-3.59297*10^6, -0.773268, -0.099122, -0.0229107, -0.000100093,
    ↪ -0.0000180379}
```

which implies Y_{∞_1} is a saddle point and Y_{∞_2} is stable.

A.5 Model II

We first substitute the second order approximations (4.69) and their derivatives (4.70) into system (4.64)-(4.68). Then we compute their difference to create polynomials that are equal to zero by using Wolfram Language

```
Element[\[Alpha] | \[Beta] | \[Gamma] | \[Delta] | \[Zeta] | \[Lambda] | \[
    ↪ Eta] | \[Theta], Reals];

zder = yeqn*(2*a1*y + b1*\[Nu]) + nueqn*(b1*y + 2*c1*\[Nu]);
wder = yeqn*(2*a2*y + b2*\[Nu]) + nueqn*(b2*y + 2*c2*\[Nu]);
vder = yeqn*(2*a3*y + b3*\[Nu]) + nueqn*(b3*y + 2*c3*\[Nu]);
yeqn = -2*(1 - (a1 + a2 + a3)*y^2 - (b1 + b2 + b3)*y*\[Nu] - (c1 + c2 + c3)
    ↪ *\[Nu]^2 - \[Nu])*y^2 + (2*\[Alpha] + \[Beta])*(a1*y^2 + b1*y*\[Nu]
    ↪ + c1*\[Nu]^2) + \[Gamma]*(a2*y^2 + b2*y*\[Nu] + c2*\[Nu]^2);
zeqn = (1 - (a1 + a2 + a3)*y^2 - (b1 + b2 + b3)*y*\[Nu] - (c1 + c2 + c3)*\[
    ↪ Nu]^2 - \[Nu])*y^2 - (\[Alpha] + \[Beta])*(a1*y^2 + b1*y*\[Nu] + c1
    ↪ *\[Nu]^2);
weqn = \[Beta]*(a1*y^2 + b1*y*\[Nu] + c1*\[Nu]^2) + \[Delta]*(a3*y^2 + b3*y
    ↪ *\[Nu] + c3*\[Nu]^2) - (\[Gamma] + \[Lambda])*(a2*y^2 + b2*y*\[Nu] +
    ↪  c2*\[Nu]^2);
```

```
veqn = -\[Delta]*(a3*y^2 + b3*y*\[Nu] + c3*\[Nu]^2) + \[Gamma]*(a2*y^2 + b2
    ↪ *y*\[Nu] + c2*\[Nu]^2);
nueqn = \[Lambda]*(a2*y^2 + b2*y*\[Nu] + c2*\[Nu]^2);

zpoly = Collect[zeqn - zder, {y, \[Nu]}];
wpoly = Collect[weqn - wder, {y, \[Nu]}];
vpoly = Collect[veqn - vder, {y, \[Nu]}];
```

We collect the coefficients of the second order terms with the Wolfram Language

```
znu2 = Coefficient[zpoly, \[Nu]^2]
zy2 = Coefficient[zpoly, y^2]
znuy = Coefficient[zpoly, \[Nu]*y]

wnu2 = Coefficient[wpoly, \[Nu]^2]
wy2 = Coefficient[wpoly, y^2]
wnuy = Coefficient[wpoly, \[Nu]*y]

vnu2 = Coefficient[vpoly, \[Nu]^2]
vy2 = Coefficient[vpoly, y^2]
vnuy = Coefficient[vpoly, \[Nu]*y]
```

Using these language segements together creates the output

```
-2 b1 y^2 - c1 y^2 - c2 y^2 - c3 y^2 - 2 b1^2 y^3 - 2 b1 b2 y^3 - 2 b1 b3 y
    ↪ ^3 - 4 a1 c1 y^3 - 4 a1 c2 y^3 - 4 a1 c3 y^3 - c1 \[Alpha] - 2 b1^2
    ↪ y \[Alpha] - 4 a1 c1 y \[Alpha] - c1 \[Beta] - b1^2 y \[Beta] - 2 a1
    ↪  c1 y \[Beta] - b1 b2 y \[Gamma] - 2 a1 c2 y \[Gamma] - 2 b2 c1 y \[
    ↪ Lambda] - b1 c2 y \[Lambda]

1 + a1 (-\[Alpha] - \[Beta]) + (-1 + 2 b1 - 3 a1 b1 (2 \[Alpha] + \[Beta])
    ↪ - a2 b1 \[Gamma] - 2 a1 b2 \[Gamma] - b1 b2 \[Lambda] - 2 a2 c1 \[
    ↪ Lambda]) \[Nu] + (-2 b1 - c1 - c2 - c3) \[Nu]^2 - 2 b1 (c1 + c2 + c3
    ↪ ) \[Nu]^3

b1 (-\[Alpha] - \[Beta])

-2 b2 y^2 - 2 b1 b2 y^3 - 2 b2^2 y^3 - 2 b2 b3 y^3 - 4 a2 c1 y^3 - 4 a2 c2
    ↪ y^3 - 4 a2 c3 y^3 - 2 b1 b2 y \[Alpha] - 4 a2 c1 y \[Alpha] + c1 \[
    ↪ Beta] - b1 b2 y \[Beta] - 2 a2 c1 y \[Beta] - c2 \[Gamma] - b2^2 y
    ↪ \[Gamma] - 2 a2 c2 y \[Gamma] + c3 \[Delta] - c2 \[Lambda] - 3 b2 c2
    ↪  y \[Lambda]

a1 \[Beta] + a3 \[Delta] + a2 (-\[Gamma] - \[Lambda]) + (2 b2 - 2 a2 b1 (2
    ↪ \[Alpha] + \[Beta]) - a1 b2 (2 \[Alpha] + \[Beta]) - 3 a2 b2 \[Gamma
    ↪ ] - b2^2 \[Lambda] - 2 a2 c2 \[Lambda]) \[Nu] - 2 b2 \[Nu]^2 - 2 b2
    ↪ (c1 + c2 + c3) \[Nu]^3
```

```
b1 \[Beta] + b3 \[Delta] + b2 (-\[Gamma] - \[Lambda])

-2 b3 y^2 - 2 b1 b3 y^3 - 2 b2 b3 y^3 - 2 b3^2 y^3 - 4 a3 c1 y^3 - 4 a3 c2
    ↪ y^3 - 4 a3 c3 y^3 - 2 b1 b3 y \[Alpha] - 4 a3 c1 y \[Alpha] - b1 b3
    ↪ y \[Beta] - 2 a3 c1 y \[Beta] + c2 \[Gamma] - b2 b3 y \[Gamma] - 2
    ↪ a3 c2 y \[Gamma] - c3 \[Delta] - b3 c2 y \[Lambda] - 2 b2 c3 y \[
    ↪ Lambda]

a2 \[Gamma] - a3 \[Delta] + (2 b3 - 2 a3 b1 (2 \[Alpha] + \[Beta]) - a1 b3
    ↪ (2 \[Alpha] + \[Beta]) - 2 a3 b2 \[Gamma] - a2 b3 \[Gamma] - b2 b3
    ↪ \[Lambda] - 2 a2 c3 \[Lambda]) \[Nu] - 2 b3 \[Nu]^2 - 2 b3 (c1 + c2
    ↪ + c3) \[Nu]^3

b2 \[Gamma] - b3 \[Delta]
```

where the coefficients of interest are determined by letting y and ν equal zero. The system then solves to

$$
\begin{gathered}
b_1 = 0, \quad b_2 = 0, \quad b_3 = 0, \\
c_1 = 0, \quad c_2 = 0, \quad c_3 = 0 \\
a_1 = \frac{1}{\alpha + \beta}, \quad a_2 = \frac{\beta}{\lambda(\alpha + \beta)}, \quad a_3 = \frac{\beta\gamma}{\delta\lambda(\alpha + \beta)}.
\end{gathered}
$$

APPENDIX B

MATLAB CODE

This code allows the user to set parameter values, import a data set to compare against simulation values, and fix values that correspond to various UDAR template structures such as the length of the toehold, palindrome site, and restriction site. The user can also choose to sequester or hold constant the polymerase concentration as described by the formula (3.3), create custom detailed inset graphs or graphs of concentrations rather than fluorescence approximations, and output the fluorescence approximation data as a .csv file. The data is set to run for one hour to simulate the experimental time series.

```
%% Input data
% rate and association constants (agreed on simulation values)
Kon = 2000; % multistep initiation (2000)
Koff = 45; % back reaction from Z to TY^2 (45)
n = 4; % Hill exponent (4)
k1 = 400; % extending Z to W (400)
k2 = 0.625; % nicking W (0.625)
k3 = 800; % extending V to W (800)
k4 = 0.013; % deactivation (0.013)
k5 = 0.1; % recycling (0.1)
k6 = 0.01; % extending to G and D (0.01)
kr = 14; % Y hill Khalf (14)
ka = 0.0075; % polymerase bimolecular association constant (0.0075)
kp1 = 0.015; % polymerase unimolecular disassociation constant (0.015)
kp2 = 0.225; % polymerase bimolecular disassociation constant (0.225)

% csv data to import [time in seconds; uM concentration of 1 nt pieces]
expdata = csvread('TypeII.csv');

% template lengths
th = 6; % toehold length in nt
pd = 6; % palindrome length in nt
rs = 10; % restriction site length in nt


%% Set switch cases
% choose system of equations to solve: 'sequestered' 'constant'
poly = 'sequestered';

% graph an inset of [0 10] nt: 'on' 'off'
inset = 'off';
% select time interval [instart inend] for inset
instart = 0;
inend = 3600;

% examine concentrations not based on molar mass: 'on' 'off'
conc = 'off';
```

```
% select time interval [coninstart coninend] for inset
coninstart = 0;
coninend = 3600;
% select max concentration value
conmax = 0.5;

% write results into .csv files: 'on' 'off'
% simdata.csv == simulated fluorescence results by each structure type and
    ↪ total DNA [t 10*Y 30*T 50*Z 60*W 50*Z 60*W* 30*J 68*G 28*D totalDNA]
createcsv = 'on';


%% Structure data
% concatenate rates
K = [Kon Koff n k1 k2 k3 k4 k5 k6 kr ka kp1 kp2];

% initial conditions
p0 = 5*10^-3;
t0 = 0.1;

% time span (3600 for 1 hour, 6000 for experimental data length)
stop = 3600;
tspan = [0,stop];

% initial conditions [y0 Z W V W* J G D]
initcond = [10^-5 0 0 0 0 0 0 0];

% sizes to approximate fluorescence
Ysize = th + pd; % design size
Tsize = 2*th + 2*pd + rs; % design size
Zsize = Tsize + 2*Ysize; % 1 template, 2 bound triggers
Wsize = 2*Tsize; % 1 template, fully extended, also W* size
Vsize = Tsize + Ysize + rs; % trigger nicked off W
Jsize = Tsize; % top of W,W*
Gsize = Wsize + 2*th; % sequestered J
Dsize = 2*Ysize + 2*th; % sequestered trigger dimer

% concatenate sizes
sizes = [Ysize Zsize Wsize Vsize Jsize Gsize Dsize Tsize];


%% Run Simulation
% run ODE solver
switch poly
    case 'sequestered'
```

```
        [t,x] = ode15s(@(t,x) seq(x,p0,t0,K),tspan,initcond);

    case 'constant'
        [t,x] = ode15s(@(t,x) con(x,p0,t0,K),tspan,initcond);

    otherwise
        % do nothing
end

% compute total DNA as a function of time
totalDNA = sizes(1)*x(:,1) + sizes(2)*x(:,2) + sizes(3)*x(:,3) + sizes(4)*x
    ↪ (:,4) + sizes(3)*x(:,5) + sizes(5)*x(:,6) + sizes(6)*x(:,7) + sizes
    ↪ (7)*x(:,8) + sizes(8)*(t0-x(:,2)-x(:,3)-x(:,4)-x(:,5));


%% Plot Results
% create a 2x1 plot of the primary results
% top == nt concentrations with exp data; bottom == detail of nt
    ↪ concentrations
figure('position',[0 0 750 1000])
subplot(2,1,1)
plot(expdata(:,1),expdata(:,2),'*', t,sizes(1)*x(:,1),'g', t,sizes(2)*x
    ↪ (:,2),'b:', t,sizes(3)*x(:,3),'r', t,sizes(4)*x(:,4),'b-.', t,sizes
    ↪ (3)*x(:,5),'r-.', t,sizes(5)*x(:,6),'m:', t,sizes(6)*x(:,7),'m-.', t
    ↪ ,sizes(7)*x(:,8),'m', t,sizes(8)*(t0-x(:,2)-x(:,3)-x(:,4)-x(:,5)),'b
    ↪ ', t,totalDNA,'k')
axis([0 stop 0 max(max(totalDNA),max(expdata(:,2)))])
legend('Exp.␣Data','Sim.␣Y','Sim.␣Z','Sim.␣W','Sim.␣V','Sim.␣W*','Sim.␣J','
    ↪ Sim.␣G','Sim.␣D','Sim.␣T','Sim.␣Total␣DNA','Location','northwest')
xlabel('Time␣(s)'); ylabel('DNA␣(nt)')
title({'Simulation␣fit',...
    strcat('k_+=',num2str(K(1)),',','␣k_-=',num2str(K(2)),',','␣k_1=',
        ↪ num2str(K(4)),',','␣k_2=',num2str(K(5)),',','␣k_3=',num2str(K(6))
        ↪ ,',','␣k_4=',num2str(K(7)),',','␣k_5=',num2str(K(8)),',','␣k_6=',
        ↪ num2str(K(9)),',')...
    strcat('n=',num2str(K(3)),',','␣k_R=',num2str(K(10)),',','␣k_A=',
        ↪ num2str(K(11)),',','␣k_p_1=',num2str(K(12)),',','␣k_p_2=',num2str
        ↪ (K(13)),',','␣y_0=',num2str(initcond(1)),',','␣t_0=',num2str(t0),
        ↪ ',','␣p_0=',num2str(p0))})

subplot(2,1,2)
plot(t,sizes(1)*x(:,1),'g', t,sizes(2)*x(:,2),'b:', t,sizes(3)*x(:,3),'r',
    ↪ t,sizes(4)*x(:,4),'b-.', t,sizes(3)*x(:,5),'r-.', t,sizes(5)*x(:,6),
    ↪ 'm:', t,sizes(6)*x(:,7),'m-.', t,sizes(7)*x(:,8),'m', t,sizes(8)*(t0
    ↪ -x(:,2)-x(:,3)-x(:,4)-x(:,5)),'b', t,totalDNA,'k')
```

```
xlabel('Time␣(s)'); ylabel('DNA␣(nt)')
title('Simulated␣System␣Behavior␣(detail)')
axis([0 stop 0 10])

% when on, create detail inset of chosen time span over [0 10] nt
switch inset
    case 'on'
        figure('position',[750 500 600 500])
        plot(t,sizes(1)*x(:,1),'g', t,sizes(2)*x(:,2),'b:', t,sizes(3)*x
            ↪ (:,3),'r', t,sizes(4)*x(:,4),'b-.', t,sizes(3)*x(:,5),'r-.',
            ↪ t,sizes(5)*x(:,6),'m:', t,sizes(6)*x(:,7),'m-.', t,sizes(7)*x
            ↪ (:,8),'m', t,sizes(8)*(t0-x(:,2)-x(:,3)-x(:,4)-x(:,5)),'b', t
            ↪ ,totalDNA,'k')
        legend('Sim.␣Y','Sim.␣Z','Sim.␣W','Sim.␣V','Sim.␣W*','Sim.␣J','Sim.␣
            ↪ G','Sim.␣D','Sim.␣T','Sim.␣Total␣DNA','Location','northwest')
        xlabel('Time␣(s)'); ylabel('DNA␣(nt)')
        axis([instart inend 0 10])
        title({strcat('Simulated␣System␣Behavior␣Fluorescence␣detail'),...
            strcat('k_+=',num2str(K(1)),',', '␣k_-=',num2str(K(2)),',', '␣
                ↪ k_1=',num2str(K(4)),',','␣k_2=',num2str(K(5)),','),...
            strcat('k_3=',num2str(K(6)),',', '␣k_4=',num2str(K(7)),',','␣k_5
                ↪ =',num2str(K(8)),',','␣k_6=',num2str(K(9)),',')...
            strcat('n=',num2str(K(3)),',','␣k_R=',num2str(K(10)),',', '␣k_A=
                ↪ ',num2str(K(11)),',', '␣k_p_1=',num2str(K(12)),',')...
            strcat('k_p_2=',num2str(K(13)),',','␣y_0=',num2str(initcond(1)),
                ↪ ',','␣t_0=',num2str(t0),',','␣p_0=',num2str(p0))})

    otherwise
        % do nothing
end

% when on, create concentrations insets of chosen time and concentrations
switch conc
    case 'on'
        figure('position',[750 500 600 500])
        plot(t,x(:,1),'g', t,x(:,2),'b:', t,x(:,3),'r', t,x(:,4),'b-.', t,x
            ↪ (:,5),'r-.', t,x(:,6),'m:', t,x(:,7),'m-.', t,x(:,8),'m', t,
            ↪ t0-x(:,2)-x(:,3)-x(:,4)-x(:,5),'b', t,p0./(1+(x(:,3)+x(:,5))
            ↪ ./kp1+x(:,1).*(x(:,7)+x(:,1))./kp2),'k')
        legend('Y','Z','W','V','W*','J','G','D','T','P','Location','
            ↪ northwest')
        xlabel('Time␣(s)'); ylabel('Concentration␣(uM)')
        axis([coninstart coninend 0 conmax])
        title({strcat('Simulated␣Concentration␣detail'),...
            strcat('k_+=',num2str(K(1)),',', '␣k_-=',num2str(K(2)),',', '␣
```

```
            ↪ k_1=',num2str(K(4)),',','␣k_2=',num2str(K(5)),','),...
        strcat('k_3=',num2str(K(6)),',', '␣k_4=',num2str(K(7)),',','␣k_5
            ↪ =',num2str(K(8)),',','␣k_6=',num2str(K(9)),',')...
        strcat('n=',num2str(K(3)),',','␣k_R=',num2str(K(10)),',', '␣k_A=
            ↪ ',num2str(K(11)),',', '␣k_p_1=',num2str(K(12)),',')...
        strcat('k_p_2=',num2str(K(13)),',','␣y_0=',num2str(initcond(1)),
            ↪ ',','␣t_0=',num2str(t0),',','␣p_0=',num2str(p0))})

    otherwise
        % do nothing
end


%% Report data
switch createcsv
    case 'on'
        simdata = [t sizes(1)*x(:,1) sizes(2)*x(:,2) sizes(3)*x(:,3) sizes
            ↪ (4)*x(:,4) sizes(3)*x(:,5) sizes(5)*x(:,6) sizes(6)*x(:,7)
            ↪ sizes(7)*x(:,8) sizes(8)*(t0-x(:,2)-x(:,3)-x(:,4)-x(:,5))
            ↪ totalDNA];
        csvwrite('simdata.csv',simdata);

    otherwise
        % do nothing
end


%% ODE systems
function sys = seq(x,p0,t0,K)
Kon = K(1); Koff = K(2); n = K(3); k1 = K(4); k2 = K(5); k3 = K(6); k4 = K
    ↪ (7); k5 = K(8); k6 = K(9); kr = K(10); ka = K(11); kp1 = K(12); kp2
    ↪ = K(13);

%Y == x(1), Z == x(2), W == x(3), V == x(4), W* == x(5), J == x(6), G == x
    ↪ (7), D == x(8)
sys = [-2*Kon*x(1)^2*(t0-x(2)-x(3)-x(4)-x(5)) + 2*Koff*x(2) + (k1*x(2) - k6
    ↪ *x(1)*(2*x(1) + x(6)))*(p0/(1+(x(2)+x(4))/kp1+(ka*x(1)*(x(6)+x(1)))/
    ↪ kp2)) + k2*x(3);... % Y
    Kon*x(1)^2*(t0-x(2)-x(3)-x(4)-x(5)) - Koff*x(2) - k1*(p0/(1+(x(2)+x(4))
        ↪ /kp1+(ka*x(1)*(x(6)+x(1)))/kp2))*x(2);... % Z
    (p0/(1+(x(2)+x(4))/kp1+(ka*x(1)*(x(6)+x(1)))/kp2))*(k1*x(2) + k3*x(4))
        ↪ - x(3)*(k2 + k4 + k5*(x(1)^n/(kr^n+x(1)^n)));... % W
    k2*x(3) - k3*x(4)*(p0/(1+(x(2)+x(4))/kp1+(ka*x(1)*(x(6)+x(1)))/kp2))
        ↪ ;... % V
    k4*x(3) - k5*x(5)*(x(1)^n/(kr^n+x(1)^n));... % W*
```

```
    k5*(x(1)^n/(kr^n+x(1)^n))*(x(3) + x(5)) - k6*(p0/(1+(x(2)+x(4))/kp1+(ka
        ↪ *x(1)*(x(6)+x(1)))/kp2))*x(1)*x(6);... % J
    k6*(p0/(1+(x(2)+x(4))/kp1+(ka*x(1)*(x(6)+x(1)))/kp2))*x(1)*x(6);... % G
    k6*(p0/(1+(x(2)+x(4))/kp1+(ka*x(1)*(x(6)+x(1)))/kp2))*x(1)^2]; % D
end

function sys = con(x,p0,t0,K)
Kon = K(1); Koff = K(2); n = K(3); k1 = K(4); k2 = K(5); k3 = K(6); k4 = K
    ↪ (7); k5 = K(8); k6 = K(9); kr = K(10);

% Y == x(1), Z == x(2), W == x(3), V == x(4), W* == x(5), J == x(6), G == x
    ↪ (7), D == x(8)
sys = [-2*Kon*x(1)^2*(t0-x(2)-x(3)-x(4)-x(5)) + 2*Koff*x(2) + (k1*x(2) - k6
    ↪ *x(1)*(2*x(1) + x(6)))*p0 + k2*x(3);... % Y
    Kon*x(1)^2*(t0-x(2)-x(3)-x(4)-x(5)) - Koff*x(2) - k1*p0*x(2);... % Z
    p0*(k1*x(2) + k3*x(4)) - x(3)*(k2 + k4 + k5*(x(1)^n/(kr^n+x(1)^n)));...
        ↪  % W
    k2*x(3) - k3*x(4)*p0;... % V
    k4*x(3) - k5*x(5)*(x(1)^n/(kr^n+x(1)^n));... % W*
    k5*(x(1)^n/(kr^n+x(1)^n))*(x(3) + x(5)) - k6*p0*x(1)*x(6);... % J
    k6*p0*x(1)*x(6);... % G
    k6*p0*x(1)^2]; % D
end
```